

---

Unterschrift (Betreuer)



# D I P L O M A R B E I T

## Automated Ending Analysis of Drawn Strokes

Ausgeführt am Institut für  
Rechnergestützte Automation,  
Arbeitsbereich für Mustererkennung und Bildverarbeitung  
der Technischen Universität Wien

unter der Anleitung von **a.o.Univ.-Prof. Dipl.-Ing. Dr.techn.  
Robert Sablatnig**

durch

**Maria Christine Vill**  
Wallensteinstrasse 28/22  
1200 Wien

Wien, 01.04.2008

---

Unterschrift (Student)

# Danksagung

Auch wenn eine Diplomarbeit wie die vorliegende per definitionem eine eigenständige Arbeit ist, sind aufmunternde Worte und fachliches Feedback eine wichtige und gerne angenommene Hilfestellung, womit ich mich hiermit bei all jenen bedanken möchte, die mich in diesem Sinne, aber auch auf andere, viel umfassendere Art und Weise unterstützt haben, so dass ich nicht nur diese Arbeit, sondern auch dieses Studium zu einem Abschluss bringen konnte.

Ein Herzensanliegen ist es mir, meinen Eltern zu danken, die das ganze Unterfangen durch ihre Unterstützung erst ermöglichten. Gleiches gilt für meine Tante. Ein besonderer Dank gilt meinen Kollegen am PRIP (Pattern Recognition and Image Processing Group) des Instituts für Rechnergestützte Automation der Technischen Universität Wien. Namentlich möchte ich mich bei Martin Lettner, Florian Kleber, Markus Diem, Sebastian Zambanini, Paul Kammerer und Ernestine Zolda bedanken. Durch die beiden letzteren fand ich im Rahmen eines Praktikums erlangte das erste Mal einen tieferen Einblick in die Materie der Bildverarbeitung und Mustererkennung in Verbindung mit geisteswissenschaftlichen Fragestellungen. Sigrid Elsinger danke ich herzlich für die Unterstützung im bürokratischen Alltag.

Bei dem Betreuer meiner Diplomarbeit, Robert Sablatnig, bedanke ich mich, dass ich die Arbeit an dieser Diplomarbeit zu einem guten Teil im Rahmen des FWF-Projekts “The Sinaitic Glagolitic Sacramentary (Euchologium) Fragments” (FWF: P19608-G12) durchführen konnte und er mir die Teilnahme an mehreren wissenschaftlichen Konferenzen ermöglichte. Im Rahmen des angesprochenen Projekts lernte ich Melanie Gau und Prof. Heinz Miklas, beide Slawisten an der Universität Wien, sowie den Kalligraphen Herrn Dietrich kennen, die mir nicht nur bereitwillig Material zur Verfügung gestellt, sondern mir auch einen Einblick in die Welt der glagolitischen Schrift gewährt haben.

Wien im März 2008

# Abstract

This thesis proposes a drawing and writing tool recognition algorithm based on features calculated from the shape of stroke endings. The analysis of strokes is an interdisciplinary field which unites different fields of research: Art History, Paleography and Computer Science, especially the field of Image Processing and Pattern Recognition. The application for this method is to help art historians to identify the drawing tool used for a drawing. Since the style of a drawing depends on the drawing tool used, drawing tool recognition is an important step toward a style analysis. A stroke is a fundamental part of drawing and writing. This means that every drawing and every handwritten document consists of an assemblage of strokes which can be arranged in different ways.

Before the endings can be extracted, the strokes need to be separated from the background. This results in a binary image which is then used to extract static open and half-open strokes. A static stroke is defined as a stroke which is delimited by two endpoints, two knots or an endpoint and a knot, where a knot is the junction of at least three strokes. If the stroke connects two endpoints, it is called open, and if it is delimited only by one endpoint, it is called half-open. This leads to the conclusion that endings can be extracted from open and half-open static strokes. They are extracted according to their varying width in contrast to the remainder of the stroke. A stroke formation is partitioned into static strokes with the help of a skeleton.

Several features regarding curvature, proportions etc. are calculated out of the shape of the endings. These features are then used to classify stroke endings with a Support Vector Machine Classifier.

Test data consists of synthetic strokes, strokes and stroke formations drawn with different drawing and writing tools and Glagolitic characters from an ancient missal from St. Catherines Monastery and made by a calligrapher.

# Kurzfassung

Die vorliegende Diplomarbeit befasst sich mit dem Erkennen von Zeichen- und Schreibwerkzeugen. Diese Erkennung ist eine unterstützende Anwendung für Kunsthistoriker und Palaeographen. Die Erkennung erfolgt mit Hilfe der Strichenden. Ein Strichende kann verschiedene Formen annehmen, die sich zwischen den einzelnen Werkzeugen unterscheiden.

Ein Strich ist ein grundlegendes Element in Zeichnung und Schrift. Er kann einzeln oder auch in Formationen, z.B. Buchstaben oder Schraffuren vorkommen. Ein einzelner Strich besitzt zwei Enden, die man analysieren kann, er wird daher auch "offen" genannt. Ist ein Strichende überdeckt oder wird ein Strich in einer Formation von einem anderen überlagert, spricht man von einem "halboffenen" Strich. In diesem Zusammenhang ist auch die Definition "statischer" Strich zu erwähnen. Ein "statischer" Strich ist ein Strich, der von einem offenen Ende zu einem Knoten führt, zwei offene Enden direkt verbindet oder von zwei Knoten begrenzt wird, wobei ein Knoten ein Zusammentreffen von mindestens drei statischen Strichen ist. Informationen aus Strichenden können daher aus offenen oder halboffenen statischen Strichen entnommen werden.

Als vorbereitende Maßnahme werden die Striche segmentiert, d.h. vom Hintergrund getrennt. Aus dem resultierenden Binärbild werden die einzelnen Striche, bzw. Strichformationen ausgeschnitten und ein Skelett berechnet. Dieses Skelett dient dazu, falls nötig, eine Strichformation in statische Striche aufzuteilen und die Endpunkte der Striche festzulegen. Von den Endpunkten ausgehend, wird nun das Ende vom restlichen Strich getrennt. Dabei macht man seine zunehmende Breite in Richtung Strichkörper zu Nutze, die das Ende vom restlichen Strich unterscheidet.

Der Umfang des Strichendes dient nun zur Berechnung bestimmter Eigenschaften, die unter anderem auf der Krümmung, auf Proportionen und statistischen Momenten basieren. Diese Eigenschaften dienen zur Klassifizierung mit einer Support-Vector-Machine.

Die Testdaten setzen sich aus synthetischen Daten, eingescannten Strichen (einzeln und Schraffuren), die mit verschiedenen Zeichenwerkzeugen auf Papier gemacht wurden. Zusätzlich wurden noch Schriftbeispiele glagolitischer Schrift, einerseits aus fotografierten Originaldokumenten aus dem Katherinenkloster am Berg Sinai, andererseits aus Datenmaterial, das von einem Kalligraphen angefertigt wurde, untersucht.

# Contents

<b>1</b>	<b>Introduction</b>	<b>1</b>
1-1	Drawings . . . . .	2
1-1.1	Historical Overview . . . . .	2
1-1.2	Function and Types of Drawings . . . . .	3
1-1.3	Elements of a Drawing . . . . .	3
1-2	Glagolitic Writing . . . . .	5
1-3	State of the Art - Related Work . . . . .	6
1-4	Main Contribution . . . . .	9
1-5	Structure of the Thesis . . . . .	10
1-6	Definitions . . . . .	10
1-7	Summary . . . . .	10
<b>2</b>	<b>Drawing Tools</b>	<b>11</b>
2-1	Drawing Tools . . . . .	12
2-1.1	Graphite . . . . .	12
2-1.2	Silver Point . . . . .	12
2-1.3	Charcoal . . . . .	13
2-1.4	Black Chalk . . . . .	14
2-1.5	Reed Pen . . . . .	14
2-1.6	Goose Quill . . . . .	15
2-1.7	Metal Pen . . . . .	15
2-1.8	Brush . . . . .	16
2-1.9	Classifications . . . . .	16
2-2	Writing Tools . . . . .	18
2-3	Summary . . . . .	20
<b>3</b>	<b>Ending Extraction</b>	<b>21</b>
3-1	Stroke Segmentation . . . . .	21
3-1.1	Thresholding and Contour Refinement with Snakes . . . . .	21
3-1.2	Evaluation . . . . .	23
3-1.3	Conclusion . . . . .	29
3-2	Skeletonization . . . . .	30
3-2.1	Skeletonization and Skeleton Beautification . . . . .	31
3-2.2	Evaluation . . . . .	36
3-2.3	Conclusion . . . . .	39
3-3	Static Stroke Partitioning . . . . .	40
3-3.1	Evaluation . . . . .	41

3-3.2	Conclusion . . . . .	43
3-4	Cutting-Off Endings . . . . .	44
3-4.1	Evaluation . . . . .	44
3-4.2	Conclusion . . . . .	47
3-5	Summary . . . . .	48
<b>4</b>	<b>Features and Classification</b>	<b>49</b>
4-1	Related Work . . . . .	49
4-2	Features . . . . .	50
4-2.1	Landmark Setting . . . . .	50
4-2.2	Statistical Features . . . . .	52
4-2.3	Curvature Based Features . . . . .	54
4-2.4	Structural Features . . . . .	55
4-3	Classification . . . . .	56
4-3.1	Support Vector Machines . . . . .	57
4-3.2	Evaluation . . . . .	58
4-3.3	Conclusion . . . . .	60
4-4	Summary . . . . .	60
<b>5</b>	<b>Evaluation and Results</b>	<b>61</b>
5-1	Drawn Strokes . . . . .	61
5-1.1	All Drawing Tools . . . . .	61
5-1.2	Dry Drawing Tools . . . . .	62
5-1.3	Transferential Drawing Tools . . . . .	63
5-1.4	Dry and Transferential Drawing Tools . . . . .	64
5-2	Glagolitic Characters . . . . .	65
5-3	Conclusion . . . . .	66
<b>6</b>	<b>Conclusion and Outlook</b>	<b>68</b>
	<b>Appendix</b>	<b>70</b>
	<b>Bibliography</b>	<b>74</b>

# Chapter 1

## Introduction

Strokes are a fundamental part of drawings [Kos77]. This means that every drawing consists of an assemblage of strokes which can be arranged in different ways. They can form hatches, shapes or curves. Handwritten characters are also built up with strokes. The analysis of strokes is therefore an interdisciplinary field which unites different fields of research: Art History, Paleography and Computer Science, especially the field of Image Processing and Pattern Recognition. This thesis confirms the following hypothesis:

*Stroke endings carry information about drawing tools to allow an automated drawing tool recognition.*

Nine different drawing tools have been examined in this thesis. These tools have been selected because they were the tools most used in making drawings since antiquity [Kos77]. Drawings were preparatory steps of paintings since the early Renaissance: sketches, to record an idea, to compose a drawing, to try out a different combination of elements and to study poses, proportions and arrangements [Kos77]. Drafts, which are nearer to the final painting than sketches, show shadows, lights and backgrounds. The final draft is the drawing which needs to be transferred to another medium, e.g. a painting or a sculpture [Kos77]. A special kind of drafts is the underdrawing, which was common during the Middle Ages and Early Renaissance [Kos77]. The artist drew the design directly onto the primed panel or canvas. These underdrawings are then covered by the painting layers [Bom02]. Therefore, drawings carry information about the synthesis of a painting, and since they are drawn by the master himself, speaking of medieval, renaissance and baroque workshops, they show the artistic development of the master in a way that changes in the style can be tracked and used for dating purposes or to ensure or discard an attribution. Autonomous drawings came up in the renaissance area [Kos77]. Even if they are not preliminary stages of a painting, their expressivity allows the same insights into an artist's work as drafts and sketches [Kos77].

Some of the tools were also used also for writing (brush, reed pen, quill and metal nib). In this thesis, in addition to drawings, the glagolitic script is examined. It is a predecessor of the kyrillic script and has special characteristics that are not present in any other kind of writing (see Section 1-2).

## 1-1 Drawings

The style of a drawing is more spontaneous and expressive than the final painting [Kos77]. It tells more about the artistic development of an artist and the creation process of a piece of art. The analysis of drafts reveals connections between painters and painting schools because drafts were used for interchanging ideas between workshops [Kos77]. An analysis of drawings and the style includes the degree of “sketchiness”, i.e. how spontaneous a drawing is, the level of detail, i.e. if a drawing is elaborated or if it gives only a general idea about a composition. The style of a drawing in general, sketchiness and level of detail depend on the drawing tool used [Kos77]. Therefore an analysis of style can be attempted only if the drawing tool is known. To make drawing analysis fully automated, also the first step, drawing tool recognition, needs to be automated and unsupervised. Such a system, which supports art historians and restorers in discovering which drawing tool(s) was/were used in a painting, is presented in this thesis. It provides a non-destructive analysis method and can therefore be applied on a photograph (if the preservation state allows it, also on a scan) of the drawing. It can also be applied if the original drawing is lost and only photographic documents are available.

### 1-1.1 Historical Overview

At first, a drawing was not an autonomous class in the fine arts. In the Middle Ages drawings were made on panels or wax tablets, while in the 13th century these drawing grounds were replaced by parchment that was again replaced by paper around 1300; the tools used were brush and pen [Kos77]. At that time drawings were bound in pattern-books that moved around with the help of wandering artists [Kos77]. This helped to assign a value to drawings, but generally, drawings were not preserved until the 15th century [Kos77]. In the 15th century the silver point became popular [Lad68]. Silver as a drawing tool was known already to the Romans and widely used during the late Middle Ages and Early Renaissance, finally going out of fashion during the 16th century. It was the first drawing tool which was used to make an autonomous drawing e.g. a drawing which is not a means to an end, but stands for itself [Kos77]. For pen drawings bistre was used as drawing media during the late Middle Ages and Early Renaissance [Lad68]. Bistre consists of oven-soot or lampblack dissolved in water. It produces a brown stroke. Later on, black Indian Ink was used, which was made of candle- or lampblack mixed with water and arabic gum. The paper could be grounded with color powder, white lead or chalk, fixed with glue or gum [Lad68].

Thin quill and silver point pens were the main drawing tools in the 15th century. The drawings have a transparent look, the objects fragile. Young Albrecht Dürer started drawing in an animated and plastic style around 1490. New themes were discovered: landscapes, portraits and nudes. Black and red chalk became more prominent as drawing materials and different drawing materials (e.g. pen and brush, so called “washed drawings”) were combined. Charcoal was also introduced and accepted as drawing material [Lad68] in that era. Washed drawings were still popular in the baroque era, but also the pure brush drawing was becoming popular [Lad68]. Movement, dramatic scenes, light and shadow became more frequent in drawings. These “chiaroscuro” drawings are a main outcome of baroque drawing art [Lad68]. In the 18th century black chalk was used to make drawings with a high materiality and elegance and drawings in general were highly

appreciated and fashionable [Lad68]. Sepia ink (extracted from cuttle fish) was used for brush drawings [Lad68]. At the end of the 18th century the drawing style changed: shapes and figures were more calm, static and precise than before [Lad68]. Graphite became popular, because it allows to draw thin and precise lines, like a pen [Lad68]. Besides this new, harmonic and precise style, a dramatic style which introduced new topics - scenes from everyday life - existed [Lad68]. This style preferred black chalk, broad pens and brush and Indian Ink.

Since the end of the 19th century all of the drawing tools mentioned above were used contemporarily and equally [Lad68]. Van Gogh drew with a broad reed pen, Seurat with black chalk and charcoal. European artists got a new inspiration: East-Asian Brush-and-Ink drawings became known in Europe. Brush with Indian Ink was used by the “*Nabis*”, a group of Symbolists and the expressionistic artists belonging to “*Die Brücke*”. The drawing tools became a matter of expression and not of fashion in the 20th century: the artist uses the drawing tool according to the effect he wants to produce and the sentiment he wants to transfer [Lad68].

## 1-1.2 Function and Types of Drawings

A drawing can have different functions, it can be for example a sketch, to record an idea. To compose a drawing, an artist needs sketches to try out different combination of elements and to study poses, proportions and arrangements. The draft is the next step towards a final painting, showing more refined details, shadows, lights and backgrounds. The final draft is the drawing which needs to be transferred to another medium, e.g. a painting or a sculpture [Kos77]. A special kind of a final draft, especially used in the Renaissance, is the cartoon. It is a drawing in the size of a final painting or fresco and is transferred by copying techniques, such as spolvero or stylus incision, on the final drawing ground [Bam99]. Another special kind of drafts is the underdrawing, which was common during the Middle Ages and Early Renaissance. The artist drew the design directly onto the primed panel or canvas. These underdrawings are then covered by the painting layers and can be made visible through infrared reflectography [Bom02, Mai03].

Figure 1.1 shows a painting by a follower of Hugo van der Goes or himself, where the chalk underdrawing has been revealed by scratching away the painting layers [Bom02].

These types of drawings are useful for art historians to get insight into the work of an artist and his workshop. The synthesis of a painting or a fresco can be reconstructed if sketches and drafts are preserved, or different artists and drawing schools can be related to each other, exchange of knowledge and drawing styles be documented.

Another type of drawing is the study. It is used to reflect the reality or a model. Main topics in studies are nature, landscapes, portraits or sculptures. It has also an educational purpose in academies to teach nascent artists to draw. A drawing can also be a copy of an existing artwork. This was done in workshops to document the workshops output or to make publicity. Copies were also an exercise for artists [Kos77].

A drawing can also have no other purpose than being a drawing, then called an autonomous drawing.

## 1-1.3 Elements of a Drawing

A drawing consists of several elements [Kos77]:



Figure 1.1: An underdrawing made visible by brute force: Attributed to Hugo van der Goes, The Virgin Majesty with Four Saints. Private Collection [Bom02].

- Points
- Spots
- Lines
- Areas, shadows

Since the notion of stroke corresponds to the graphical element “line”, different types of lines are explained.

A line is the basis of a drawing [Kos77]. A line can be a contour line that abstracts an object in a way the viewer can still recognize it. A contour can consist of a single line or of line fragments. It can be filled with interior structure to emphasize the representation. Single lines, line structures and hatches or smooth shadows can fulfill this task. From the technical point of view it can be a member of the following classes [Kos77]:

**Straight Lines:** A straight line is defined by the shortest connection between two points. The straight line is considered technical and incapable of carrying artistic expression. Its main use is in perspective, architectural drawings but in the 20th century also in the art of the Constructivism.

**Angled Lines:** An angled line is the conjunction of two straight lines at a certain angle.

**Curved Lines:** Curved lines can be divided into geometrical curves and freeforms. The freeform curved line was preferred by artists, because it left scope for individual design [Kos77].

For the artistic viewpoint of the formation process lines can be divided as follows [Kos77]:

**Mechanical Lines:** A mechanical line is drawn with precision and discipline and does not allow the artist’s personality to emerge. It can be drawn with auxiliary means, e.g. rulers.

**Spontaneous Lines:** This type of line originates in spontaneous improvisation and artistic expression.

**Virtuous Lines:** These lines combine artistic expression and discipline. Virtuous lines are known from east-asian brush drawings, but appear also in other cultural environments [Kos77].

Most drawings consist of freeform curved lines which are drawn spontaneously [Kos77]. These lines are useful for an analysis, because they carry artistic expression.

## 1-2 Glagolitic Writing

Not only drawings, but also handwritten characters consist of strokes. Therefore, in addition to drawings, we analyze the glagolitic script or “Glagolica”. As a byproduct, in addition to ending analysis, we also analyze paleographic features derived from a static stroke partitioning of the characters. The glagolitic script was invented in 863 AD by the Slav apostle Constantin-Cyrill during the Moravian mission [Mik03]. This script was newly created for the Slavonic language and was invented as a book script for sacral purposes [Mik03]. The Glagolica was replaced by the Cyrillic script in the eastern Balkan regions from the 10th century; it survived in Croatia in an angular form until the 20th century [Mik03].

There was no taking over of other alphabets letter forms. No contemporary alphabet was suitable to write down the Slavonic language, because none covered all the Slavonic sounds. The order of the letters of the glagolitic alphabet is based upon the Greek alphabet. The Glagolica has no cursive or lower case letters. A characteristic feature of the glagolitic script is loops. The glagolitic alphabet consists in its canonical form of 36 letters, of which 25 have these loops [Tka00]. The whole glagolitic alphabet can be seen in the Appendix.

In 1975 new Glagolitic codices were discovered in the St. Catherine Monastery on Mount Sinai [Mik08]. These codices allow new discoveries in the research about glagolitic writings [Mik04]. The St. Catherine Monastery has one of the largest collections of early manuscripts since the 4th century which contains also some codices written in Old Church Slavonic in the glagolitic script [Mik08]. A documentation and analysis of these scripts consists according to [Mik08] of:

1. Documentation of undocumented or insufficiently documented objects
2. Codiological and paleographic description
3. Examination of contents
4. Alignment with Greek/Latin sources
5. Edition
6. Composition of a comparative history of the collection

Some of the codices are in a bad state of preservation, therefore different image acquisition and image processing methods have been or are to be applied. This is the task of a project supported by the Austrian Science Foundation (FWF) under grant P19608-G12. Multispectral analysis should help to make erased scripture readable again. Stroke and stroke ending analysis are performed on grayscale and binarized RGB images or on registered and binarized multispectral images. This kind of analysis leads to a paleographic description of glagolitic letters according to discussion with Miklas and Gau, two slavists supporting the project. In this thesis, images from the Missale Sinaiticum are used as test data.

Miklas presents a division between static and dynamic strokes for paleographic analysis:

**Static Strokes:** A static stroke is the connection between an endpoint or a knot or between knots.

**Dynamic Strokes:** A dynamic stroke corresponds to the original pen trajectory.

**Knot:** A knot is a joint of at least three strokes.

In this thesis the static definition of strokes is used. Miklas defined also features for characters based on both stroke definitions. The full list of features for static strokes is listed in the Appendix. The method presented in this thesis includes the calculation of some of these features, namely the following:

1. Multistroke: Number of static strokes/character
2. Multiknot: Number of knots/character
3. Straight: Number of straight static strokes/character
4. Round: Number of round static strokes/character
5. Vertical: Number of vertical static strokes/character
6. Horizontal: Number of horizontal static strokes/character
7. Closed Elements: Number of closed elements (number of holes) per character

Other tasks divided amongst project group members consist of extracting the lineament, skew detection, character analysis and image enhancement with the help of multispectral imaging. For the latter each page of the codex was acquired nine times. Seven images with different cut-off filters were taken in addition to a UV-fluorescence and an RGB image. The filtered images were acquired by a Hammamatsu C9300-124 grayscale camera with a spectral response between 330 and 1000 nm. It has a resolution of  $4000 \times 2672$  pixels. The RGB and the UV-fluorescence picture were taken with a Nikon D2Xs. The image acquisition system is shown in Figure 1.2 [DLS07].

## 1-3 State of the Art - Related Work

Image processing is a technology which gained importance in the fields of art history and restoration. An overview of the beginnings and achievements of this interdisciplinary field of work can be found in [MCSP02], [MSL01] and [BPP05]. Regarding painting analysis Berezhnoy et al. [BPvdH05b] show the application of image processing methods on Van Gogh paintings. They analyze the occurrences of opponent colors to determine the evolution of color use in Van Gogh's paintings. They propose also a brush stroke based method to examine the way Van Gogh applied brushstrokes on the canvas (see also [BPvdH05a] and [BPvdH07]). This method consists in enhancing brushstroke structures with a circular filter and filling closed contours (which should correspond to a single brush stroke). These brush strokes are skeletonized and fitted to a polynomials. The coefficients of these polynomials are used to describe the texture of a painting.

Sablatnig et al. [SKZ98] use color, shape and stroke classification to relate portrait miniatures to artists. They use mean RGB-values to make a rough classification and refine it by segmenting the portrait into elliptic regions of interest and comparing their

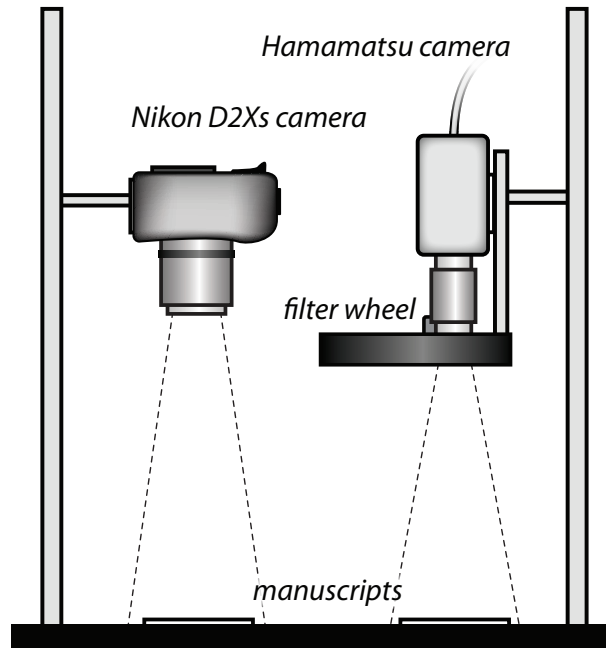


Figure 1.2: The image acquisition system (*courtesy M. Diem [DLS07]*).

size. Afterward brushstrokes are extracted from these regions. Their structure allows a final classification of the miniature. Stork et al. [Sto06, SJ06, SD07] focus on optical properties of paintings. They show results of a perspective analysis and illuminant projection direction estimation. Moreover they show how shape descriptors can be applied on modern and medieval paintings.

Image processing as an aid in painting restorations can be found in Nikolaidis and Pitas [NP01]. They propose a method for digital crack resaturation, color restoration, mosaicking of paintings on curved surfaces and an image database management tool. Crack restoration has also been proposed by Hanbury et al. [HKZ03]. They use morphological operations to remove cracks from painting while preserving the original brushstrokes.

Drago and Chiba [DC04] present an algorithm to simulate canvas aging, while Romero and Candela [RC06] worked out a mathematical model for restoration of baroque paintings. They want to simulate the cleaning process and consider that dust and dirt are distributed uniformly on a painting. They pose the cleaning as a deconvolution problem with a Gaussian kernel.

An approach to distinguish artistic painting styles is discussed in Li and Wang [LW04]. They extract stroke styles using a mixture of 2-D Hidden Markov Models to classify ancient Chinese brush paintings. Widjaja et al. present a painter identification approach based on color profiles of skin patches [WLW03]. Lyu et al. use wavelet statistics to attribute paintings to an artist [LRF04], while Deac et al. [DvdLB06] use a decision tree to classify paintings and relate them to an artist. Guan et al. [GPW05] classify traditional Chinese paintings into subject classes with the help of statistical features. A new colorspace designed especially for oil painting indexing and retrieving is introduced by [YJ05] based on human perception and pigment color mixing. An analysis of photographic accuracy of paintings is done by [Fal07].

Drawing tool classification has been proposed by [KLZS07]. They use two approaches,

one is based on stroke contour analysis and the other on stroke texture analysis. The contour analysis consists in comparing the fit of a rigid and non-rigid snake. This serves as a measure of roughness of the boundary. The texture features are derived from a Discrete Wavelet Transformation. They classify brush, black chalk and graphite strokes on different grounds and different cover layers in infrared reflectograms. Kröner et al. [KL98] propose a drawing authentication method for free hand drawings using global features, i.e. black and white ratios of subimages. Drawing stroke segmentation techniques based on snakes have been proposed by [VK06] and [KLSZ03]. [VK06] use a combination of ribbon and ziplock snakes to segment straight and bent single and crossed strokes, while [KLSZ03] utilizes an edge based approach and classical snakes [KWT88] for boundary refinement.

Related to drawing and painting analysis is document image analysis (DIA) [Let05]. An overview of DIA techniques developed can be found in [Nag00]. According to [Nag00], document image analysis is *“the subfield of digital image processing that aims at converting document images in symbolic form for modification, storage, retrieval, reuse and transmission”*. [Nag00] divides document image analysis into different levels:

**Pixels:** In this level, preprocessing techniques apply: representation, noise reduction, binarization, skew detection, zoning, character segmentation, thinning, vectorization, script, language and font recognition.

**Primitives:** Here, different primitive structures (glyphs) are extracted from the document: connected components, strokes, characters, punctuation and words.

**Structures:** This level deals with text recognition tasks: word segmentation, text line reconstruction, table analysis, morphological context, lexical context, syntax and semantics.

**Documents:** Page layouts and document interpretations are analyzed here: text vs. non-text, physical component analysis, logical component analysis, functional components (content tags) and compression.

**Corpus:** The final level is about information retrieval: document classification and indexing, search, security, authentication and privacy issues are concerned.

This thesis covers the pixel and primitives level according to these definitions.

Handwriting recognition of different scripts is a part of DIA which covers virtually all levels [Nag00]. Overviews of on-line and off-line handwriting recognition for Latin scripts can be found in Plamondon et al. [PS00] and more recently in [Bun03]. A survey of arabic handwriting recognition has been published by Lorigo and Govindaraju [LG06] while Liu et al. report the state-of-the-art in online chinese character recognition in [LJN04]. Signature verification for forensic applications has been attempted by Franke and Köppen [FK01]. An overview of camera-based DIA can be found in [DLL03].

The analysis of historical documents has gained importance in this field of research. Moalla et al. [MBEA06] introduce a paleographical analysis in DIA. They try to distinguish Latin writings from Caroline Letters to the Gothic Rotunda Textualis with the help of co-occurrence between letters to extract features for a writing style. A similar goal for Hebrew handwriting has been pursued by Yosef et al. [YKD<sup>+</sup>04]. They recognize two hebrew characters based on difference regions from the binary character and its convex

hull. Manmatha and Rothfeder [MR05] propose an approach to segment words of historical documents. They apply their scale space approach on letters of George Washington to provide a preprocessing for retrieval and recognition tools.

A special kind of artifact, so called bleed-through distortion concerns the method presented by Tonazzini et al. [TSB07]. These artifacts originate in seeping ink from the reverse paper side. They decompose the signal into two blind sources where the overlapping text and the paper texture has to be recovered. Eglin et al. [EBR07] presents a method based on discrete Hermite-Filters to remove noise in document images. They use the knowledge that noise has lower frequencies than writing. Further, they use Gabor-Filters to measure the complexity of the handwriting in order to classify the hands. Kokla [KPK06] presents in his paper a method to recognize historical inks by building a statistical model upon inks in infrared images.

Several researchers deal with the analysis and restoration of characters. Character analysis on carved stones to identify hands has been proposed by Tracy et al. [TPR<sup>+</sup>07]. They extract the contour of a carved letter and determine the turning points in each letter. From this, the letter's shape is reconstructed and different features are extracted (ratios and angles). Allier et al. [ABE06] present a method to reconstruct broken characters in documents. Their input is a set of segmented document images. They use active contours to model the missing parts of a character and introduce a priori knowledge to calculate the external force, recognizing the broken characters beforehand with the help of features gained from a Gabor filter bank. Work has also been published on Asian writings, e.g. Chiu and Tseng provide stroke based features for classification of chinese characters. They use a run-length-based stroke segmentation, while Lee and Wu [LW98] present a stroke extraction algorithm based on contour information.

Multispectral imaging has been applied on a ancient manuscript to make palimpsests visible in [EJKCB03]. They examined a medieval prayer-book which has been written on an erased manuscript from the 10th century containing the seven treaties of Archimedes and try to visualize the erased writing so that scholars are able to read the text. They use different illuminations to extract the different spectral responses of ink, erased ink and parchment. Rapantzikos and Balas [RB05] present a multispectral imaging system which images a palimpsested document with 34 bands. They utilize PCA-Analysis to determine the bands which contain most information.

## 1-4 Main Contribution

The analysis of stroke endings has never been attempted before. This thesis presents a drawing and writing tool recognition algorithm based on shape features of stroke endings. After a preprocessing phase, where the stroke endings are extracted from an image, landmarks are set on the resulting curve of a stroke ending. These landmarks are used to calculate features, based on the ending's shape and curvature. These features serve as distinguishing criteria to recognize drawing tools.

Drawing tool recognition has been attempted by Lettner [LS05, Let05] and Kammerer [KLSZ03, KLZS07]. They use stroke texture and boundary-based features to classify strokes into different drawing tools. Both approaches have difficulties in dealing with transferential drawing tools, because, in contrast to dry drawing tools, strokes made with them exhibit similar boundary and texture characteristics. This thesis finds a way to overcome this problem by introducing features based on the shape of stroke endings.

## 1-5 Structure of the Thesis

Following this introductory chapter different drawing tools are presented in Chapter 2. Their characteristics are outlined, as well as their historical development. Image examples are shown in order to visualize the different appearance of each tool. Chapter 3 shows the steps which are used to extract stroke endings from an image. These steps consist of the segmentation of strokes and stroke formations, the skeletonization of the segmented strokes, the partitioning of stroke formations into static strokes and the cutting-off of the endings. Afterwards, Chapter 4 presents the shape features which are used to characterize the shape of an ending and the classifier used to divide the stroke endings into classes. Chapter 5 shows the result of the classification algorithm applied on different test data. The thesis closes with Chapter 6 where conclusions are drawn.

## 1-6 Definitions

In this thesis, terms are used as follows:

**Drawing Tool:** A drawing tool is a tool which can be used to draw or write, no matter if it is transferring another medium or if it is a medium itself brought into a suitable shape.

**Drawing Media:** A pigmented or colored matter which leaves traces when drawn over a ground. These traces can be produced by the rubbing of color particles which stick to the drawing ground or fluid drawing media which transports pigments to the ground and binds them to the ground during the drying process.

**Drawing or Writing Ground:** The matter on which a drawing was produced or a text written. The most popular grounds are paper and parchment.

**Stroke:** The result of drawing a drawing or writing tool over a drawing or writing ground.

**Stroke Formation:** A stroke formation is the connected combination of strokes with different angles, curvatures and lengths. Characters are also considered as stroke formations.

**Static Strokes:** A static stroke is the connection between an endpoint or a knot or between knots.

**Dynamic Strokes:** A dynamic stroke corresponds to the original pen trajectory.

**Knot:** A knot is a joint of at least three strokes.

## 1-7 Summary

This chapter gave an introduction on the topic and introduced background knowledge on drawings and glagolitic writings, i.e. the data material used in this thesis. Afterwards an overview of the state of the art and related work in computer aided analysis of art and documents was given. Then the structure of the thesis was presented and finally definitions of relevant terms were given.

## Chapter 2

# Drawing Tools

This chapter introduces the characteristics of different drawing tools. A total of nine tools is described. It shows the differences in use and appearance and gives a brief historical overview. Image examples are given to allow for a visual comparison of the tools. Figure 2.1 shows a selection of writing and drawing tools, which have been examined in this thesis. Stroke examples for these tools can be observed in Figure 2.2.



Figure 2.1: Drawing and writing tools. From left to right: Brush (pointed), Quill, Reed Pen (bamboo), Metal Nib Pen (broad), Reed pen (Juniper), Graphite, Charcoal, Black Chalk.

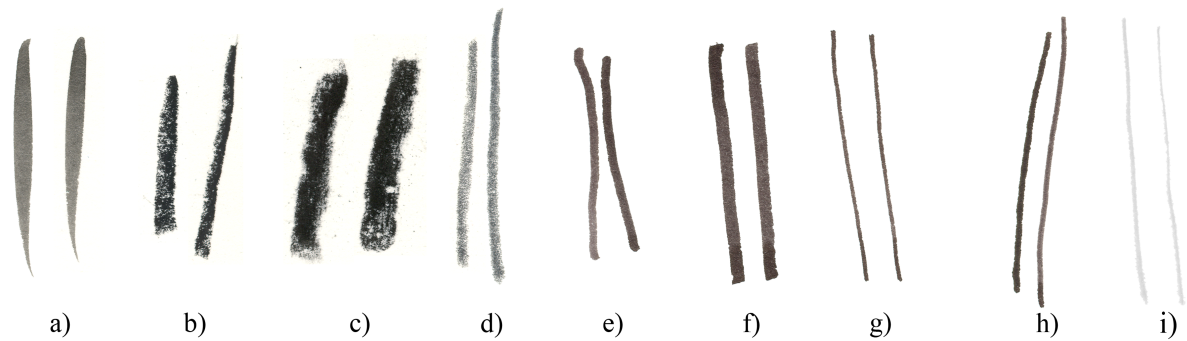


Figure 2.2: Sample strokes. a) Brush, b) Black Chalk, c) Charcoal, d) Graphite, e) Juniper, f) Metal Nib Pen, g) Goose Quill, h) Reed Pen, i) Silver Point Pen.

## 2-1 Drawing Tools

This section gives a brief overview about different drawing tools. In this work, nine drawing tools have been examined.

### 2-1.1 Graphite

The word “*graphite*” derives from the greek word “*graphein*” which means to write or to draw. Graphite is a mineral and consists of carbon. A stroke drawn with graphite in its natural form has a black and greasy effect. It smears in the unevenness of the paper [Kos77].

Graphite has been known since ancient times [Kos77]. It has not only been used in drawing, but also to line medieval manuscripts [Kos77]. The first known traces in drawings derive from the 15th century in underdrawings by Jan van Eyck [Kos77]. Until the 18th century graphite was not much used in art, because graphite strokes were too easy to smudge and scratchy due to the low quality of the material [Kos77]. Only high quality graphite which was then imported from England satisfied the needs of artists and writers [Kos77]. In 1795 a patent was released for a mixture of pulverized graphite and clay, invented by Jaques Louis Conté [Kos77]. This mixture, surrounded by a wooden mantle, is what we now call a pencil. Since this invention graphite was a booming drawing tool [Kos77]. Figure 2.3 shows a drawing with pencil <sup>1</sup>.

### 2-1.2 Silver Point

The height of silver point drawings was in the second half of the 15th century [Kos77]. An example of a silver point drawing is shown in Figure 2.4 <sup>2</sup>. The silver drawing technique was rediscovered for portrait miniatures in the 18th century and was afterwards constantly used [Kos77]. Silver produces a clean, fine, light gray stroke and is economic in consumption [Kos77]. The high price of silver, which was comparable to that of gold, led to the fact that only the point of a pencil was made of silver. A silver pencil needs a compact paper surface, but rough enough to rub off the metal particles [Kos77]. Silver

<sup>1</sup>Source: [www.zeno.org](http://www.zeno.org)

<sup>2</sup>Source: [www.wga.hu](http://www.wga.hu)



Figure 2.3: A graphite drawing. Amadeo Modigliani (1884-1920), Portrait of Lunia Czechowska (1919), 41 x 24 cm, Private Collection.

point drawings darken with time as a result of the formation of brown silver sulfide and can turn out black due to this oxidation process [Bom02].

### 2-1.3 Charcoal

Charcoal is basically a carbonized stick of wood. It was cheap because it was always available where a fire was. The best wood to produce charcoal are vine or willow twigs. An advantage of charcoal is that it can be corrected, e.g. with bread. Twigs are bundled and carbonized in a hermetically sealed pot and slowly cooled down afterward [Fug05]. Since its particles do not stick on paper, they have somehow to be fixed. Therefore it was not commonly used for artwork since the end of the 15th century [Kos77]. Before, it was only used for sketches or underdrawings. Then a fixation method based on glue was invented and charcoal was used for autonomous drawings. It is a versatile drawing tool: it can be



Figure 2.4: A silver point drawing. Jan van Eyck (1390-1441), Portrait of Cardinal Niccolo Albergati (1432), 21.4 x 18 cm, Kupferstichkabinett, Dresden.

used for linear drawings but also for smudged shadows. It produces black, saturated and velvety strokes and it is often confused with black chalk. The thickness of a stroke depends on the applied pressure and it allows quick modeling of shapes [Kos77, Bom02, Fug05]. Figure 2.5<sup>3</sup> shows an example of a charcoal drawing.

The charcoal sticks are fragile, therefore since the 19th century a charcoal stick consists of pulverized carbonized wood mixed with a binder and pressed in sticks [Kos77].

## 2-1.4 Black Chalk

Natural black chalk consists of clay-like shale containing carbon and was mined all over Europe [Kos77]. It was used by artists since around 1500. It produces a black, dull stroke and it is a hard material which had to be moistened before use. Since the 17th century it was replaced by an artificially produced black chalk [Kos77]. It consists of lampblack mixed with a binder. Therefore it can be produced in different hardness degrees. The black particles of artificially produced black chalk stick better to the paper than the particles of natural black chalk [Kos77]. A black chalk drawing from the Rococo era is shown in Figure 2.6<sup>4</sup>.

## 2-1.5 Reed Pen

A reed pen is a cut piece of reed or bamboo used to draw or write with ink or bistre. The effect of a stroke depends on the thickness or the obliquity of the nib. It was already

---

<sup>3</sup>Source: [www.wga.hu](http://www.wga.hu)

<sup>4</sup>Source: [www.zeno.org](http://www.zeno.org)



Figure 2.5: A charcoal drawing. Albrecht Dürer (1471-1528), Portrait of the Artist's Mother (1514), 42.1 x 30.3 cm, Staatliche Museen, Berlin.

known to the Romans and rediscovered in the early Renaissance. While it was replaced by the quill as a writing tool, its characteristics (strong, angular strokes) inspired artists also in the following centuries [Kos77]. An example of a reed pen drawing is shown in Figure 2.7<sup>5</sup>. A reed pen can also be a juniper or an elder stick. This type of pen was also used through the Middle Ages [Kos77].

## 2-1.6 Goose Quill

The goose quill is known to be used in drawings since the 12th century [Kos77]. Its advantages compared to the reed pen are the fine drawing style and the litheness of the duct [Kos77]. A pen-stroke is characterized by square ends [Bom02]. Quills are mainly made of goose feathers, but also other birds produce quills suitable for drawing and writing: swan, crow and raven [Pig05]. Figure 2.8<sup>6</sup> shows a quill drawing.

## 2-1.7 Metal Pen

Metal pens are known since the 19th century. They are more durable than reed pens or goose quills and can be produced in different sizes, widths and shapes [Kos77].

<sup>5</sup>Source: [www3.vangoghmuseum.nl](http://www3.vangoghmuseum.nl)

<sup>6</sup>Source: [www.wga.hu](http://www.wga.hu)



Figure 2.6: A black chalk drawing. Antoine Watteau (1684-1721), *The Violinist* (around 1717-1718), 30 x 21.3 cm, National Gallery of Art, Washington (D.C.).

## 2-1.8 Brush

The brush is not only a drawing, but also a painting tool. It was used constantly over the last millennia. It is composed of bristles set into a handle. The bristles can be from squirrels, dogs, cattle etc. The brush is often combined with other drawing tools, e.g. goose quill. It can be broad or pointed and was used according to the desired level of detail [Kos77, Fug05]. A brush drawing with black ink and with heights on a dark ground is shown in Figure 2.9<sup>7</sup>.

## 2-1.9 Classifications

Two different ways to group drawing tools are presented in this section. One classification has been made by Koschatzky [Kos77]. He divides drawing tools into thinly drawing pencils, broadly drawing pencils and transferential means. These classifications are used to group drawing tools for the evaluation of the method and results differ between them (see Section 5).

**Thinly Drawing Pencils:** Drawing tools in this category produce fine strokes that are durable.

---

<sup>7</sup>Source: [www.wga.hu](http://www.wga.hu)



Figure 2.7: A reed pen drawing: Vincent van Gogh (1853-1890), 61 x 49 cm, Van Gogh Museum, Amsterdam.

- Graphite
- Silver Point

**Broadly Drawing Pencils:** This kind of drawing tool produces broad strokes.

- Charcoal
- Black Chalk

**Transfereential Means:** These drawing tool have no color pigments of their own, but are used as a transfereential matter for ink, bistre or Indian Ink.

- Reed Pen
- Goose Quill
- Brush
- Dip Pen

David Bomford uses a different classification [Bom02]. He divides the drawing tools into fluid and dry drawing media:

**Dry Drawing Media:** This category of drawing media consists of those that are dry in nature.

- Charcoal
- Black Chalk
- Graphite
- Silver Point

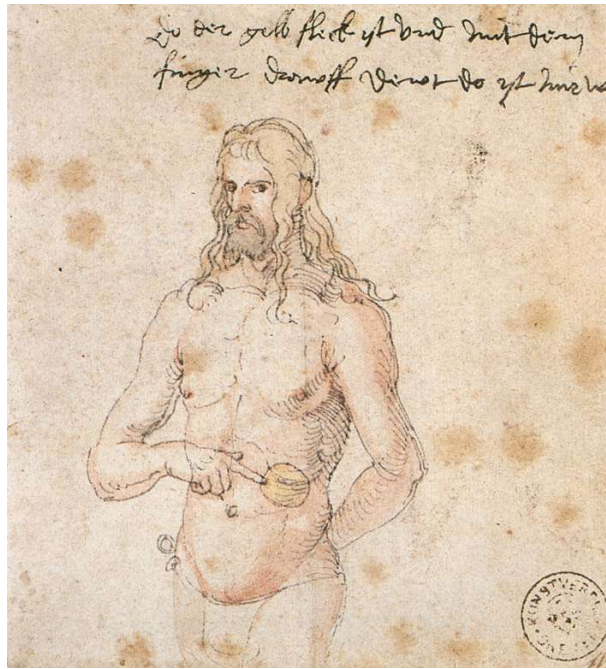


Figure 2.8: A pen drawing. Albrecht Dürer (1471-1528), Self-portrait (1521), 12.7 x 11.7 cm, Kunsthalle, Bremen.

**Fluid Drawing Media:** The characteristic of fluid drawing media is that color, in the form of a pigment mixed with a fluid binding or a dye, is applied on the drawing matter by an appropriate tool which can be:

- Reed Pen
- Goose Quill
- Brush

They are easy to use, both for design and for shading. The lines are continuous and can form a droplet at the end of a stroke, depending on the degree of fluidness of the drawing media.

Inspired by these classifications, in this thesis tools are divided into dry drawing tools (black chalk, charcoal, graphite, silver) and transferential drawing tools (brush, reed pen (reed, juniper), goose quill, metal nib pen).

## 2-2 Writing Tools

Some of the drawing tools were also used for writing. In the European area quill or reed and ink dominated since 1500 years, while in Asia brush and Indian Ink were used. Jewish and Islamic writers used writing tools similar to those used in Europe, but mainly reed [Kun92]. All alphabets written in these areas are based mainly on lines. The pens and quills were predominantly broad-nibbed, because pointed nibs are worn off more easily than broad nibs [Kun92]. The ending shape of broad pens depends on the angle between pen and drawing direction [Gum02]. Figure 2.10 shows examples of writings with different tools<sup>8</sup>.

<sup>8</sup>Source: a,b,d,f: commons.wikimedia.org

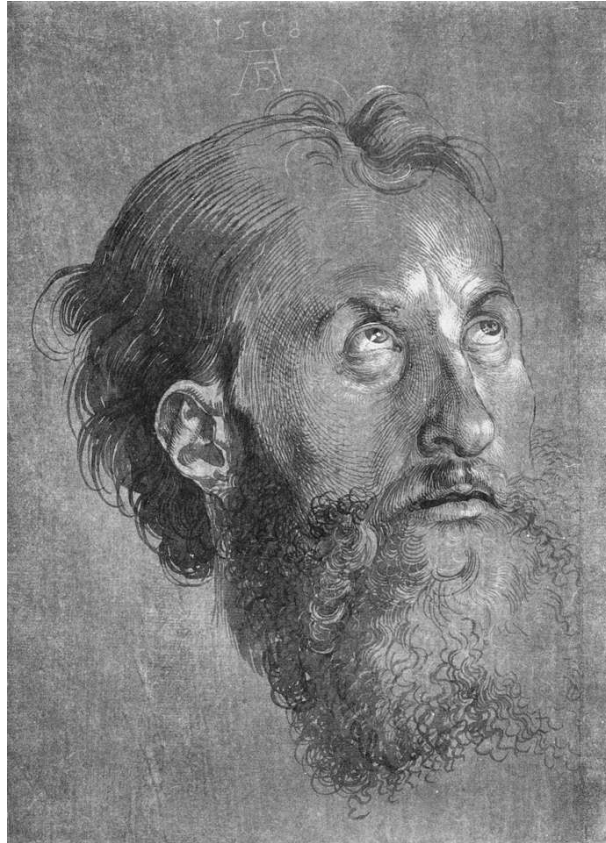


Figure 2.9: A brush drawing. Albrecht Dürer (1471-1528), Head of an Apostle Looking Upward (1508), 28.8 x 20.7 cm, Staatliche Museen, Berlin

The reed pen or “calamus” (lat.) is the oldest form of pen and was used since antiquity [Kun92]. It is the traditional writing tool in the Arabic world. It should be made of hard and stable wood, forming a tube, with a marrow core (e.g. juniper) or with many capillaries like, for example, rattan. Reed can also be used and modern pens made for calligraphers are bamboo sticks. Reed pens can be pulled and pushed [Kun92].

Goose quill pens were used in the European area since the year 500 AD. [Kun92]. They produce finer hairlines than other writing tools presented here and are elastic, which allows an expressive writing. Their disadvantage is that they wear off fast. Only the outer, large flight feathers are suitable to produce a quill [Kun92]. Goose, swan, turkey or raven feathers can be used. Quills were usually only pulled and not pushed, because of the resistance on the writing ground when doing otherwise [Kun92].

A dip-pen consists of a metal nib with capillary channels mounted on a wooden handle. The nib can assume different shapes: broad, pointed or round. The mass production of metal nibs started at the beginning of the 19th century [Kun92].

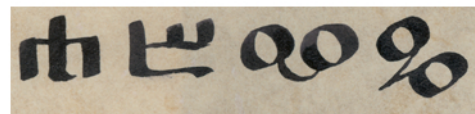
Brushes were and are used mainly in Asian writings. They can have broad or pointed tips [Kun92].



a)



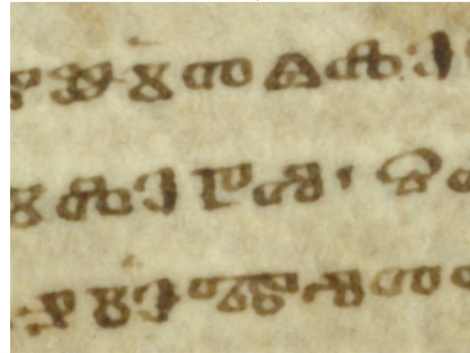
b)



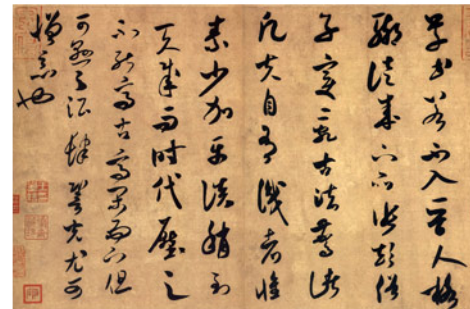
c)



d)



e)



f)

Figure 2.10: Examples of writing tools: a) Quill: first page of the Rijmkroniek by Melis Stoke, Manuscript A, 14th century (detail), b) Quill: Latin Bible of AD 1407, Malmesbury Abbey, Wiltshire, England, by Gerard Brils (detail), c) Metal Nib: Glagolitic characters, d) Reed Pen (calamus): Arabic Manuscript, Anatomy of the Eye, by al-Mutadibh, 1200 CE (detail), e) Reed Pen: Missale Sinaiticum 5n, page 11x (detail), f) Brush: Chinese Calligraphy by Mifu, Song Dynasty, Jingsan Province.

## 2-3 Summary

This chapter introduced background knowledge about drawing and writing tools used as test data in this work. Nine tools were presented with their characteristics and historical developments. Image examples of master drawings and handwritings support the descriptions. Some of the drawing tools can also be used as writing tools, they were described under this aspect, too. Further, two different classification schemes for drawing tools were introduced.

# Chapter 3

## Ending Extraction

The previous chapter gave an introduction to the historical, art-historical and paleographic environment of this thesis. This chapter gives information on the technical part of stroke ending analysis. The first four sections tell about the preprocessing steps which have been taken in order to calculate the features presented in Chapter 4. Section 3-1 shows the segmentation of the strokes, Section 3-2 the skeletonization of the segmented strokes and Section 3-3 the partitioning of segmented stroke formations into static strokes. The open and half-open static strokes are then further processed to cut off their endings as described in Section 3-4.

### 3-1 Stroke Segmentation

Before the endings can be analyzed, they have to be cut off the strokes and still before that, the strokes have to be segmented. This segmentation has to preserve shape of the stroke and its endings. It is achieved by combining a thresholding operation for a coarse segmentation and a snake to refine the contours.

#### 3-1.1 Thresholding and Contour Refinement with Snakes

To achieve a first segmentation, a thresholding algorithm is applied on a grayscale stroke image. This threshold divides the stroke image into strokes and background. Thresholding methods can be global or local. A global threshold is calculated over the whole image and applied equally on all pixels, while a local or adaptive threshold method calculates the threshold for a limited neighborhood. These methods work better than global methods [dTT95], but they are adapted to special applications (document analysis) and the results depend on the size of the neighborhood window [dTT95]. Therefore a global thresholding is preferred in this thesis. The thresholding algorithm proposed by Otsu [Ots79] was used for our test strokes. This global threshold selection method has the advantage of being unparameterized and unsupervised. It calculates the threshold by maximizing the variance between the two pixel classes for back and foreground. It works both with drawings and documents without adapting any parameters.

Trier and Taxt [dTT95] evaluate binarization algorithms for document images. They compare local adaptive algorithms with and without postprocessing and global methods. Otsu's method performed best for global thresholding methods and better than some of

the local adaptive methods (Mardia/Hainsworth, Taxt/Flynn/Jain, White/Rohrer IFA; see [dT95] for more details).

Other methods considered were a multistage adaptive binarization method developed by Gatos et al. [GPP04]. First the image is denoised with a Wiener filter. On the result, Niblack's method [Nib86] is applied to estimate background and foreground regions. The resulting background regions are interpolated into foreground areas. This interpolated background is combined with the original image. Kavallieratou presents a binarization algorithm specialized for documents [Kav05]. He uses the fact that only around 6% of the pixels of a document image belong to text and subtracts the average value of the image from it. The histogram of the resulting image is equalized. These steps are repeated until they retain the document without noise. Finally, all pixels, which do not have the value 1 (white) are turned into black (0). An algorithm that works both in grayscale and color domain and can handle degradation in historical documents is proposed by [GPH06]. They use a connected component labeling to find similar pixels. From these background blocks are extracted which are processed separately. They are binarized with a k-means approach. Wang et al. [WLLH05] present a binarization algorithm for color images. After a dimensionality reduction to facilitate further processing they reduce data size with a graph clustering algorithm working on the color histogram. For each cluster they extract binary texture features and construct several binary images. According to the texture features, the best of the binary images is selected. Sauvola and Pietikäinen [SP00] propose an adaptive algorithm for documents with textual and non-textual areas. These areas are found with the help of the average gray value of a neighborhood window and the transient difference. According to the decision made, different binarization algorithms are applied on textual or non-textual document areas. On non-textual areas, a soft-control algorithm is applied. The textual areas are binarized with a modified Niblack [Nib86] algorithm. The problem of the Niblack adaptive thresholding is that it does not work well when the background contains light texture, because gray values in the texture "easily exceed threshold values" [SP00] and therefore cause noise. Sauvola and Pietikäinen solve this by adding a parameter that amplifies the influence of the standard deviation. They compose the threshold only for every  $n$ -th pixel and interpolate bilinearly between these base pixels. Since all these methods include some parameters depending on the structure of the image to segment, Otsu's method is still preferred.

If a stroke image cannot be segmented by a thresholding operation, the segmentation algorithms proposed by Vill [VK06] or Kammerer [KLSZ03] can also be used. Both approaches use active contours (snakes) to extract the stroke. [VK06] propose an algorithm to segment straight, crossed and bent strokes. The semi-automated algorithm is based on ribbon and ziplock snakes. The algorithm requires two endpoints of a stroke as user-input. Then two ziplock snakes start at each endpoint of the stroke. These ziplock snakes stop when they have reached a region of stable stroke width. Then two ribbon snakes start to segment the middle part of the stroke. These ribbon snakes ensure that the segmentation of a crossed stroke is not influenced by the crossings. The approach of [KLSZ03] segments straight strokes. A segmentation based on parallel stroke boundaries is refined with the help of traditional snakes.

Thresholding the image results in a binary representation of the strokes. From this the contour pixels of the strokes are extracted and sorted to get a boundary representation of the strokes in an image. Since the contours are discretized, a snake [KWT88, XP97] is applied on them to achieve a smooth contour. Snakes have the advantage that grayscale

information can be introduced as a force to draw the snake toward the true contour. This means that the contour derived from the binarized image can be corrected with the snake and moved toward its true location.

Snakes were first introduced by Kass, Witkin and Terzopoulos in 1988 [KWT88]. They distinguish two different energy types, the internal energy ( $E_{int}$ ) and the external, or image energy ( $E_{ext}$ ). Internal energies consider smoothness, coarseness or stiffness of the resulting curve and depend on its intrinsic properties while external energies take the structure of the underlying image into account. A 2-dimensional snake  $v(s)$  is defined with coordinates  $x$  and  $y$  as

$$v(s) = (x(s, t), y(s, t)) \quad (3.1)$$

where  $s$  is proportional to the arc length of the curve and  $t$  the current time. The total energy of the snake is defined as

$$E_v = E_{int} + E_{ext}. \quad (3.2)$$

with

$$E_{int} = \frac{1}{2} \int_0^1 \left( \alpha(s) \left| \frac{\delta v(s, t)}{\delta(s)} \right|^2 + \beta(s) \left| \frac{\delta^2 v(s, t)}{\delta s^2} \right|^2 \right) ds \quad (3.3)$$

where  $\alpha(s)$  and  $\beta(s)$  are arbitrary functions that regulate the curves tension and rigidity. Based on Neuenschwander et al. [NFI<sup>+</sup>97], the functions are replaced by constants in this thesis.  $E_{ext}$  is defined as

$$E_{ext} = \int_0^1 P(v(s)) ds \quad (3.4)$$

where  $P$  is a function of the image, e.g. the magnitude of the image gradient and  $v$  stands for either  $x$  or  $y$ . A traditional snake requires a complex initialization. It consists of a polygon which lies near to the contour to adhere to. Therefore the approximate shape of the object to segment has to be known. The position of the snake is optimized iteratively until the energies are minimized.

Simple external energies, such as the gradient magnitude, have problems to draw the snake to contours, especially when the snake is initialized far from the contour to which it should adhere or when this contour has concave features. In 1997, Xu and Prince [XP97] presented an alternative, the Gradient Vector Flow Field. The method consists in the diffusion of gradient vectors obtained from an edge map of an image. The algorithm presented in this thesis uses the Gradient Vector Flow Field as external energy to draw the calculated contour toward the true contour.

### 3-1.2 Evaluation

The stroke segmentation has been evaluated with different kinds of data. A first evaluation has taken place with synthetic data. This shows the correct functioning of the proposed method and points out pathological cases. Then the method is evaluated on strokes drawn with the drawing tools presented in Section 2-1. These sheets are scanned with a flatbed scanner at a resolution of 600dpi. Additionally the method has been tested also on Glagolitic writings acquired with the system presented in Section 1-2. These are compared to Glagolitic writings made by a calligrapher, which are again scanned with a flatbed scanner at a resolution of 600dpi.

The evaluation of the stroke segmentation includes several measures. First of all, the number of strokes or stroke formations found in the ground truth (SGT) is compared to the number of stroke configurations found in the test image (STEST). The Rand Index (RI) is a measure which measures segmentation similarities. Unnikrishnan et al. [UPH07] evaluate different segmentation evaluation measures and show that the RI is closer to human perception than other measures. The RI is defined as

$$R(S, S') = \frac{1}{\binom{N}{2}} \sum_{\substack{i,j \\ i \neq j}} [I(l_i = l_j \wedge l'_i = l'_j) + I(l_i \neq l_j \wedge l'_i \neq l'_j)] \quad (3.5)$$

$S$  and  $S'$  are two label assignments with labels  $\{l_i\}$  and  $\{l'_i\}$  while  $N$  is the number of points and  $I$  is the identity function. The RI is therefore the ratio of the number of pairs of points having compatible label relationship in both assignments [UH05]. A value of 0 means no similarity between the segmentations and a value of 1 stands for maximal similarity. The Rand Index counts the fraction of pairs of pixels whose labellings are consistent between the computed segmentation and the ground truth. The RI is compared to the Global Consistency Error (GCE) proposed by Martin et al. [MFTM01]. It is defined by the weighted minimum of the sum of all Local Refinement Errors (LRE) for each pixel in the images in both directions. The LRE is defined in the following equation:

$$LRE(S, S', x_i) = \frac{|R(S, x_i) \setminus R(S', x_i)|}{|R(S, x_i)|} \quad (3.6)$$

$R(S, x_i)$ , respectively  $R(S', x_i)$  is the set of pixels which belongs to the same class as the pixel  $x_i$ . Therefrom the GCE can be computed as follows:

$$GCE(S, S') = \frac{1}{N} \sum_i \min \{LRE(S, S', x_i), LRE(S', S, x_i)\} \quad (3.7)$$

Since the GCE is a measure of error and the RI a measure of similarity,  $1 - GCE$  is used. It measures the extent to which one segmentation can be viewed as a refinement of the other. The Boundary Displacement Error (BDE) is also calculated [FMR<sup>+</sup>02]. It calculates the mean distance between the boundaries of the ground truth image and the boundaries found in the segmented test image and it is related to the number of boundary pixels found in the images. It can be regarded as the average displacement error of boundary pixels between two segmented images. Particularly, it defines the error of one boundary pixel as the distance between the pixel and the closest pixel in the other boundary image. Further a visual inspection of the segmentation results has been performed which lead to the following criteria:

- **Number of Misshaped Strokes (MSS)** denotes the number of stroke configuration which have large distortions in comparison to the ground truth. Not included are split or merged stroke formations.
- **Number of Merged Strokes (MS)** is the number of single stroke configurations in the ground truth which have been merged by the segmentation process.
- **Number of Split Strokes (SS)** is the number of single stroke configurations in the ground truth which have been split up by the segmentation process.

- **Number of False Positives (FP)** is the number regions in the test image that have been identified as stroke, but have no correspondent region in the ground truth. They can also be single, isolated pixels or small isolated pixel areas which are considered as belonging to a stroke formation, but are neither connected to the stroke formation region nor have a correspondent part in the ground truth. They can also be filled holes in characters.
- **Number of False Negatives (FN)** is the number of regions in the test image that have been identified as background, although they should have been identified as stroke according to the ground truth. False negatives can also originate in the rough texture of some drawing tools. Lighter areas inside a stroke are then considered as background, although they should belong to the stroke region.

### 3-1.2.1 Synthetic Data

The synthetic data consists of black strokes applied on white background with software. The resulting binary images are considered as the ground truth segmentation for the evaluation. These images are applied on an uneven background and distorted with noise and blur. Figure 3.1 shows an example for such a synthetic input. The strokes belong to six classes of stroke ending shapes. Some of them can be divided into subclasses. The classes of synthetic stroke endings are listed in Table 3.1.

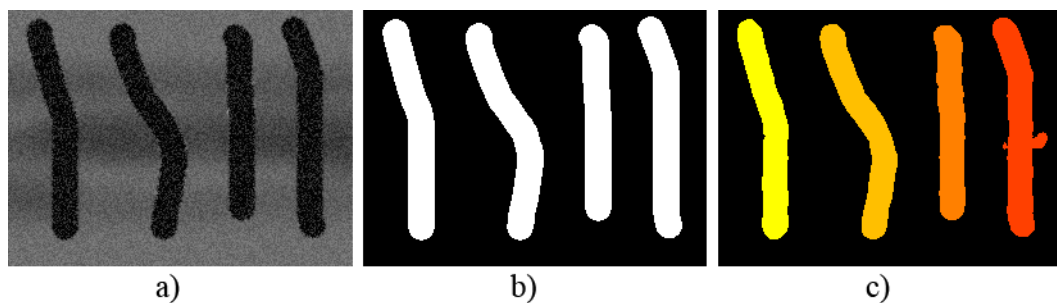


Figure 3.1: An example for a synthetic stroke input. a) shows the distorted image, b) shows the ground truth and c) the resulting segmentation.

Table 3.2 shows the evaluation results for the synthetic data. The segmentation results show a high level of accuracy of the segmentation for all the classes. The GCE and the RI confirm each other and the boundary displacement error is also low with two exceptions. The rough ended strokes show the highest number of misshaped strokes. Since rough endings lose fine details when they are distorted by noise, they can not be segmented according to the ground truth. This is also reflected in the BDE which is the second highest (0.505) in the test. The ending class “pointed 4” produced the highest BDE. This originates in the fact that more stroke regions than in the other classes were recognized as background. The RI (0.649) and the GCE (0.961) reflect this fact too, the values are the lowest for all classes. All other classes produced similar values: the RI lies between 0.975 and 0.989 and the 1-GCE between 0.971 and 0.986. Besides the “rough” and “pointed 4” ending classes, angular and round ended strokes produce both one misshaped stroke and the segmentation of the class “elliptic 1” resulted in two misshaped strokes. Only in the class “pointed 2”, two nearby single strokes are merged into one stroke with four endings. No strokes in the whole test set were split up. In the class “elliptic 1” two areas, which in

Class	Subclass	Description	Example
Angular		Angular endings are characterized by two angles near to $90^\circ$	
Rough		Rough endings have rough contour	
Elliptic	Elliptic 1	The longer axis of the ellipse is perpendicular to the drawing direction	
	Elliptic 2	The longer axis of the ellipse has an angle of $45^\circ$ in relation to the drawing direction	
Pointed	Pointed 1	$\theta = 90^\circ$	
	Pointed 2	$\theta = 45^\circ$ , endpoint is on the middle axis of the stroke	
	Pointed 3	$\theta = 45^\circ$ , endpoint lies on the outer border of the stroke	
	Pointed 4	$\theta = 110^\circ$	
Round		A round stroke ends in a half-circle	
Dovetail		A dovetail shaped stroke has a pointed cavity at his endings	

Table 3.1: Classes of synthetic stroke endings.

the ground truth belong to the background, were detected as belonging to a stroke, the same for the class “round”. Besides “pointed 4”, the segmentation of “elliptic 1” results in one False Negative area.

### 3-1.2.2 Drawn Strokes

The segmentation has also been tested on strokes drawn on test panels. Nine different drawing and/or writing tools have been applied on artist paper and scanned on a flatbed scanner with 600dpi:

1. Brush

Class	SGT	STEST	RI	1-GCE	BDE	MSS	MS	SS	FP	FN
Angular	17	17	0.988	0.984	0.138	1	0	0	0	0
Rough	15	15	0.972	0.970	0.505	9	0	0	0	0
Elliptic 1	15	15	0.987	0.983	0.242	2	0	0	2	0
Elliptic 2	16	16	0.987	0.984	0.141	0	0	0	0	1
Pointed 1	16	16	0.984	0.979	0.188	0	0	0	0	0
Pointed 2	18	18	0.989	0.986	0.113	0	0	0	0	0
Pointed 3	18	18	0.983	0.981	0.164	1	2	0	0	0
Pointed 4	14	14	0.649	0.961	1.388	0	0	0	0	3
Round	14	14	0.975	0.971	0.330	1	0	0	2	0
Dovetail	15	15	0.989	0.986	0.128	0	0	0	0	0
Mean			0.950	0.978	0.333	1.400	0.200	0	0.400	0.400

Table 3.2: Evaluation of the segmentation of synthetic data.

2. Black Chalk
3. Charcoal
4. Graphite
5. Juniper
6. Metal Nib Pen
7. Goose Quill
8. Reed Pen
9. Silver Point Pen

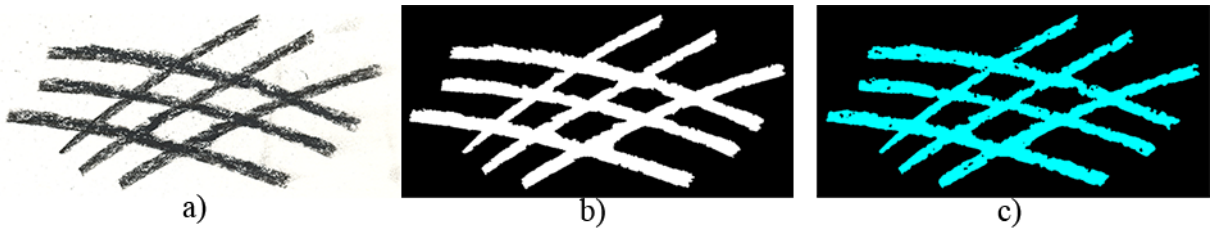


Figure 3.2: An example for a charcoal stroke input. a) shows the original image, b) shows the ground truth and c) the resulting segmentation.

Table 3.3 shows the evaluation results for these strokes. The number of false negatives encountered in Black Chalk, Charcoal and Graphite classes can be explained by the rough texture of these dry drawing tools. In Figure 3.2 a charcoal hatch shows how the texture of the strokes causes segmentation problems. Regions within a stroke have been identified as background. The BDEs for black chalk (5.632), charcoal (8.900) and graphite (6.643) confirm this observation. Since no fountain-pens were used in the tests performed in this paper, strokes can be distorted when the dip-pen, goose quill or reed pen contains little ink. Figure 3.3 illustrates this problem. Strokes drawn with enough ink are segmented correctly, while strokes drawn with little ink are split up or otherwise segmented incorrectly. Above all, juniper shows this behavior confirmed by the BDE (4.670). Although the GCE suggests that the segmentation of the silver strokes is correct with respect to the ground truth, the visual results are not satisfying enough to continue

Class	SGT	STEST	RI	1-GCE	BDE	MSS	MS	SS	FP	FN
Brush	21	21	0.992	0.992	0.586	0	0	0	0	0
Chalk	21	21	0.920	0.934	5.632	0	0	0	3	31
Charcoal	19	19	0.923	0.936	8.900	4	0	0	1	30
Graphite	27	27	0.948	0.960	6.643	1	0	1	0	1
Juniper	26	23	0.968	0.980	4.670	4	0	2	0	3
Metal	24	24	0.934	0.982	1.136	2	0	0	0	2
Quill	27	25	0.985	0.995	1.505	0	0	2	0	2
Reed	27	27	0.930	0.942	1.130	0	0	0	0	3
Silver	27	15	0.847	0.985	240.132	0	0	6	0	22
Mean			0.938	0.967	30.037	1.222	0	1.222	0.444	10.444

Table 3.3: Evaluation of the segmentation of drawn strokes in different formations.

an analysis. The BDE (240.132) and the RI (0.847) confirm these observations. Therefore silver point is excluded from further analysis.

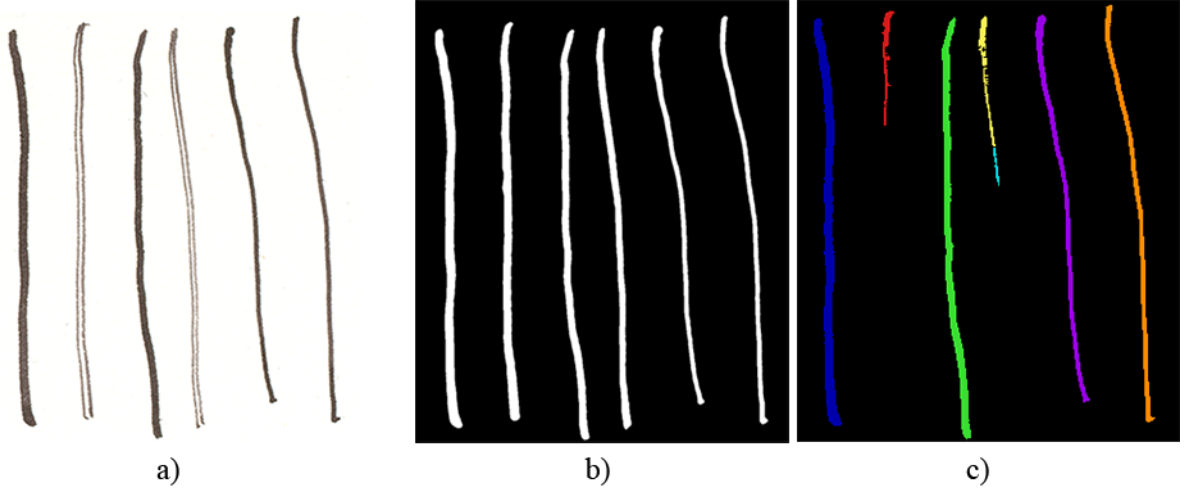


Figure 3.3: An example for a quill stroke input. a) shows the original image, b) shows the ground truth and c) the resulting segmentation.

### 3-1.2.3 Glagolitic Characters

In addition, the segmentation of Glagolitic characters is evaluated. The test data is either derived from photographs in the visual range taken at the St. Catherines monastery from the Missale Sinaiticum or written by a calligrapher. The test data consists of arbitrary patches from both sources with different backgrounds. The evaluation results are reported in Table 3.4.

Figure 3.4 shows an example of test data from the Missale Sinaiticum. The images c1-c5 are the test data from the calligrapher. c1 is a metal nib writing on yellowish paper, c2 a reed pen writing on dark green paper, c3 a reed pen writing on light yellow paper, c4 a metal nib writing on light paper and c5 a reed pen writing on brown, speckled paper. Supralinears and linears which can be found between lines or characters are missed. These special signs are structure or punctuation marks and can take the shapes of short straight

Image	SGT	STEST	RI	1-GCE	BDE	MSS	MS	SS	FP	FN
003y	43	26	0.929	0.941	1.365	0	15	0	2	6
011x	22	15	0.913	0.924	0.986	6	8	2	1	9
012y	32	21	0.947	0.962	1.185	2	4	1	0	6
017y	30	17	0.911	0.918	1.332	10	7	1	2	6
030x	44	31	0.899	0.894	1.325	3	0	0	0	13
031y	48	22	0.943	0.950	1.123	0	10	0	0	6
033y	57	47	0.904	0.901	1.570	7	2	3	0	7
c1	11	11	0.995	0.994	0.188	0	0	0	0	0
c2	21	18	0.952	0.950	0.739	0	0	1	3	11
c3	8	8	0.951	0.954	0.440	0	0	0	0	0
c4	15	14	0.992	0.993	0.471	0	0	0	0	0
c5	23	22	0.974	0.971	0.380	0	0	0	2	2
Mean			0.942	0.946	0.930	2.333	3.833	0.667	0.833	5.500

Table 3.4: Evaluation of the segmentation of glagolitic characters.

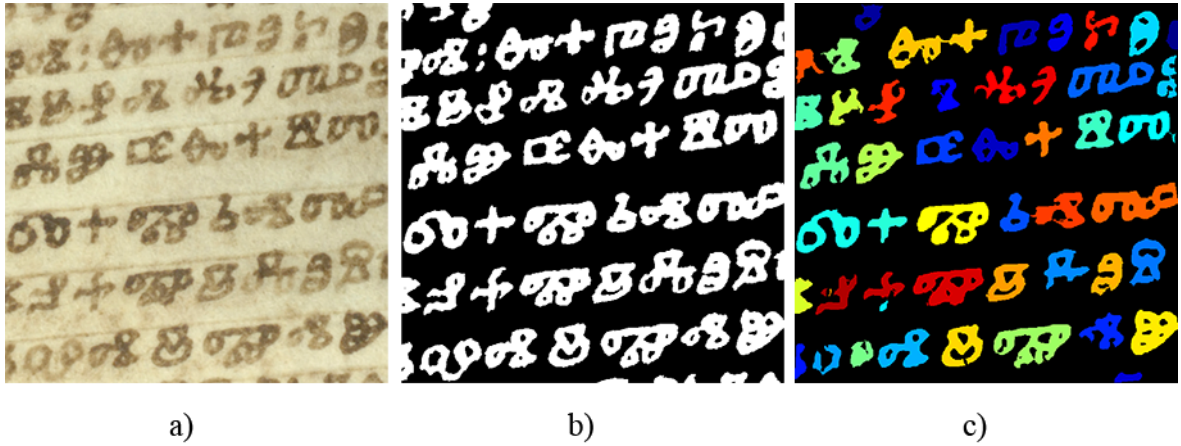


Figure 3.4: Input image 033x (detail) from the Missale Sinaiticum. a) shows the original image, b) shows the ground truth and c) the resulting segmentation.

lines, v- or roof-shaped lines, points or diamonds. They are comparatively small and written with little pressure. They cause a high false negative number, as can be seen for image 030x. Another problem is merged characters in the test data from the Missale. Since the characters are written in a narrow style, the ink-flow caused characters to merge. The results of the test data produced by a calligrapher are better because the background is more uniform than in the Missale data. Further the calligrapher made a larger space between single characters.

### 3-1.3 Conclusion

The evaluation of the segmentation showed how the proposed solution (Otsu's method refined with a snake) works on the test data. Its advantage is that no parameters have to be changed between drawn strokes and writings. Since silver point strokes exhibit a low contrast with respect to the background, they were segmented so badly that they are

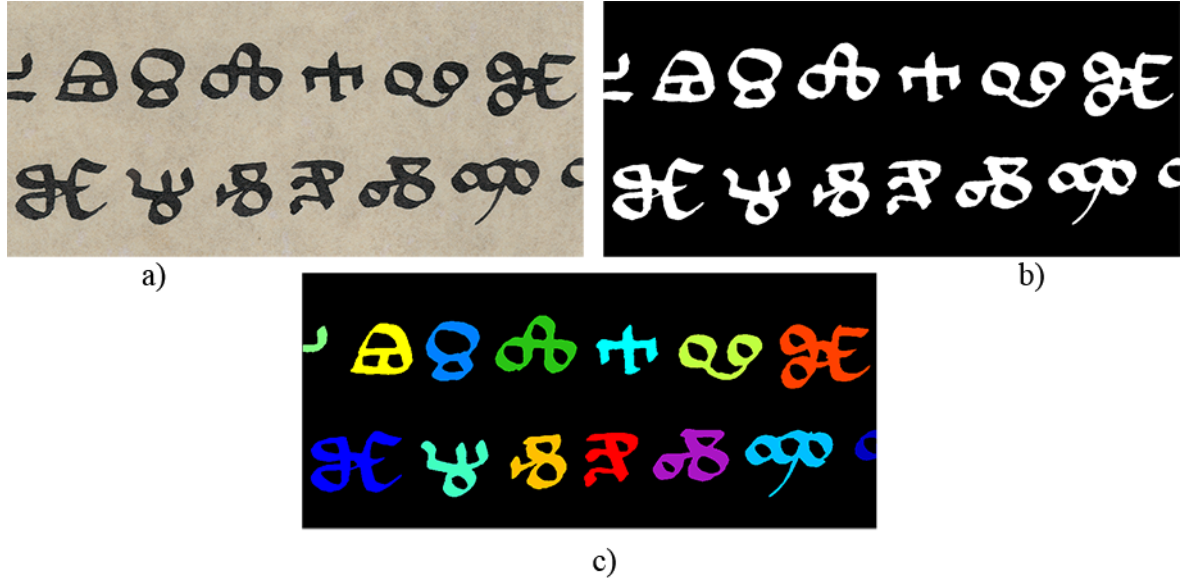


Figure 3.5: Input image c4 (detail) from the dataset made by a calligrapher. a) shows the original image, b) shows the ground truth and c) the resulting segmentation.

excluded from further processing.

The Boundary Displacement Error has proved to be more reliable for this kind of segmentation than the RI and the GCE. The latter measure only the correctness of existing segment labels, but do not include information about the number of objects found. The RI and 1-GCE take the fact into account that segmentations of the same image can have different levels of refinement, which is not the case in the segmentation method presented in this thesis.

Therefore we conclude, that if the BDE is low, RI and 1-GCE are measures of similarity which correspond to human intuition [UH05], otherwise they only provide information if the, badly segmented image (according to human perception) still has some similarities with the ground truth or if it is totally different.

## 3-2 Skeletonization

The structure of a stroke or stroke formation is characterized by a skeleton. Stroke extraction techniques in the field of art history are described in Section 1-3. The task of extracting strokes in document images has been attempted also by researchers who deal with Asian writings [YF95]. Yeung and Fong [YF95] present an algorithm to extract natural strokes from Chinese handwritten characters and propose a hierarchical model of strokes and substrokes. After thinning the character, predefined stroke models are matched to it in order to reconstruct the strokes. Chiu and Tseng [CT99] use a run-length based method to extract straight lines from Chinese characters. Lee [LW98] extracts the boundary and corner points from a digitized character. Then he constructs a sequence graph with the help of cross-sections of the character strokes. This information helps to build a structure graph which can then be simplified with the goal to connect stroke segments belonging together. Liu et al. [LHS99] use feature points from skeletons

(endpoints and fork points, corners) to get a polygonal representation of stroke trajectories from a character. All these methods operate with the notion of dynamic strokes (see Section 1-6) and attempt to reconstruct pen trajectories and connect stroke segments belonging together. In this thesis we deal with the static definition of strokes. Therefore we interpret the stroke skeleton in a different way (see Section 3-2 and Section 3-3).

### 3-2.1 Skeletonization and Skeleton Beautification

Skeletonization, or thinning is a technique widely used in the preprocessing stage of pattern recognition systems to reduce the amount of data and to enhance feature extraction in the subsequent stage [SW93]. Lam et al. [LLS92] state that a skeleton is a representation of a pattern by a collection of thin arcs and curves. “Thinning” and “skeletonization” are synonymous words for the process, “skeleton” or “thinned image” name the result. A skeleton  $S(A)$  of a shape  $A$  is formally defined with the notion of largest disks or medial axis transform [GW01]: If  $z$  is a point of  $S(A)$  and  $(D_z)$  is the largest disk centered at  $z$  and contained in  $A$ , one cannot find a larger disk (not necessarily centered at  $z$ ) containing  $(D_z)$  and included in  $A$ . This *maximum disk*  $(D_z)$  touches the boundary of  $A$  at two or more different points.

Skeletons can be divided into raster or vector skeletons. Raster skeletons contain the coordinates of every skeleton pixel, while vector skeletons are stored as polygons or splines. Furthermore, thinning algorithms can be divided into iterative and non-iterative algorithms. Iterative algorithms delete successive layers of pixels on the boundary of the pattern, until a one pixel wide skeleton (4- or 8-connected) remains. They can be divided further into sequential and parallel algorithms. In a sequential algorithm the boundary pixels are processed in a fixed sequence and marked for deletion depending on all the operations performed so far. A parallel algorithm examines all boundary pixels independently. Non-iterative thinning methods produce a skeleton directly in one pass. Methods include run-length encoding, line following and medial-axis transform by circle fitting [LLS92].

Recently presented skeletonization techniques for characters and/or elongated shapes include Tang and You, who present a skeletonization algorithm for characters based on a wavelet function [TY03]. You et al. [YFY<sup>+</sup>05] propose a thinning algorithm for characters based on multiscale wavelets. An approach based on splines was proposed by Pervouchine et al. [PLM05]. They calculate spline points by fitting rectangles on a handwritten character. The splines represent branches of the character which are merged into a complete skeleton. Kuijper and Olson [KO05] propose a skeletonization algorithm based on symmetry sets while Sakai et al. [SS06] introduce a normalized boundary distance based on touching circles to create a skeleton. However, these techniques deal with special cases and do not generalize or depend on parameters (see corresponding papers).

In this thesis, the parallel thinning algorithm by Zhang and Suen [ZS84] has been applied. This algorithm looks for pixel configurations in a  $3 \times 3$  window moving over a binary image. A point on the contour is then either preserved or deleted according to the pixel configurations in the window. This algorithm was examined by Lam and Suen [LS95] in their comparative paper about character skeletonization algorithms and showed good performance and results (for more details see [LS95]). Since the algorithm does not always guarantee 8-connectedness ([LLS92]), the last iteration is performed with different conditions, according to [LS95]. This algorithm has the advantage that it works

on strokes, stroke formations and characters and is parameter free.

Skeletons show spurious branches and split-up junctions. These branches are produced by non-uniformities in the strokes [GW01] e.g. a rough outer contour of dry drawing tools or irregular ink flow of transferential drawing tools. When two strokes cross at a sharp angle, skeletonization methods produce two vertices connecting three skeleton segments rather than a vertex connecting four segments. The distance between the two vertices is inversely proportional to the angle at which two strokes cross [KK02]. Figure 3.6 shows this effect. It shows two stroke crossings with the corresponding skeletons and illustrates the different distance between skeleton junctions depending on the crossing angle. Several attempts to remove and compensate these distortions have been made. Liu et al. [LHS99] use the maximum circle criterium to remove spurious branches from character skeletons. They use a distance threshold to merge split-up joints. Lin and Tang [LT02] use joint-templates to detect surplus pixel in joint regions. Bai et al. [BL07] propose a skeleton pruning algorithm based on discrete curve evaluation to solve this problem.

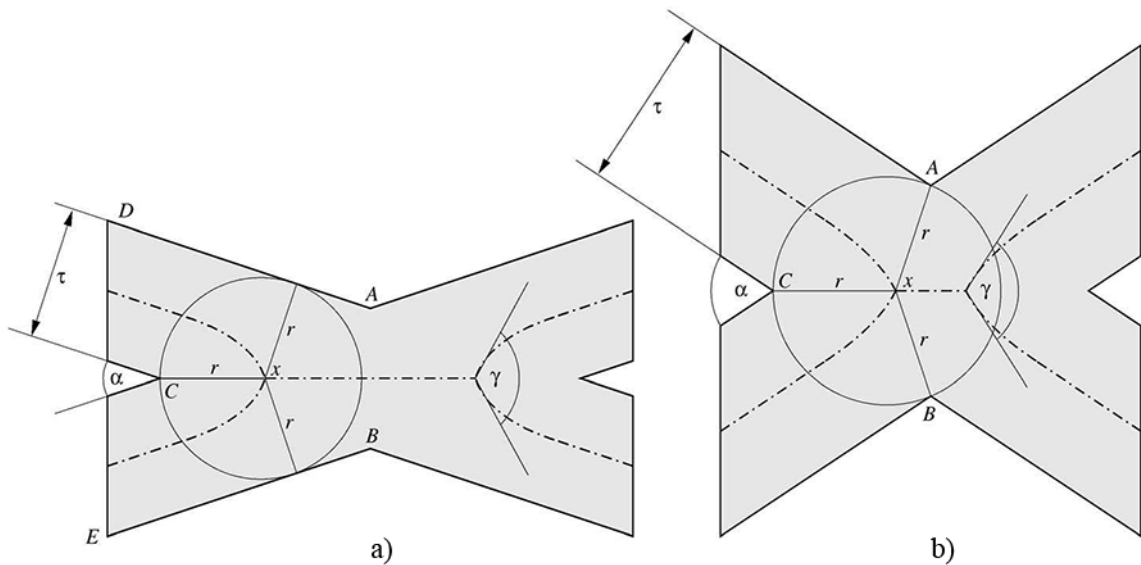


Figure 3.6: The behavior of the skeleton at the crossing point of two strokes [KK02]. Every skeleton point (dashed line) is the center of a maximum disc inscribed into the geometrical object. The endpoint  $x$  of the short path is equidistant from (a) contour lines  $AD$  and  $BE$  and contour point  $C$  if  $\alpha \leq 60^\circ$ , and (b) contour points  $A, B$  and  $C$  if  $60^\circ \leq \alpha \leq 90^\circ$ .

As the algorithm proposed in [ZS84] is also subject to these phenomena, the following skeleton beautification [KK02] algorithms have been examined.

### 3-2.1.1 Principal Curves

This algorithm proposed by Kegl and Krzyzak [KK02] uses a graph representation of a skeleton to improve it. The algorithm is divided into four steps: after the *initialization* of the skeleton graph, the graph is subject to a *fitting and smoothing* method. This already improved skeleton is then *restructured* and the *fitting and smoothing* step is applied again on the graph.

**Initialization:** Every raster based skeletonization algorithm which preserves the connectedness and structure of the shape can be used to build an initial skeleton. The pixels of the resulting skeleton serve as vertices of the graph, and two pixels are connected by an edge if the corresponding pixels are 8-connected. This approach can generate small loops in the graph if two or more junction pixels are 8-connected. These anomalies are detected and adjacent junction pixels are replaced by one graph node located at their center of gravity.

**Fitting and Smoothing:** In this step, the skeleton graph is optimized by minimizing a penalized distance function  $E(G)$ :

$$E(G) = \Delta(G) + \lambda P(G) \quad (3.8)$$

where  $\Delta(G)$  is the averaged squared distance of the points belonging to the original shape from the graph  $G$  and  $P(G)$  is the curvature penalty of the whole graph.  $\lambda$  is a penalty coefficient which balances the influence of  $\Delta(G)$  and  $P(G)$ . The average squared distances is defined as

$$\Delta(G) = \frac{1}{n} \sum_{i=1}^n \Delta(x_i, G) \quad (3.9)$$

$\Delta(x_i, G)$  is the Euclidean squared distance of a point  $x_i$  belonging to the original shape. A low  $\Delta(G)$  secures the close fitting of the skeleton graph to the data.  $P(G)$  is a curvature penalty:

$$P(G) = \frac{1}{m} \sum_{i=1}^m P_v(v_i). \quad (3.10)$$

$m$  is the number of vertices of the graph and  $P_v(v_i)$  is the curvature penalty at vertex  $i$ . This penalty is small when the incident edges join smoothly at  $v_i$ , therefore it ensures a smooth skeleton graph. Kegl and Krzyzak define different types of vertices with different penalty functions.

To find the minimum of  $\Delta(G)$  is analytically impossible. Therefore [KK02] iterate a projection and a vertex optimization step. The projection partitions the shape data into nearest neighbor regions, according to which vertex or edge is nearest to the graph (see also Equations 3.20 and 3.21). This projection is considered as an objective function and optimized with a gradient based method in order to find a minimum  $\Delta(G)$ . These two steps are executed until convergence.  $\Delta(G)$  drives the skeleton graph toward the true position of the medial axis, i.e. it tries to place the skeleton graph midway between the shape borders.

**Restructuring:** In the restructuring step, geometric properties of the skeleton graph are used to modify the configuration of vertices. The first task of this step is to delete short, spurious branches. These branches are deleted according to their length and their angle to a connected path. The threshold is determined by the thickness  $\tau$  of the shape.

$$\tau = \frac{4}{n} \sum_{i=1}^n \sqrt{\Delta(x_i, G)} \quad (3.11)$$

A problem to be solved is the merging of split-up junctions. These are two junctions, where three paths meet (3star), connected through a short path, instead of

one junction connecting four paths. The length of the connecting short path depends on the thickness of the strokes and crossing angle. The sharper the crossing angle, the longer is the connecting path, relative to the stroke thickness. A threshold depending on these parameters determines if two junctions belong together or not. Such detected split-up junctions are then merged into one. Two junctions are therefore merged, if

$$l(p_{i,\dots,j}) < \epsilon_{3star} \frac{\ell(\frac{\gamma_{i_1,i_2}}{2}, \tau) + \ell(\frac{\gamma_{j_1,j_2}}{2}, \tau)}{2} \quad (3.12)$$

This means that if the length of the path  $(p_{i,\dots,j})$  with two 3star-vertices  $v_i$  and  $v_j$  as its endpoints is less than the length of a short segment which should connect these vertices, with the crossing angle of two strokes  $\alpha = \frac{\gamma}{2}$  which are  $\tau$  pixels wide, the vertices  $v_i$  and  $v_j$  are merged (see Figure 3.6). The length of the theoretical short segment connecting two such vertices is determined by:

$$\ell(\alpha, \tau) = \begin{cases} \tau \frac{\frac{1}{\sin \frac{\alpha}{2}} - 1}{\sin \frac{\alpha}{2} + 1} & \text{if } \alpha \leq 60^\circ \\ \tau \frac{\cos \alpha}{\sin \alpha \cos \frac{\alpha}{2}} & \text{if } 60^\circ \leq \alpha \leq 90^\circ \end{cases} \quad (3.13)$$

In short, for a narrow crossing angle the segment is longer than for a wider crossing angle.

### 3-2.1.2 Maximal Circles

This skeleton revision algorithm uses a different approach to compensate skeleton irregularities. It was presented by Nakamura et al. [NEIH98] and uses Maximum Circles to beautify the skeleton. Their algorithm is divided in three steps.

**Thinning:** Every thinning algorithm which produces a raster-skeleton can be used.

**Removal of Spurious Pixels:** A Maximum Circle with a fixed radius is centered at each point of the skeleton. Its diameter is the stroke width. If this circle touches the shape border at two points, the skeleton point in the circle center is preserved. If a Maximum Circle touches the shape border at three or more points, the angles between the touching points should be narrow at opposite sides of the shape border. If those conditions do not hold, the point is deleted. Since the radius of the Maximum Circles remains stable over all the skeleton, points at angles, short branches and junctions are deleted. The result of this step is a skeleton with gaps at such critical points.

**Skeleton Reconstruction:** These gaps have to be reconstructed through a point  $P_c$ . This point is chosen as follows:

- $P_c$  can only be at a location where the distances from the incident skeleton segments to the shape boundary is minimal
- $P_c$  is at the point where all direction vectors of the incident stroke segments meet. The direction vectors are calculated through a least square matching of the broken segments. The least square error weights the direction vector of an incident segment.

The Maximum Circle algorithm is modified into a “Triple-Circle” algorithm. The fixed radius circles have the disadvantage that the conditions hold only for e.g. characters with a stable stroke width. To compensate changing stroke widths, for each vertex  $v_i$  on the graph  $G$  three circles with the center at  $v_i$  are constructed. Their radii are calculated as follows:

$$r_{small} = \min(\tau_B(G)) \quad (3.14)$$

$$r_{medium} = \text{mean}(\tau_B(G)) \quad (3.15)$$

$$r_{large} = \max(\tau_B(G)) \quad (3.16)$$

where  $\tau_B$  is a vector holding the distances from all boundary pixels  $x_b$  of a shape to graph  $G$ . Now a reward function based on the intersection of all three circles with the shape boundary is calculated. After the calculation of the crossing points  $x_c$ , they are sorted clockwise and nearby points within  $10^\circ$  are merged into one point. The reward function  $R(v_i)$  for a vertex  $i$  and a circle  $j$  depends on the length  $l$  of  $x_c$ . If a circle has no or only one touching point,  $R$  is not increased. For two or three crossing points, the reward functions are inspired by [NEIH98]. Equation 3.17 shows how  $R$  is calculated for two crossing points  $x_{c_1}, x_{c_2}$ .

$$R(v_i, j) = \text{abs}(\cos(\phi(x_{c_1}, x_{c_2}))) \quad (3.17)$$

The same equation holds for three crossing points. Instead of the angle  $\phi$  between two crossing points, the mean of the two largest angles between all three crossing points is considered. For four and more crossing points, all circles are divided into quarters. These are determined by the direction of the path in the graph on which the center vertex lies and its orthogonal direction. The reward function for vertex  $v_i$  and circle  $j$  is increased if a crossing point can be found in every quadrant. The reward functions of all circles centered at vertex  $v_i$  are added. All vertices which could reward less than a third of the maximum value of the rewarding function are deleted. The reward function increases at skeleton endpoints, to prevent their excessive pruning. The gaps created by deleting vertices are filled according to [NEIH98].

Both methods have drawbacks. The principal curve method by Kegl [KK02] has parameters to set. The most critical is  $\lambda$  which balances the distance function and the curvature penalty. If  $\lambda$  favors the distance function too much, the graph suffers from overfitting and tends toward a zig-zag-like behavior.

While the algorithm based on principal curves, although applied on written numbers, works on all kind of shapes, the Maximum Circle approach is especially designed for characters with a stable stroke width. In this case, the radius of the Maximum Circles corresponds to the width of the strokes. Therefore the skeleton is degenerated at open stroke endings with decreasing width. It is not possible to select a single radius for the Maximum Circles, when the stroke width is varying. Therefore the algorithm is extended to use three differently sized circles.

The steps taken in this work to create a clean skeleton are the following:

**Thinning:** The thinning algorithm by Zhang and Suen [ZS84] is used to create a skeleton from a binary character or a stroke assembly in a drawing. A skeleton graph is created according to [KK02].

**Elimination of Minor Inconsistencies:** Here both the Triple Circle and the smoothing step from the Principal Curve algorithm can be used.

**Restructuring:** The restructuring step is taken from [KK02], since it is based on a mathematical derivation of 3star merging and not on a simple threshold as for example [LHS99]. All the branches and split-up junctions which have not been removed by the prior step algorithm are processed. The thresholds concerning the merging of 3star-vertices and removing spurious branches are multiples of the shape thickness  $\tau$ .

### 3-2.2 Evaluation

The synthetic data are the same as used in the evaluation of the segmentation, with some additions. A series of hatches with different angles have been introduced to evaluate the skeletonization algorithms, for the same purpose also a set of synthetic strokes with rough borders is used. The stroke and writing data is the same as in Section 3-1.2.

First, the two skeleton beautification algorithms presented in Section 3-2.1 are compared. The measures are the number of changed pixels in comparison to the initial skeleton, related to the total number of pixels in the initial skeleton. Table 3.5 shows

Test Data	Circles	Principal curve
Synthetic Strokes	0.020	0.054
Synthetic Hatches	0.075	0.133
Synthetic Rough border	0.109	0.162
Drawn strokes	0.024	0.052
Glagolitic writings	0.178	0.112
Average	0.085	0.103

Table 3.5: Evaluation of two skeleton beautification algorithms.

the results of this evaluation. One can observe, that the principal curve method causes more changes to the initial skeleton (0.103 compared to 0.085 for the circle algorithm). However, the number of moved pixels does not actually define the “beauty” of a skeleton. Therefore a sample of 50 randomly selected strokes or stroke formations has been examined by a human to judge the correctness and the nearness to human perception of a skeleton. If a method produced a clearly more consistent skeleton than the other, the better method awarded 1, the other 0. If both methods produced the same result or if the results were of a comparably quality, both methods will get 0.5.

The principal curve algorithm “won” with an average result of 0.68, while the modified maximum circle algorithm earned an average voting of 0.32. Based on these results, the principal curve method is used further on.

As mentioned in Section 3-2, skeletons are subject to noisy branches and split up junctions. The restructuring algorithm proposed by Kegl et al. [KK02] and presented in Section 3-2.1.1 is used to eliminate these phenomena. Here, the algorithm is tested on synthetic data: one set of hatches of different angles to evaluate the correct merging of split up junctions and the removal of short branches is tested on a set of synthetic strokes with a rough border. Table 3.6 shows the evaluation of the removal of short branches. The criteria are as follows:

- **Removed Short Branches:** Tells the number of removed branches.

- **True Positives:** Denotes the number of deleted branches which should have been removed.
- **False Positives:** Denotes the number of deleted branches which should not have been removed.
- **True Negatives:** Is the number of open skeleton branches which were not deleted, but are not noise.
- **False Negatives:** Counts the number of skeleton branches which should have been removed, but still form a part of the skeleton.
- **False Positive Rate:** This measure is defined as

$$\text{False Positive Rate} = \frac{\# \text{ of false positives}}{\# \text{ of negative instances}} \quad (3.18)$$

- **False Negative Rate:** This measure is defined as

$$\text{False Negative Rate} = \frac{\# \text{ of false negatives}}{\# \text{ of positive instances}} \quad (3.19)$$

Test Data Set	Removed Short Branches	TP	FP	TN	FN	FPR	FNR
1	16	26	0	10	22	0	0.48
2	13	13	0	7	6	0	0.31
3	8	8	0	6	5	0	0.38
4	26	23	3	8	3	0.27	0.11
5	23	23	0	9	7	0	0.24
6	33	33	0	14	0	0	0
7	5	5	0	10	0	0	0
8	4	4	0	9	0	0	0
Average						0.03	0.19

Table 3.6: Evaluation of the removal of short branches.

The overall False Positive Rate is low. This means that the branches which have been removed, were really noisy and not essential parts of the skeleton. Compared to it, the overall False Negative Rate is higher. It indicates the number of noisy branches which have not been removed. Figure 3.7 shows several synthetic and drawn strokes with their skeletons and pruned skeletons.

The merging of split up junctions is evaluated on cross hatches. These cross-hatches consist of three straight strokes which are crossed by three strokes at a certain angle  $\alpha$ . All strokes have the same width. There are two sets of cross-hatches regarding the distance between the strokes. In one set, the gap between the strokes in a triplet is approximately the stroke width (narrow). In the other set (wide), the gap is doubled. [KK02] suggest a value for the scaling parameter  $\epsilon_{3star}$  between 2 and 4. We choose both values for our test runs. The criteria are defined similar to the evaluation of the removal of noisy branches:

- **Joined Junctions (JJ):** Tells the number of junctions, which have been merged.
- **True Positives:** Is the number of split up junctions, which are correctly merged.
- **False Positives:** Denotes the number of merged junctions which should be two independent junctions.

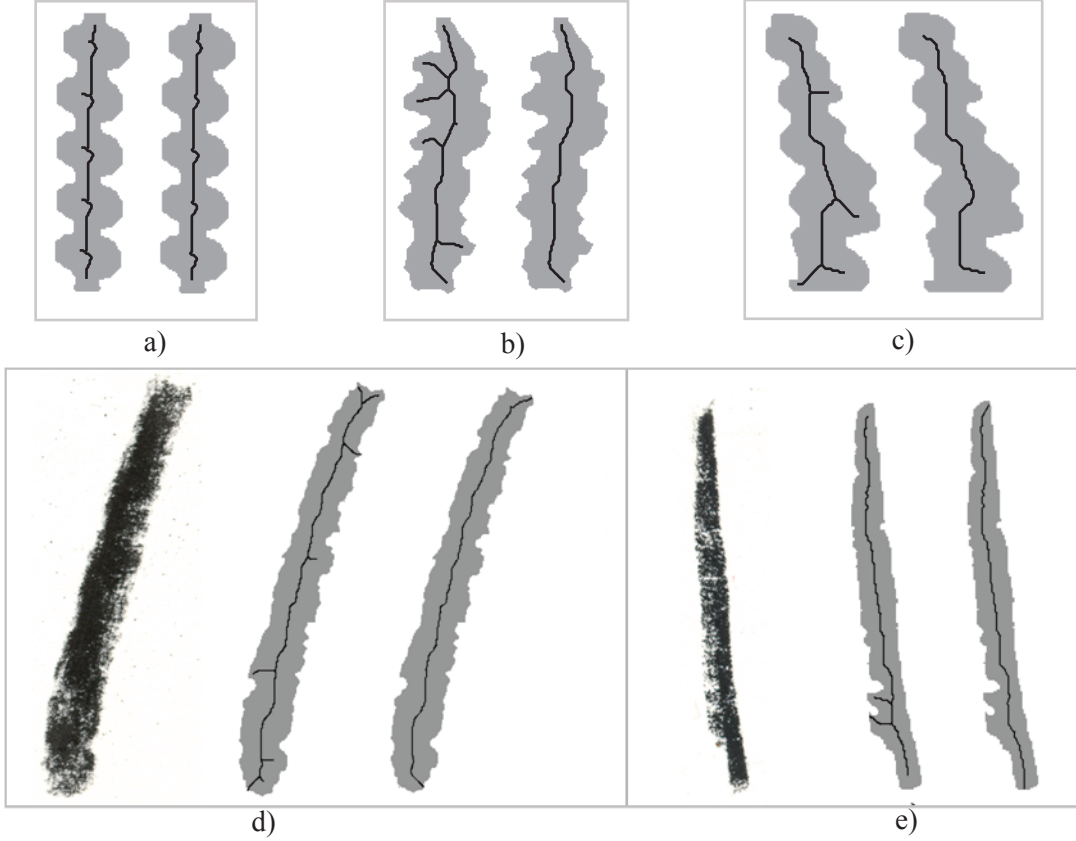


Figure 3.7: Illustration of the pruning: a), b) and c) show three synthetic strokes with noisy skeleton branches and the respective clean skeleton; d) shows a charcoal stroke with skeleton and pruned skeleton and d) the same for a black chalk stroke.

- **True Negatives:** Is the number of independent 3star-junctions which have not been merged.
- **False Negatives:** Counts the number of split up junctions which should have been merged, but are not.
- **False Positive and False Negative Rate**

Figure 3.8 shows hatches used in this tests. The first row shows the initial skeletons for wide and narrow hatches with a crossing angle of  $10^\circ$ . The second row shows the merging with  $\epsilon_{3star} = 2$ , while the third row shows the merging with  $\epsilon_{3star} = 4$ . The fourth row shows the initial skeletons of wide and narrow hatches with  $\alpha = 45^\circ$ . The next row shows the merging with  $\epsilon_{3star} = 2$ , while the last row shows the merging with  $\epsilon_{3star} = 4$ . It can be observed that the merging results differ more between narrow and wide hatches than between the same hatch merged with a different  $\epsilon_{3star}$ .

Tables 3.7 and 3.8 show the result. The mean False Positive Rate with  $\epsilon_{3star} = 2$  is about 0.085 compared to 0.1 when  $\epsilon_{3star} = 4$ . The False Negative Rate is 0.32 in  $\epsilon_{3star} = 2$  and 0.31 with  $\epsilon_{3star} = 4$ . Since the difference of the False Positive Rate is larger than the difference of the False Negative Rate, the first is used as decision value, therefore  $\epsilon_{3star} = 2$  is used further on. Both rates decrease inversely proportional to the angle  $\alpha$ .

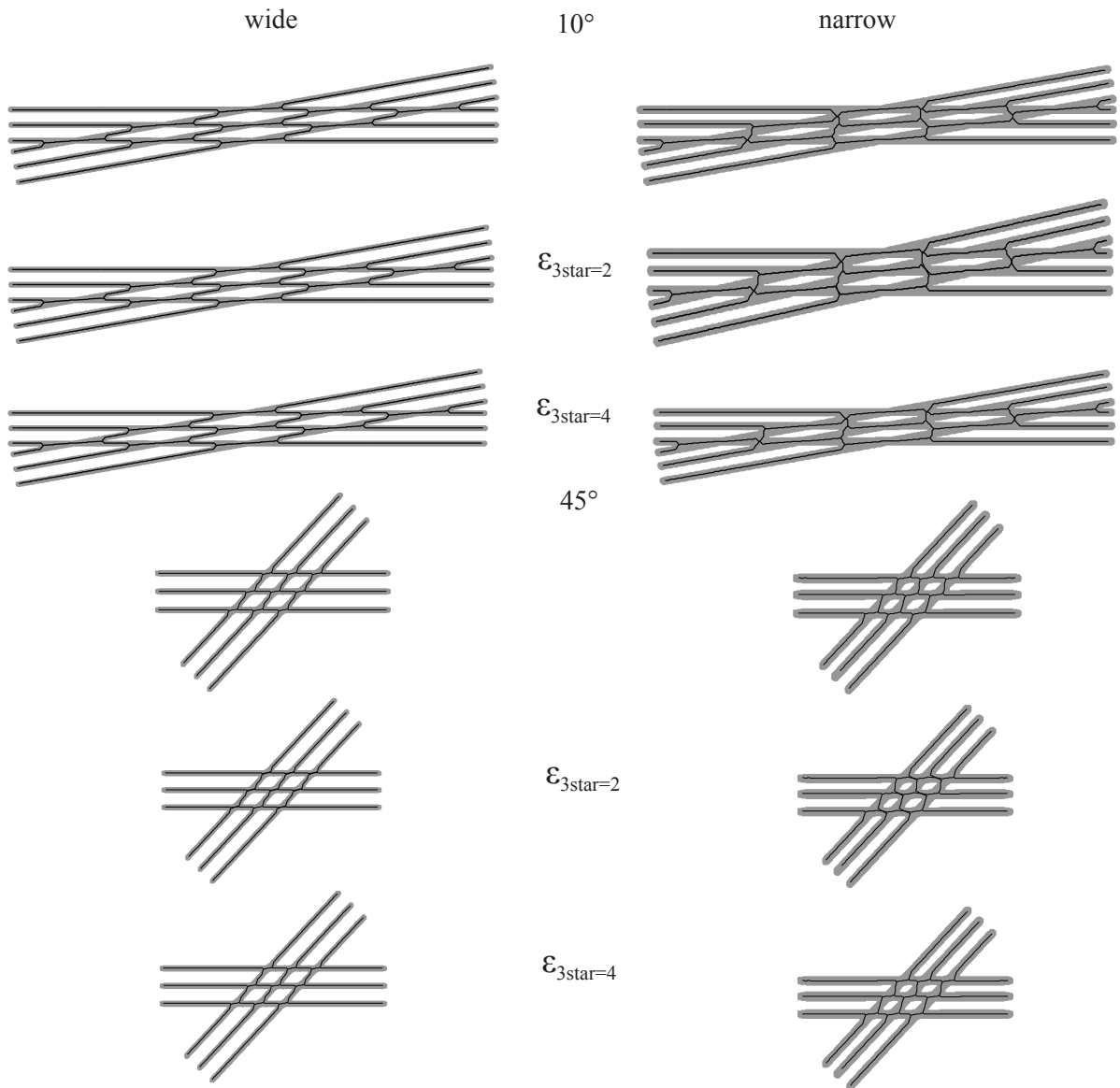


Figure 3.8: Examples for hatches used in the test and their skeletons.

### 3-2.3 Conclusion

A skeletonization algorithm is used to extract the structure of a stroke formation. Two beautification algorithms have been compared. One is based on fitting a principal curve into the shape and the other on the relation of circles centered on the skeleton to the shape boundary. The evaluation of both favored the principal curve algorithm which is used further on. The method used for restructuring the skeleton eliminates split up junctions and noisy branches. All junctions in hatches with a crossing angle  $\alpha \geq 45^\circ$  were merged correctly.

	narrow							wide							
$\alpha$	JJ	TP	FP	TN	FN	FPR	FNR	JJ	TP	FP	TN	FN	FPR	FNR	
10°	0	0	0	12	9	0	1	0	0	0	12	9	0	1	
20°	5	0	5	5	7	0.41	0.77	0	0	0	12	9	0	1	
30°	6	0	6	6	6	0.5	0.66	0	0	0	12	9	0	1	
45°	6	0	6	6	6	0.5	0.66	8	8	0	12	1	0	0.11	
60°	9	9	0	12	0	0	0	9	9	0	12	0	0	0	
70°	9	9	0	12	0	0	0	9	9	0	12	0	0	0	
80°	9	9	0	12	0	0	0	9	9	0	12	0	0	0	
90°	0	0	0	12	0	0	0*	0	0	0	12	0	0	0*	
Average						0.17	0.26	Average						0	0.38

Table 3.7: Evaluation of split up junction merging with  $\epsilon_{3star} = 2$ . \*Since there are no split up junctions at a crossing angle of 90°, the number of positive instances is zero. The False Negative Rate is assumed to be 0 in this case.

	narrow							wide							
$\alpha$	JJ	TP	FP	TN	FN	FPR	FNR	JJ	TP	FP	TN	FN	FPR	FNR	
10°	0	0	0	12	9	0	1	0	0	0	12	9	0	1	
20°	6	0	6	6	9	0.5	1	4	4	0	12	5	0	0.55	
30°	6	0	6	6	9	0.5	1	7	4	3	9	3	0.25	0.33	
45°	6	1	5	1	9	0.41	1	9	9	0	12	0	0	0	
60°	9	9	0	12	0	0	0	9	9	0	12	0	0	0	
70°	9	9	0	12	0	0	0	9	9	0	12	0	0	0	
80°	9	9	0	12	0	0	0	9	9	0	12	0	0	0	
90°	0	0	0	12	0	0	0*	0	0	0	12	0	0	0*	
Average						0.17	0.5	Average						0.03	0.11

Table 3.8: Evaluation of split up junction merging  $\epsilon_{3star} = 4$ . \*Since there are no split up junctions at a crossing angle of 90°, the number of positive instances is zero. The False Negative Rate is assumed to be 0 in this case.

### 3-3 Static Stroke Partitioning

The skeleton created in the previous section is used to extract static strokes from an stroke formation. The meeting point of the skeleton and the stroke border is the endpoint of the stroke. If there is no meeting point, the skeleton branches are extended until they meet with the stroke border. The direction of this extension is obtained by calculating the average direction of the line segments connecting the skeleton endpoint to its next following neighbors.

A tessellation as proposed by Kegl [KK02] is computed. It consists in calculating the distance of each point to the skeleton graph  $G_{V,S}$ . Then the shape is partitioned into nearest-neighbor regions. Each region contains the points  $x_{v_i}$  of a shape where the distance to a vertex  $\Delta(v_i)$  is less than the distance to all other vertices  $V$ . Since also the edges  $S$  have to be included in this distance calculation, the tessellation of the nearest-

neighbor-sets  $V_i$  and  $S_i$  can be calculated as follows:

$$\begin{aligned} V_i = \{x \in X_n : \Delta(x, v_i) = \Delta(x, G_{V,S}), \\ \Delta(x, v_i) < \Delta(x, v_j), j = 1, \dots, i - 1\} \end{aligned} \quad (3.20)$$

and

$$\begin{aligned} S_i = \{x \in X_n : x \notin \cup_{j=1}^m V_j, \Delta(x, x_i) = \Delta(x, G_{V,S}), \\ \Delta(x, s_i) < \Delta(x, s_j), j = 1, \dots, i - 1\} \end{aligned} \quad (3.21)$$

where  $m$  is the number of vertices,  $X_n$  all points which belong to the shape. The skeleton is divided up into branches, which either go from an endpoint to the nearest junction on the path or consist of paths between junctions. A static stroke is defined as all nearest neighbor sets which belong to vertices or edges of a skeleton branch.

The ending extraction consists of several steps (see Chapter 3). These steps are evaluated separately for each type of test data (synthetic, drawn strokes, Glagolitic writing).

### 3-3.1 Evaluation

We test the partitioning only with stroke formations, since the task is trivial with single strokes and we concentrate on Glagolitic characters, because static stroke partitioning is the base of a paleographic character analysis.

The static strokes can be seen on a clean skeleton, since they correspond to skeleton segments which are either delimited by two vertices, two endpoints (the trivial single stroke case) or an endpoint and a vertex. Additionally, the open skeleton segments are extended toward the stroke boundary until they meet. In this way, the endpoint of an open or half-open stroke is defined. Figure 3.9 shows the partition into static strokes of a brush stroke hatch with the skeleton overlaid. The extraction of static strokes identifies half-open strokes, but it also plays a role in the paleographic analysis of Glagolitic characters. The perceptive features mentioned in Section 1-2 are based on the number or arrangement of static strokes.

In Figure 3.10 one can find examples of a static stroke partitioning of different Glagolitic characters. In the first row, five instances of the character  $l$  are shown. It can be observed, that the static stroke partitioning is consistent over all characters. A Glagolitic  $l$  consists therefore of four static strokes. The second row depicts the characters  $t$  and  $v$ , as they have the same structure, only rotated by  $180^\circ$  (other characters with similar structure are  $d$  (round form) and  $o$ ). The stroke partitioning of the first three characters in the row is consistent (three static strokes), the last character is written in a slightly different way with an additional short stroke. This stroke is part of an individual style of a writer and not caused through noise. It increases the number of static strokes for this character to five.

In the third row, two  $d$ 's (pointed form) are partitioned into five static strokes. There one can argue that the pointed angle connecting the two circles consists of two strokes instead of three. However, this issue is not yet sufficiently clarified with the slavists. The same effect can be observed with the letter  $g$  in the same row, which is virtually a rotated and elongated version of the  $d$ . The fourth row contains five  $a$ 's, which are all partitioned into four static strokes. The fifth row contains two instances of the letter  $b$  and three instances of the letter  $\check{s}$ , which has the same shape, but without the hook characterizing

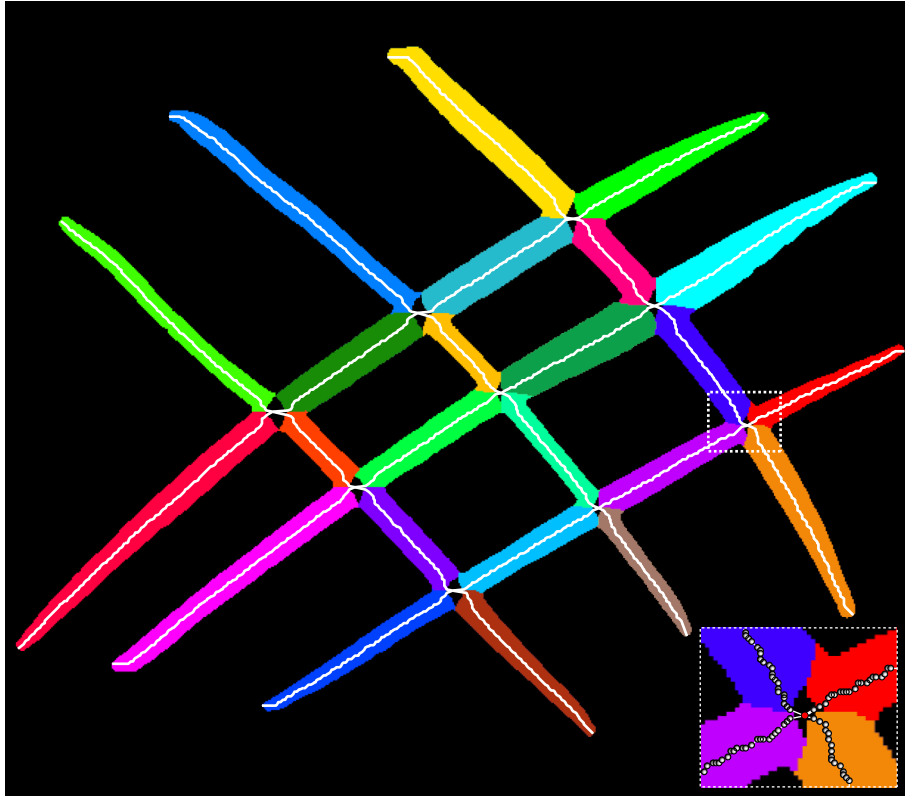


Figure 3.9: A brush stroke hatch with the static strokes colored in different colors and the skeleton overlaid in white and a detail of a crossing.

the *b*. The *b*'s are partitioned into five static strokes each and the first *š* consequently into three strokes. The last *š* in this row has the same characteristic as the rightmost *t* in the second row. The sixth row starts with two instances of the letter *e* which are correctly partitioned into six strokes, the following two *ç*'s into five strokes. The last letter in this row, *jq*, is partitioned into sixteen static strokes.

The last row starts with two instances of the letter *m*, both partitioned into eight static strokes. Two instances of *i*, both partitioned into six static strokes, conclude this inspection. Here, the same issue as with the letters *d* and *g* takes place.

Figure 3.11 shows some problematic static stroke partitionings. In the first row, three letters *b* show an underestimation of static strokes. The letters *t* in the first row has a wrongly merged 3star, the same holds for the last two letters in the second row *n* and *r*. The first three letters in the second row of Figure 3.11 (*l*, *n* and *č*) suffer from noisy branches, which have not been deleted.

In addition to the partitioning of the characters into static strokes there are features presented in Section 1-2 which can be calculated straightforward from the skeleton. Figure 3.12 shows examples for a static stroke analysis. Arbitrary characters have been selected arbitrarily to show the results of the analysis. The decision, if a stroke is bent or straight, horizontal or vertical has been made with the help of the formfactor of the skeleton of a static stroke. In accordance with the slavists, we consider a stroke straight, if its formfactor is above 4. However, there are still discussions with the slavists about these features.

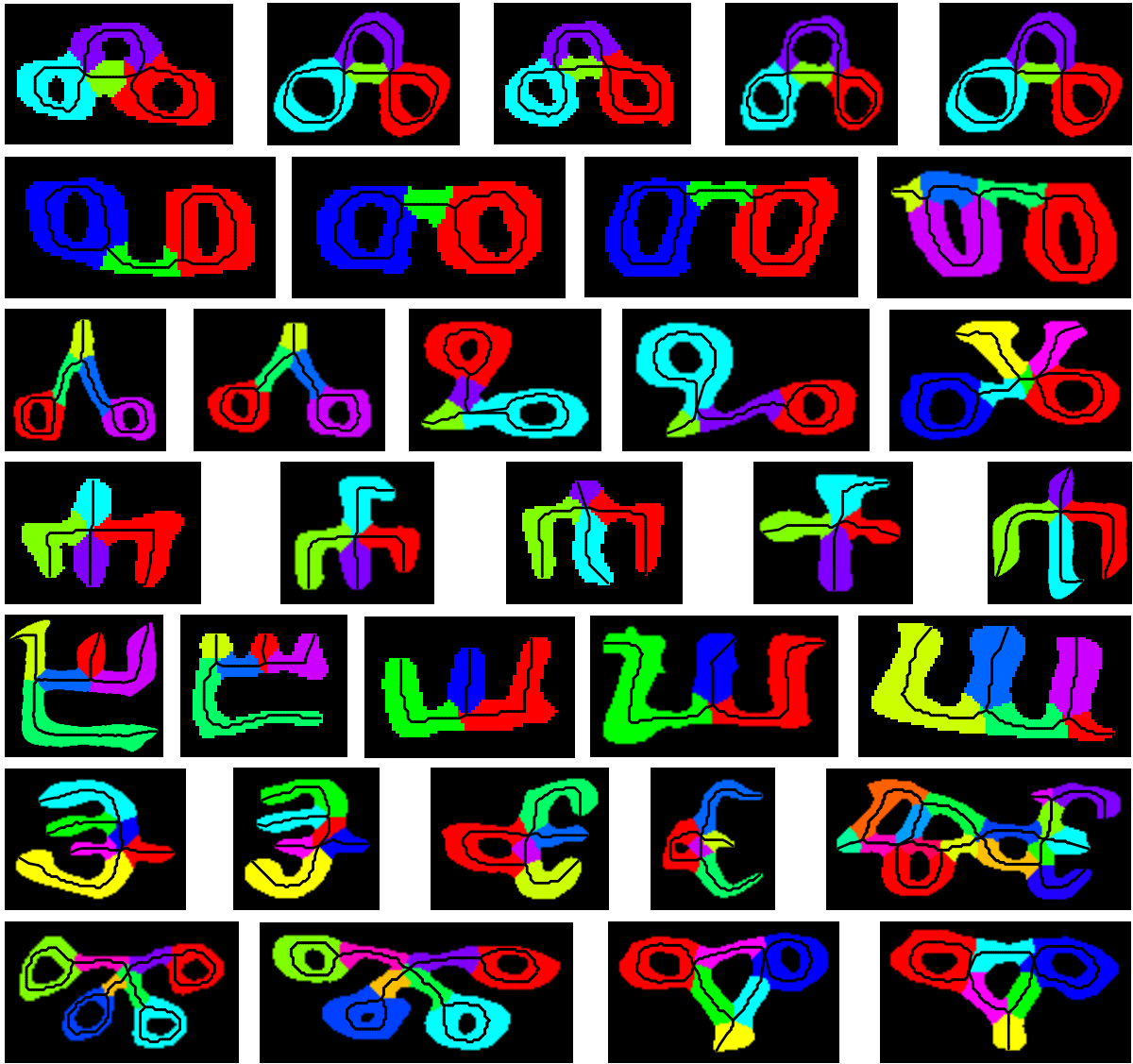


Figure 3.10: Static strokes partitioning of Glagolitic characters. From left to right, first row: l (5x); second row: v (1x), t (3x); third row: d (2x), g (2x), ž (1x); forth row: a (5x); fifth row: b (2x), š (3x); sixth row: e (2x), ę (2x), jq (1x); seventh row: m (2x) and i (2x). The colors of the strokes are arbitrary.

### 3-3.2 Conclusion

The static stroke partitioning can be used to find open and half open strokes which are then processed further in Section 3-4 to extract endings. The static stroke partitioning implies also information for the paleographer. Features for a paleographic description of characters as shown in Section 1-2 are calculated from the static strokes.

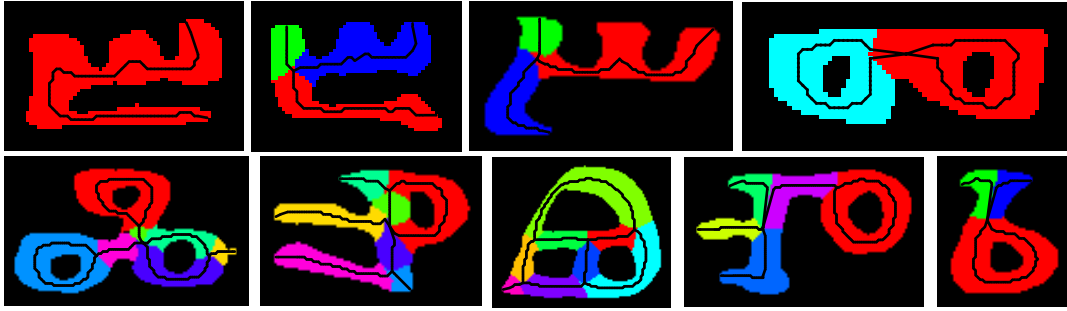


Figure 3.11: Examples of erroneous static stroke partitioning of glagolitic characters. From left to right, first row: a (3x), d (1x); second row: l (1x), n (1x), ě (1x), n (1x) and r (1x). The colors of the strokes are arbitrary.

### 3-4 Cutting-Off Endings

A static stroke, as depicted in the previous section, can be open, half-open or closed. An open stroke has two free-standing, clear endings. A half-open stroke has one free ending. The other part of the stroke joins either another stroke at some angle or an area or a shadow. A closed stroke has both endings covered. Since endings are visible only on open and half-open strokes, only these types of strokes are considered in ending analysis. An open stroke consists of a body connecting two endings, delimited by endpoints. Figure 3.13 shows a schematic stroke with body and endings. These endings are distinguished from their body by their decreasing width toward the endpoints.

This characteristic is used to cut-off the endings. To find out the transition point between ending and body, the distance  $w$  between both sides of a stroke is calculated. This distance is regarded as a function with a certain limit. This limit is approximately the mean width of the body. For open strokes, the stroke is divided in halves, normal to the stroke direction, and this calculation is performed for each half separately. For half-open strokes, the whole length of the stroke is considered. The distance  $w$  is then smoothed and simplified with a least square approximating spline to reduce the influence of a noisy stroke contour. This spline can be interpreted as a function as mentioned above. From this function the point where this function reaches its limit is calculated. A 5% tolerance interval is put around the limit to compensate a noisy contour. This point marks the transition between ending and body. There, the ending is cut from the body. The contour of the ending is used for further processing. Figure 3.14 shows this procedure. A chalk stroke is depicted in the middle with marks where the endings are cut off. The corresponding functions are shown at the left and right side of the stroke.

#### 3-4.1 Evaluation

The extraction of the endings of open or half open strokes has first been tested with the synthetic stroke data presented in Table 3.1. Further it has been tested with drawn strokes and with glagolitic characters. The following criteria have been used to evaluate the ending extraction:

- **Number of Detected Endings (Det. End.):** Denotes the total number of endings found in a class.

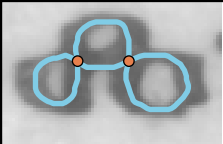
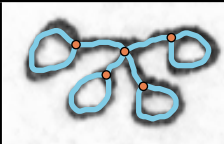
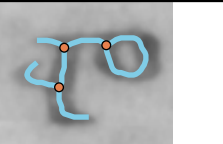
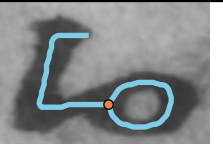
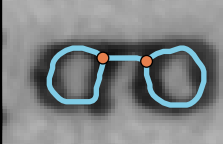
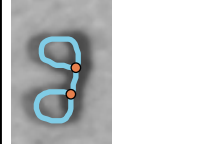
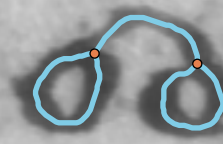
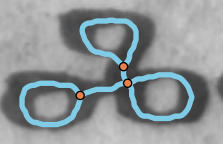
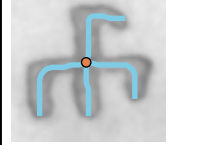
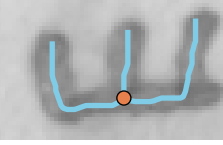
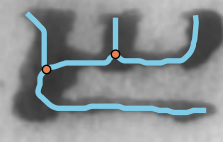
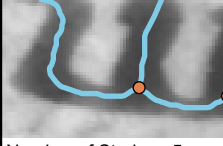
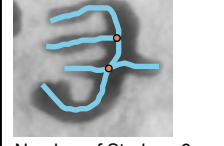
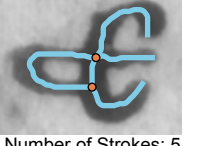
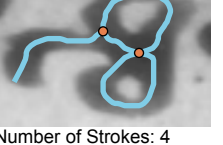
			
Number of Strokes: 4 Number of Knots: 2 Number of Straight Strokes: 1 Number of Horizontal Strokes: 1 Number of Vertical Strokes: 0 Number of Bent Strokes: 3 Number of Enclosed Areas: 3	Number of Strokes: 8 Number of Knots: 5 Number of Straight Strokes: 4 Number of Horizontal Strokes: 1 Number of Vertical Strokes: 0 Number of Bent Strokes: 4 Number of Enclosed Areas: 4	Number of Strokes: 6 Number of Knots: 3 Number of Straight Strokes: 3 Number of Horizontal Strokes: 1 Number of Vertical Strokes: 1 Number of Bent Strokes: 3 Number of Enclosed Areas: 1	Number of Strokes: 2 Number of Knots: 1 Number of Straight Strokes: 0 Number of Horizontal Strokes: 0 Number of Vertical Strokes: 0 Number of Bent Strokes: 2 Number of Enclosed Areas: 1
			
Number of Strokes: 3 Number of Knots: 2 Number of Straight Strokes: 1 Number of Horizontal Strokes: 1 Number of Vertical Strokes: 0 Number of Bent Strokes: 2 Number of Enclosed Areas: 2	Number of Strokes: 3 Number of Knots: 2 Number of Straight Strokes: 1 Number of Horizontal Strokes: 0 Number of Vertical Strokes: 1 Number of Bent Strokes: 2 Number of Enclosed Areas: 2	Number of Strokes: 3 Number of Knots: 2 Number of Straight Strokes: 0 Number of Horizontal Strokes: 0 Number of Vertical Strokes: 0 Number of Bent Strokes: 3 Number of Enclosed Areas: 2	Number of Strokes: 5 Number of Knots: 3 Number of Straight Strokes: 1 Number of Horizontal Strokes: 0 Number of Vertical Strokes: 0 Number of Bent Strokes: 4 Number of Enclosed Areas: 3
			
Number of Strokes: 4 Number of Knots: 1 Number of Straight Strokes: 1 Number of Horizontal Strokes: 0 Number of Vertical Strokes: 1 Number of Bent Strokes: 3 Number of Enclosed Areas: 1	Number of Strokes: 4 Number of Knots: 1 Number of Straight Strokes: 1 Number of Horizontal Strokes: 0 Number of Vertical Strokes: 1 Number of Bent Strokes: 3 Number of Enclosed Areas: 0	Number of Strokes: 3 Number of Knots: 1 Number of Straight Strokes: 1 Number of Horizontal Strokes: 0 Number of Vertical Strokes: 1 Number of Bent Strokes: 2 Number of Enclosed Areas: 0	Number of Strokes: 5 Number of Knots: 2 Number of Straight Strokes: 3 Number of Horizontal Strokes: 1 Number of Vertical Strokes: 2 Number of Bent Strokes: 2 Number of Enclosed Areas: 0
			
Number of Strokes: 5 Number of Knots: 2 Number of Straight Strokes: 4 Number of Horizontal Strokes: 1 Number of Vertical Strokes: 2 Number of Bent Strokes: 1 Number of Enclosed Areas: 0	Number of Strokes: 6 Number of Knots: 2 Number of Straight Strokes: 3 Number of Horizontal Strokes: 3 Number of Vertical Strokes: 0 Number of Bent Strokes: 3 Number of Enclosed Areas: 0	Number of Strokes: 5 Number of Knots: 2 Number of Straight Strokes: 2 Number of Horizontal Strokes: 1 Number of Vertical Strokes: 1 Number of Bent Strokes: 3 Number of Enclosed Areas: 0	Number of Strokes: 5 Number of Knots: 2 Number of Straight Strokes: 3 Number of Horizontal Strokes: 1 Number of Vertical Strokes: 2 Number of Bent Strokes: 2 Number of Enclosed Areas: 1
			
Number of Strokes: 6 Number of Knots: 3 Number of Straight Strokes: 3 Number of Horizontal Strokes: 0 Number of Vertical Strokes: 1 Number of Bent Strokes: 3 Number of Enclosed Areas: 1	Number of Strokes: 3 Number of Knots: 2 Number of Straight Strokes: 1 Number of Horizontal Strokes: 1 Number of Vertical Strokes: 0 Number of Bent Strokes: 2 Number of Enclosed Areas: 2	Number of Strokes: 6 Number of Knots: 3 Number of Straight Strokes: 4 Number of Horizontal Strokes: 1 Number of Vertical Strokes: 1 Number of Bent Strokes: 2 Number of Enclosed Areas: 2	Number of Strokes: 4 Number of Knots: 2 Number of Straight Strokes: 1 Number of Horizontal Strokes: 0 Number of Vertical Strokes: 0 Number of Bent Strokes: 3 Number of Enclosed Areas: 2

Figure 3.12: Static stroke analysis: the figure shows a grid with analyzed Glagolitic characters. First row: l, m, p, ch; second row: t, o, d, l; third row: a (2x), š, b; fourth row: š, e, e, n; fifth row: gj, s, jer (2x).

- **True Positives (TP):** Is the number of found endings, which are true endings.
- **False Positives (FP):** The number of found endings, which should not be an ending.



Figure 3.13: Schematic illustration of a stroke. The dark part in the middle is the stroke body, the endings are highlighted in light gray and the endpoints are denoted as circles.

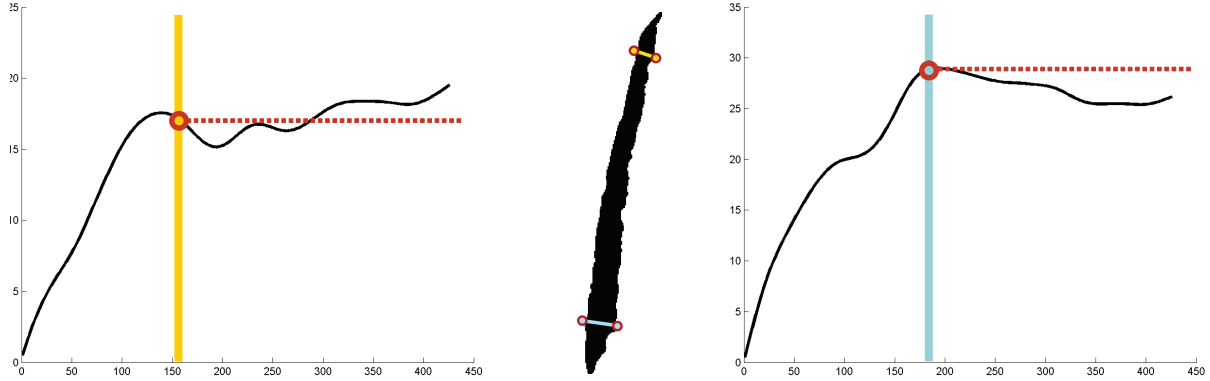


Figure 3.14: Ending extraction of a chalk stroke: left: shows the distance function for the lower end of the stroke shown in the middle; the dashed line marks the threshold where to cut off the ending, right: shows the distance function for the same stroke. The y-axis represents the width for each opposed contour point (x-axis) (note that the x- and y- axis are scaled differently to enhance the readability of the plots).

- **False Negatives (FN):** Tells the number of stroke endings, which have not been found by the algorithm.
- **Number of Distorted Endings (Dist. End.):** Depicts the number of actual true positives, which however are too short, do not cover the whole ending or are split up.
- **Faulty Ending Rate (FER):** This ratio relates the sum of false negatives, false positives and distorted endings to the positives instances in a class.

$$\text{Faulty Ending Rate} = \frac{\# \text{ false negatives} + \# \text{ false positives} + \# \text{ distorted endings}}{\# \text{ of positive instances}} \quad (3.22)$$

Table 3.9 shows the evaluation results for synthetic data. It shows that all types of synthetic endings but dovetail were extracted correctly. The problem with the dovetails was that some noisy branches at the tips were not removed due to their length and therefore two endings were detected, where there should be one. Another problem was that if the cut between the tips is very deep and one endpoint was detected at one tip, the algorithm stopped before the other tip could be included in the ending. Figure 3.15 shows extracted endings from different types of strokes. The first row a) shows synthetic strokes from each class with cut off endings. Further examples for all drawing tools ( b)-i ) are shown, where the extracted ending shape is emphasized.

The evaluation of the ending extraction for drawn strokes is shown in Table 3.10. Here a problem was noisy branches which cause false positives, especially with the dry drawing tools. Endings which lie too near to the image border have been discarded, because they

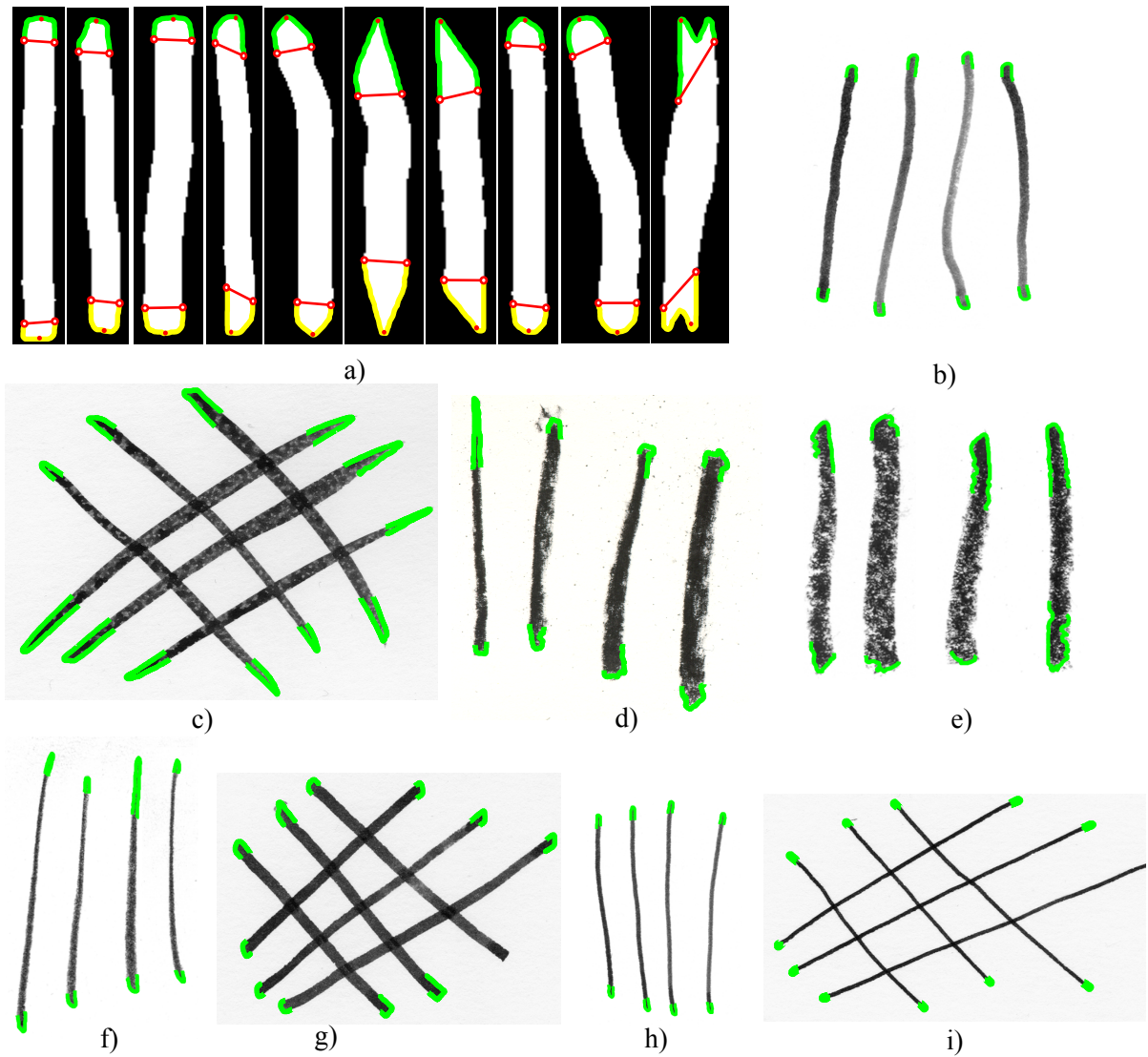


Figure 3.15: a) Synthetic strokes with cut off endings; b) juniper strokes with emphasized endings, c) brush hatch, d) charcoal strokes, e) black chalk strokes, f) graphite strokes, g) metal nib hatch, h) goose quill strokes, i) reed pen hatch, all with emphasized endings.

could be confounded with strokes that are cut off at the image border and cause wrong ending shapes. These result as false negatives.

The algorithm was also evaluated with Glagolitic writings (see Table 3.11). Only characters which actually are composed of at least one half open static stroke were evaluated. The results of the calligraphers writings are better than the one of the Missale. The main problem with the Glagolitic writings is that the data is noisy. Therefore segmentation errors are propagated through the whole procedure. Further, the same problems which are explained in Section 3-3.1 come into effect.

### 3-4.2 Conclusion

The partitioning of stroke formations, mainly Glagolitic characters depends of the structure of the skeleton. Therefore segmentation errors and skeletonization errors propagate

Class	# Det. Endings	TP	FP	FN	# Dist. Endings	FER
Angular	34	34	0	0	0	0
Rough	30	30	0	0	0	0
Elliptic 1	32	32	0	0	0	0
Elliptic 2	30	30	0	0	0	0
Pointed 1	32	32	0	0	0	0
Pointed 2	36	36	0	0	0	0
Pointed 3	36	36	0	0	0	0
Pointed 4	28	28	0	0	0	0
Round	38	38	0	0	0	0
Dovetail	29	24	0	1	5	0.2

Table 3.9: Evaluation of cutting of endings of synthetic strokes.

Drawing tool	# Det. Endings	TP	FP	FN	# Dist. Endings	FER
Brush	54	54	0	0	0	0
Black Chalk	54	52	2	0	0	0.038
Charcoal	47	47	0	2	3	0.16
Graphite	65	64	1	0	1	0.031
Juniper	56	56	0	0	2	0.035
Metal Nib	58	58	0	0	2	0.034
Goose Quill	60	60	0	0	1	0.016
Reed Pen	64	64	0	0	0	0

Table 3.10: Evaluation of cutting of endings of drawn strokes.

Source	# Det. Endings	TP	FP	FN	# Dist. Endings	FER
Missale	228	204	20	42	23	0.335
Calligrapher	113	111	2	3	6	0.098

Table 3.11: Evaluation of cutting of endings of Glagolitic characters (Missale: 81 characters, calligrapher: 37 characters).

through the whole process and affect the partitioning. If the preparatory steps cause no problems, the portioning is consistent and corresponds to the notion of static strokes. However, there are still ambiguous cases which are still under discussion with the slavists.

### 3-5 Summary

This chapter gave an overview of the preprocessing steps which have to be completed in order to get the shape of an ending. First of all, strokes and stroke formations were segmented from the background. This was achieved with a thresholding operation and a refining snake. A skeleton is then calculated out of the binarized shapes. This skeleton is optimized and cleaned and used as a base for a static stroke partitioning of the stroke or stroke formation. Endings are then extracted from open and half open strokes from this partitioning. The fact that endings show a varying width in comparison to the stroke body is used to cut them off the body.

# Chapter 4

## Features and Classification

This chapter presents the features used for classifying stroke endings. The features are calculated on the endings extracted in the previous chapter. It starts with a brief introduction of different approaches for shape description and analysis to deliver insight into related work. Then all features used to characterize endings are described in Section 4-2. Finally, in Section 4-3, the classifier used to categorize strokes is presented.

### 4-1 Related Work

Two-dimensional shapes have typical properties when belonging to the same class. Humans can distinguish objects by their typical silhouettes. To model this behavior, shape analysis techniques have been developed [CMCJ00]. An overview of these techniques can be found in [CMCJ00, Lon98] and [ZL04]. Statistical shape descriptors are described in [DM98]. Otterloo gives an overview about shape analysis based on contours in [vO88].

Caiani et al. [CPZ<sup>+</sup>99] use a polar contour representation of endocardial structures to calculate shape features, among them curvature and eccentricity. A similar approach has been presented by Arica et al. [AVF05]. They show a shape representation based on beam angle statistics (BAS). Mohanty et al. [MRLM05] use centroid and profile based features and compare different machine learning systems (Support Vector Machines, Naive Bayes and Relevance Language Models). Both polar contour representation and BAS basically represent shapes as a function of the distance to the shape's centroid. This representation and features calculated from it have also been used in this thesis.

Contour features based on a curve bend function classified by a neural network are discussed by [FY97b]. A curvature scale space (CSS) contour description and shape matching method was introduced by Mokhtarian [Mok95]. Kopf et al. present an enhanced CSS which is also able to handle convex features [KHE05]. Curve-structure invariant moments are discussed in [LZLL05]. Gottfried et al. [GSH07] introduce numeric features, among them also curvature based ones, based on a qualitative relational system. Dudek et al. [DT97] introduce a shape representation and recognition system with a curve decomposition from multiscale curvature. Fu and Yan propose a classification system based on curve segment properties [FY97a]. They use a curve bend function (CBF) to locate critical points on a curve and use them as shape descriptors. Jin et al. [JCKL06] use modified Hu moment invariants [CT93] for shape classification. Huang et al. [HPM07] use curvature information to classify shapes with Hidden Markov Models.

The results achieved by the above methods were encouraging enough to include curvature based features in the feature set used in this thesis.

## 4-2 Features

To be able to classify the strokes, features which are distinctive for a class of strokes have to be found. Therefore besides classical shape features and moments, features based on curvature and distance relations of the shape are used to distinguish between different drawing tools. The input data are the landmark vectors calculated in the following section.

### 4-2.1 Landmark Setting

To simplify feature calculation, the amount of contour data has to be reduced and endings are rectified and aligned. This can be achieved by setting “*landmarks*”. Further, the sampling of the ending boundary has to ensure that salient points are not missed or oversmoothed because of sampling intervals that are too small or too large in comparison to the size of the ending. Therefore a landmark-based sampling method has been preferred over a fixed-interval sampling. A landmark is a point that identifies a salient feature on an object and which is present on every example in a shape set [HTB00]. Therefore landmarks should be set in a way that their locations correspond through a shape set and landmark setting can also be seen as point correspondence problem. Attempts to solve this problem in 2D and 3D have been published.

Hill et al. [HTB00] propose a method based on a binary tree with the mean shape on the root. Passing from the root to the leaves gives the relation between the mean shape and the original shapes. The homologous points are calculated with the help of a polygonal approximation of the shape and optimizing a cost function based on polygonal arc length. Bookstein [Boo96] uses Procrustes squared distance and thin-plate-splines to locate homologous points on shapes without salient features. Kelemen et al. [KSG99] rotate a parameter net over the surface to a position based on global surface parametrization and use spherical harmonic descriptors to parametrize 3D shapes. Rueckert et al. [FRSN03] use nonrigid registration based on B-splines. They manipulate a mesh of control points lying under the object. Its optimal transformation is found using a gradient descent minimization of a cost function associated with global transformation parameters. Kotcheff and Taylor [KT98] find the shape parametrization optimizing an objective function based on the PCA-Analysis of a shape set.

An algorithm called “Minimum Description Length (MDL) shape modeling” for landmark setting was introduced and expanded by [DCT01, DTC<sup>+</sup>02, Tho03]. Their goal is to choose a model to allow the construction of statistical shape models, which creates a dense correspondence between equivalent points on a boundary. They propose a method which establishes correspondences between points on the shape boundaries over a set of training shapes. The landmark setting algorithm presented by [DTC<sup>+</sup>02] is based on an optimization approach. They use an explicit representation of a shape boundary, therefore a shape  $S_i$  of a set of shapes  $\{S_i\}$  can be represented by a set of points, sampled on the boundary and represented by a vector  $x_i$ . They use a genetic algorithm to optimize the parametrization  $\phi_i$  of a shape in order to construct a shape model with a parametrization  $\phi_i$ . They require a parametrization to be compact, i.e. the variation of the shapes is explainable with “few” parameters. This requirement is met by the MDL (Minimum

Description Length) principle. The idea comes from sending an encoded message where the coding is based on a set of parametric statistical models. The transmission includes coded data and the model parameters. This means that MDL balances the cost of sending the model parameters (the complexity of the model) against the length of the coded data. The description length of a single class of shape data is then used as an objective function for optimization. A linear model for a shape vector in a shape set  $\{S_i\}$  is defined as

$$x_i = \bar{x} + \sum_{m=1}^{n_s-1} p^m b_i^m \quad (4.1)$$

where  $n_s$  is the number of shapes in the set,  $\bar{x}$  is the mean shape over the set,  $p^m$  are the eigenvectors of the covariance matrix describing the variation within the shape set and  $b^m$  are the shape parameters which control the modes of variation. The eigenvectors  $p^m$  are sorted by increasing eigenvalue. Then  $x_i$  is projected into the subspace which is spanned by the eigenvectors  $p^m$  and its axis is rotated about the original origin.

$$y^m \equiv x \cdot \tilde{p}^m, \quad (4.2)$$

$$\text{where } \tilde{p}^m = \frac{p^m}{\|p^m\|}, m = 1 \text{ to } n_s - 1 \quad (4.3)$$

Transmission costs for the  $n_s$  normalized eigenvectors (directions)  $\tilde{p}^m$  are constant for a given shape set. The description length  $D_m$  for the data  $y^m$  is defined as follows:

- if  $\sigma^m \leq \sigma_{min}$

$$D_m = \ln\left(\frac{R}{\Delta}\right) + D^{(1)}(\hat{Y}^m, R, \Delta) \quad (4.4)$$

- if  $\sigma^m < \sigma_{min}$  but the range of  $\hat{Y}^m > \Delta$

$$D_m = \ln\left(\frac{R}{\Delta}\right) + D^{(2)}(\hat{Y}^m, R, \Delta) \quad (4.5)$$

- else

$$D_m = \ln\left(\frac{R}{\Delta}\right) \quad (4.6)$$

$\hat{Y}^m$  is the quantized set of values  $y_i^m : i = 1 \text{ to } n_s$  with quantization parameter  $\Delta$ ,  $\sigma^m$  is the variance of  $\hat{Y}^m$ , while  $\sigma_{min}$  is defined as  $2\Delta$ .  $R$  is defined as the bound for the coordinates  $y_i^m$ , so that  $-\frac{R}{2} \leq y_i^m \leq \frac{R}{2}$  for all  $i, m$ .

The objective function for the optimization is obtained by removing the first term (the cost of transmitting the mean shape) of all equations, because it is constant for a shape set. Combining then the equations which satisfy the first and the second condition leads to the objective function  $F$ . Let  $n_g$  be the number of directions which satisfy the first condition and  $n_{min}$  the number which satisfy the second. The objective function is then defined as:

$$F = \sum_{p=1}^{n_g} D^{(1)}(\hat{Y}^m, R, \Delta) + \sum_{q=n_g+1}^{n_{min}} D^{(1)}(\hat{Y}^m, R, \Delta) \quad (4.7)$$

with

$$D^{(1)}(\hat{Y}^m, R, \Delta) \approx f(R, \Delta, n_s) + (n_s - 2) \ln \sigma^m \quad (4.8)$$

$$D^{(2)}(\hat{Y}^m, R, \Delta) \approx f(R, \Delta, n_s) + (n_s - 2) \ln \sigma^m + \frac{(n_s + 3)}{2} \left[ \left( \frac{\sigma^m}{\sigma_{min}} \right)^2 - 1 \right] \quad (4.9)$$

where  $f$  is a function which depends only on  $R$ ,  $\Delta$  and  $n_s$ .

The point correspondence problem is defined as finding the parametrization function  $\pi_i$  of each shape. The parametrization defines how points are sampled on the shape border. The objective function  $F$ , defined in Equation 4.7 is minimized by manipulating the parametrization functions. The parametrization of a shape must be a monotonically increasing function. This ensures that the right sequence of the sampled points is maintained. Davies et al. [DTC<sup>+</sup>02] choose a piecewise-linear representation of the parametrization that guarantees a diffeomorphic mapping. The parametrization is done by recursively placing landmarks between those already present. The position of these landmarks is denoted as a fraction of the distance between their parent nodes. The number of landmarks inserted determines the degree of refinement. [DTC<sup>+</sup>02] state that the degree of refinement needed depends also on the shape complexity. A reference shape, whose parametrization is fixed, is defined to avoid that all points collapse to one point during the optimization process.

The MDL Algorithm described above has been reviewed by Thodberg [Tho03]. He divided shape sets into three classes:

- Closed curves
- Open curves with fixed endpoints
- Open curves with free endpoints

The stroke endings analyzed in this thesis are considered open curves with fixed endpoints. He specifies the landmark locations the same way as [DTC<sup>+</sup>02] and uses a total of 65 marks. Then he aligned and centered the shape to the mean shape (see also [DM98]). The covariance matrix and the eigenvalues of the aligned shapes are calculated. He introduces a new cost function, which has the advantage to tend to zero when all eigenvalues tend to zero. Thodberg provides also a new method to avoid the collapsing of the landmarks. Instead of fixing the node parameters of the master, he introduces a target  $a_i^{target}$  for the average parameter  $a_i^{average}$  for each node  $a_i$  by means of a quadratic cost.

$$NodeCost = \frac{\sum (a_i^{average} - a_i^{target})^2}{T^2} \quad (4.10)$$

$T$  is a tolerance value. In this thesis the reviewed MDL-Algorithm by Thodberg is used to set landmarks because it improves the state-of-the-art algorithm [Tho03] proposed by [DTC<sup>+</sup>02].

## 4-2.2 Statistical Features

This section describes features which are used in general statistical analysis of open shapes [CMCJ00].

**Distance from Centroid:** The centroid  $C_{xy}$  of a stroke ending is defined as

$$C_{xy} = \left( \frac{1}{N} \sum_{n=1}^N x(n), \frac{1}{N} \sum_{n=1}^N y(n) \right). \quad (4.11)$$

The distances  $\Delta_x$  from every contour point  $x$  to the centroid are calculated. The following statistical terms calculated from  $\Delta_x$  serve as features:

- Minimum
- Mean
- Maximum
- Standard Deviation
- Skewness
- Kurtosis

These features describe the structure of an ending [CMCJ00]. Figure 4.1 a) shows the distance from centroid shape representation. The blue arrows denote the distance.

**Moments:** Chen and Tsai introduce seven moment invariants in [CT93] based on Hu-Moments. These Chen-Moments are defined for boundaries. For a discrete boundary the central moment is defined as follows:

$$\mu_{pq} = \sum_{i=0}^{N-1} (x_i - \bar{x})^p (y_i - \bar{y})^q, p + q = 2, 3, \dots \quad (4.12)$$

where  $\bar{x}$  and  $\bar{y}$  are the respective mean values. The central moment is normalized as

$$\eta_{pq} = \frac{\mu_{pq}}{(\mu_{00})^{p+q+1}}, p + q = 2, 3, \dots \quad (4.13)$$

They then calculate seven moments, which are invariant under translation, rotation and scaling:

$$\begin{aligned} \phi_1 &= \eta_{20} + \eta_{02} \\ \phi_2 &= (\eta_{20} - \eta_{02}) + 4\eta_{11}^2 \\ \phi_3 &= (\eta_{30} - 3\eta_{12})^2 + (3\eta_{21} - \eta_{03})^2 \\ \phi_4 &= (\eta_{30} + \eta_{12})^2 + (\eta_{21} + \eta_{03})^2 \\ \phi_5 &= (\eta_{03} + 3\eta_{12})(\eta_{30} + \eta_{12}) [(\eta_{30} + \eta_{01})^2 - 3(\eta_{21} + \eta_{03})^2] \\ &\quad + (3\eta_{21} - \eta_{03})(\eta_{21} + \eta_{03}) [(3\eta_{30} + \eta_{12})^2 - (\eta_{21} + \eta_{03})^2] \\ \phi_6 &= (\eta_{20} - \eta_{02}) [(\eta_{30} + \eta_{12})^2 - (\eta_{21} + \eta_{03})^2] + 4\eta_{11}(\eta_{30} + \eta_{12})(\eta_{21} + \eta_{03}) \\ \phi_7 &= (3\eta_{21} - \eta_{03})(\eta_{30} + \eta_{12}) [(\eta_{30} + \eta_{12})^2 - 3(\eta_{21} + \eta_{03})^2] \\ &\quad + (3\eta_{21} - \eta_{30})(\eta_{21} + \eta_{03}) [3(\eta_{30} + \eta_{21})^2 - (\eta_{21} + \eta_{03})^2] \end{aligned} \quad (4.14)$$

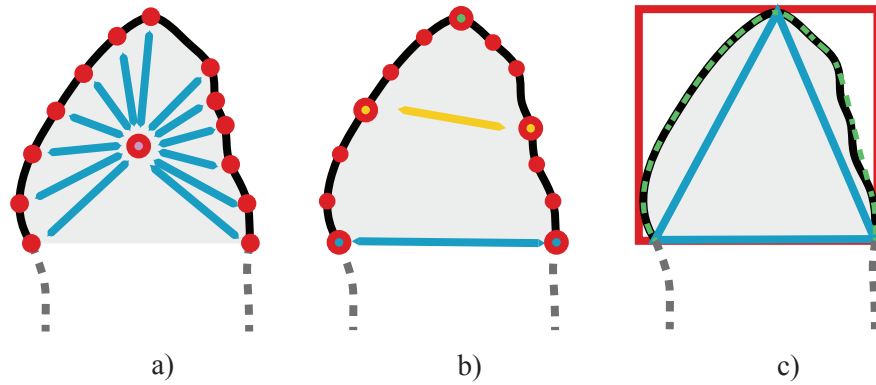


Figure 4.1: a) shows the distance from centroid representation, b) shows the marks for the distance relation and the curvature development and c) shows the comparison perimeters for rectangularity (red), triangularity (blue) and convex hull area measure (green).

### 4-2.3 Curvature Based Features

It can be observed in Figure 2.1 that the drawing tools exhibit different curvature patterns at the endings. The curvature is calculated according to [CMCJ00]. They use a multiscale approach, the so called *curvegram*. A Fourier-based approach is implemented to calculate curvature and low-pass-filtering allows a multiscale analysis. A curvegram shows the contour curvature in different scales. The increasing scale parameter causes the curvegram to be less sensitive to high frequency noise and fine details. The shape tends toward a shape with low positive curvature; it reflects its global structure. Figure 4.2 a) shows the curvegram for a rough charcoal-stroke ending. It shows that the roughness of the shape is smoothed continually. Figure 4.2 b) shows the curvegram of a pointed brush stroke ending. Brighter pixels represent higher curvature values. The curvature remains high in the middle of the ending curve. The horizontal axis displays the movement along the contour and the vertical axis the scale parameter.

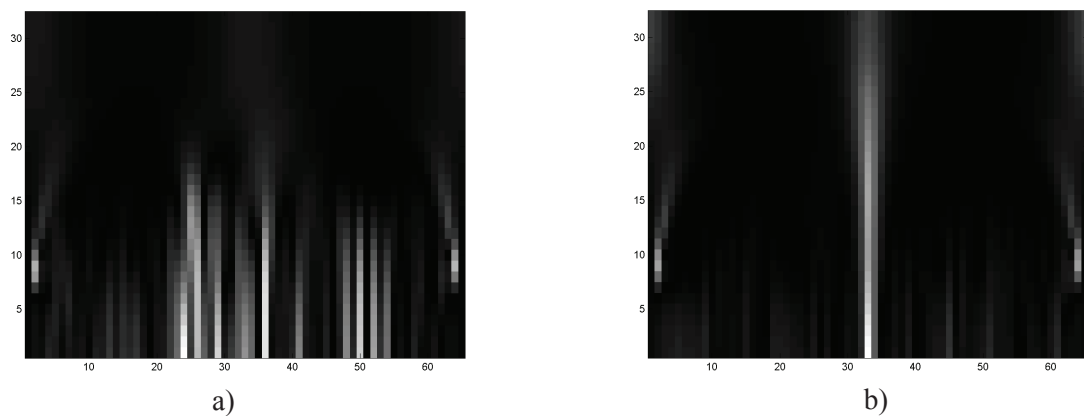


Figure 4.2: a) The curvegram of a rough charcoal ending and b) of a pointed brush-stroke ending. The x-axis shows the position on the ending curve while the y-axis shows the scale.

**Bending Energy:** The mean bending energy, also known as boundary energy, is defined as [CMCJ00]

$$\bar{B} = \frac{1}{N} \sum_{n=0}^{N-1} c(n)^2 \quad (4.15)$$

where  $c$  is the curvature at a landmark on the curve and  $N$  the number of landmarks. Since the mean bending energy of the original shape is subject to noise, the bending energy of the low-pass filtered curve is also considered. This feature is a measure for shape complexity.

**Standard Deviation:** This feature is the ratio of the standard deviation of the original curvature and the smoothed curvature.

**Curvature Development:** The feature examines the relation between the curvature at 50% of the curve length and the mean curvature at 25%, respectively 75% of the curve length. It is related to the distance relation. It compares the curvature at the endpoint to the mean of the curvatures at half way through the ending. It distinguishes endings with a high curvature at the endpoint and low curvature at midway (pointed) and endings with low curvature at the endpoint and higher curvature at midway (angular). Figure 4.1 b) shows the marks for curvature calculation: the green mark at 50% and the yellow marks at 25%, respectively 75% of the curve length.

**Maximal Curvature:** This feature introduces the relation between the maximum curvature of the original curve and the one of the smoothed curve:

$$\frac{\overline{c_{max}}}{c_{max}} = \frac{\max(c_{smooth})}{\max(c_{original})}. \quad (4.16)$$

This feature is an indicator of the smoothness of a curve.

## 4-2.4 Structural Features

These features describe the structure, i.e. the roughness and the width evolution of an ending.

**Area to Perimeter Ratio:** denotes the relation between the area which includes the ending and its perimeter [CMCJ00].

**Rectangularity:** is the ratio between the ending and its rectangular bounding box [CMCJ00]. Figure 4.1 c) shows the rectangular bounding box.

**Distance Relation:** Let  $dw$  be the distance of the open ends of the stroke ending boundary (e.g. approximately the width of the stroke body) and  $dn$  be the distance between the point at 25% and the one at 75% of the curve length. The relationship  $\frac{dn}{dw}$  is used as feature. This feature relates the thickness of the stroke to the thickness of the ending at midway. It can distinguish pointed or blunt endings. Figure 4.1 b) shows this feature. The distance of the blue marks is compared to the distance of the yellow marks.

**Temperature:** The temperature  $Temp$  of a contour is defined on a thermodynamics formalism and has a strong relationship to the fractal dimension [CMCJ00, DKM86]. It is defined as follows

$$Temp = \left( \log_2 \left( \frac{2P}{P-H} \right) \right)^{-1} \quad (4.17)$$

$P$  is the perimeter of an ending and  $H$  its convex hull.

**Triangularity:** This feature is inspired by the work of Shen et al. in [SZD03]. A triangle is fitted into an ending. The three points defining it are the endpoint of the stroke and the open endpoints of the stroke ending. The area of this triangle  $A_{TR}$  is compared to the area  $A_{xy}$  of the stroke ending:

$$Triang = \frac{A_{TR}}{A_{xy}} \quad (4.18)$$

Figure 4.1 shows c) shows the inscribed triangle.

**Convex Hull Area Measure:** This feature compares the area of the ending to the area of its convex hull. It is defined as follows [DK04]:

$$A_{AH} = \frac{A_H - A_{xy}}{A_H} \quad (4.19)$$

It is a measure for the roughness of an ending. Figure 4.1 c) shows the convex hull in green.

## 4-3 Classification

According to [CMCJ00] “to classify means to *assign* classes or categories to items according to their properties”. The properties which are used to classify stroke endings are the feature vectors calculated in Section 4-2. Classification approaches can be grouped into three types [CMCJ00]:

**Imposed Criteria:** Here the criteria are specified from outside, e.g. samples below a given threshold are classified differently than other samples.

**By Example (Supervised Classification):** A training set provides prototypes for classifying additional objects. This type of classification needs the knowledge of “experts” who define classes for the training set. These knowledge and the calculated features form the training set. This learning stage is followed by the recognition when new samples are compared to the trainingset with the help of a classification algorithm which should then predict a class. This type of classification is used, when knowledge about the dataset is available.

**Open Criteria (or Unsupervised Classification):** This method solves the task to assign classes to a set of features, while no knowledge about the data is introduced into the process. This technique is called clustering, because it maximizes similarities inside a class and minimize it between different classes. This method considered, when no knowledge about categories is present. Otherwise, a supervised classification is preferred, because it is less complex [CMCJ00].

A supervised classification approach is used in this thesis, because a priori knowledge about the classes is available. This means, that a training set of stroke endings is manually classified before a classification algorithm is trained with them. Mohanty et al. compare in [MRLM05] a bayesian approach, cross-media relevance language models and Support Vector Machines (SVM) with a linear kernel. Cross-media relevance models annotate each sample of the trainingset with the probability that it is generated from every class which occurs in the set. This discrete model can also be extended to multiple class labels. SVM with linear kernels has outperformed the bayesian approach but the relevance model reached better results than the SVM. Bacardit et al. compared different classifiers with a protein set as data [BSK<sup>+</sup>06]: a Learning Classifier System, a rule induction system, naive bayes and SVM using RBF kernels where SVM outperformed all three classifiers. A comparison between SVM, different bayes classifiers (naive, multinomial),  $k$ NN, the decision tree based classifier C4.5, another tree based system (logistic model tree) and a feed-forward neural network is reported by Kumar et al. [KZ06]. They calculate shape features from hands in order to identify people from their hands. Their results show that the SVM with a polynomial kernel outperformed all other classifiers. Golland et al. [GGSK01] state that SVM's are less subject to over-fitting problems than neural networks.

Kammerer et al. used a k-Nearest-Neighbor (kNN) approach to classify drawing tools [KLZS07]. Guan [GPW05] used kNN to classify chinese paintings with the help of statistical features. Lettner et al. [LS05] classified drawing tools with the help of a k-means clustering algorithm. Widjaja et al. [WLW03] use Support Vector Machines (SVM) to identify painters with the help of color profiles of skin patches. A Bayes classifier was used to identify drawings from Delacroix by [KL98].

### 4-3.1 Support Vector Machines

The Support Vector Machines (SVM) were first introduced by [CV95]. They are classifiers which were designed to solve two-class problems. The underlying idea is to map the feature vectors into a higher dimensional space to create a hyperplane which separates the classes. This hyperplane should create a maximal margin between the feature vectors of two classes. The training vectors with the least distance to the optimal training plane are called *support vectors*. An overview about SVM's is given in [Gun98]. The type of the classification is a c-support vector classification, according to [CV95].

Let  $x_i \in R^n, i = 1, \dots, l$  be a set of training vectors and  $y_i \in R^l$  be a vector containing the classlabels, so that  $y_i \in \{1, -1\}$ . The decision function is calculated as follows:

$$f(x) = \text{sign} \left( \sum_{i=1}^l y_i \alpha_i K(x_i, x) + b \right) \quad (4.20)$$

$K(x_i, x)$  is the kernel. This kernel function maps the training vectors into a higher dimensional space. It can be for example a polynomial, a gaussian or an exponential function. In the tests, a radial exponential kernel was used [CL01].  $\alpha$  is a parameter which is  $\alpha > 0$  for support vectors and  $\alpha = 0$  for non-support vectors.  $b$  is a scalar which defines the distance of the hyperplane to the support vectors.

Since the classification problem in this thesis requires more than two classes to be separated and SVMs are originally designed for a two class problem, several approaches to extend SVM to multiclass classification have been presented [HL02, IWNL05]. These approaches can be constructing and combining binary classifiers or considering all data in

one optimization formulation. The latter method is considered computationally expensive, therefore methods based on binary classification are preferred [HL02, IWNL05].

These can be divided in one-against-all, one-against-one and Directed-Acyclic-Graph (DAG) approaches. The one-against-all method creates  $k$  SVM models ( $k$  is the number of classes). The SVM  $i$  is trained with all of the feature vectors in class  $i$  with considering them to belong to class  $i$  and all the other feature vectors belonging *not* to class  $i$ . This results in  $k$  decision functions. A sample  $x$  belongs then to the class with the maximum value of the decision function. One-against-one builds up  $k(k - 1)/2$  classifiers where each is trained on data from two classes. If the decision function assigns a class to a sample  $x$ , the vote for this sample and this class is increased by one. The class with the maximum value wins. The DAG-SVM uses the same training process as the one-against-one approach. For testing, it uses a DAG with  $k(k - 1)/2$  internal nodes and  $k$  leaves. A test sample  $x$  starts its way through the DAG at the root. The binary decision value is calculated and according to the result, the sample  $x$  moves on the left or the right. The class is predicted by the leaf node finally reached [HL02]. In this thesis, a DAG-SVM is used.

The feature vectors have to be scaled before processing them in the SVM. Otherwise, features in a greater numeric range would dominated those with a smaller range [CL01]. Therefore the feature vectors used for training are linearly scaled to  $[-1, 1]$ , to those for testing the same scale factor has to be applied.

## 4-3.2 Evaluation

The ending data is rectified and aligned to each other with the help of the landmark setting procedure described in Section 4-2.1 and landmarks are set in salient positions throughout a class. Therefrom the features described in Section 4-2 are calculated. The classifier used is an SVM with RBF-Kernel. The input data are as in the previous sections synthetic strokes, drawn strokes on paper and glagolitic writings.

The synthetic data are the strokes described in Section 3-1.2 in Table 3.1. The evaluation is made as follows: First, all features are calculated for all classes and subclasses. Each subclass is therefore considered as an own class. Then these strokes are classified using a leave-one-out-cross-validation with an SVM. There, all endings except one serve as training-set and the one left out is the test sample. This is done over the whole set. To compare the results to another classifier, a kNN classifier with different values of  $n$  was also used to classify the synthetic data (see also [Let05]).

The next step was to reduce the feature space to eliminate irrelevant features. This was achieved by calculating the F-Score as described in [CL06]. The F-score measures the discrimination of two sets of numbers. If  $x_k, k = 1, \dots, m$  ( $m$  is the number of features) and if the numbers of positive and negative instances are  $n_+$  and  $n_-$ , the F-score of feature  $i$  is calculated as follows:

$$F(i) \equiv \frac{\left(\bar{x}_i^{(+)} - \bar{x}_i\right)^2 + \left(\bar{x}_i^{(-)} - \bar{x}_i\right)^2}{\frac{1}{n_+ - 1} \sum_{k=1}^{n_+} \left(x_{k,i}^{(+)} - \bar{x}_i^{(+)}\right)^2 + \frac{1}{n_- - 1} \sum_{k=1}^{n_-} \left(x_{k,i}^{(-)} - \bar{x}_i^{(-)}\right)^2} \quad (4.21)$$

where  $\bar{x}_i, \bar{x}_i^{(+)}, \bar{x}_i^{(-)}$  are the average of feature  $i$  of the whole, positive and negative data sets, respectively;  $x_{k,i}^{(+)}$  is the  $i$ th feature of the  $k$ th positive instance, and  $x_{k,i}$  is the  $i$ th

feature of the  $k$ th negative instance. The larger the F-score, the more discriminating a feature is. The features are then sorted descending by F-score and the first half of the features (12) is used once again for a leave-one-out-cross-validation with SVM and kNN. These 12 features are:

1. Rectangularity
2. Convex Hull Area Measure
3. Chen Moment 2
4. Distance from Centroid: Minimum
5. Area to Perimeter Ratio
6. Distance from Centroid: Skewness
7. Distance from Centroid: Standard Deviation
8. Distance from Centroid: Kurtosis
9. Maximal Curvature
10. Distance from Centroid: Maximum
11. Distance from Centroid: Mean
12. Chen Moment 1

		All Features	Reduced Feature Set
<b>kNN</b>	3	83.91	84.54
	5	83.59	83.59
	7	81.38	82.96
	9	79.49	81.70
	11	79.49	80.44
	avg	81.63	82.64
<b>SVM</b>		89.27	90.53

Table 4.1: Evaluation of the SVM and the kNN classifier over the whole feature space compared to a reduced feature space.

Table 4.1 shows a comparison of the classification results of kNN and SVM over the whole and the reduced feature set. There is a difference of 1% regarding the whole and the reduced feature set. The difference between the kNN (mean) and the SVM Classifier is more notable: 7.64% for the whole feature set and 7.89% for the reduced feature set.

The next test groups the data set into less classes, as listed in the first column of Table 3.1. This also includes, that the intraclass difference is higher as with more classes. The features selected by the F-score are:

1. Convex Hull Area Measure
2. Rectangularity
3. Distance from Centroid: Minimum
4. Chen Moment 2
5. Distance from Centroid: Skewness
6. Maximal Curvature
7. Area to Perimeter Ratio

8. Distance from Centroid: Kurtosis
9. Distance from Centroid: Standard Deviation
10. Distance Relation
11. Bending Energy: Original Curvature
12. Curvature: Standard Deviation Ratio

		All Features %	Reduced Feature Set%
<b>kNN</b>	3	87.91	88.00
	5	89.27	88.60
	7	87.69	88.32
	9	86.43	87.69
	11	86.43	88.11
	avg	87.50	87.74
<b>SVM</b>		88.64	88.95

Table 4.2: Evaluation of the SVM and the kNN classifier over the whole feature space compared to a reduced feature space with less classes.

The results of this test are shown in Table 4.2. Here the difference between SVM and kNN decreased, SVM did better for about 1% (compared to the average of all  $n$ ). But however, since the SVM produced better results with more classes, it is used further on.

### 4-3.3 Conclusion

The classifier was tested with the whole feature-set presented in this chapter on synthetic data. A reduced feature set was derived by calculating the F-Score. The SVM classifier outperformed the kNN and is therefore used to classify stroke endings.

## 4-4 Summary

This section introduced the features used for the classification. These are statistical features which are used to characterize open shapes, features based on curvature and structural features. The statistical features include distance from centroid based statistical values and moments based on the endings contour. Curvature based features are bending energy, mean curvature, standard deviation of curvature, maximal curvature and curvature development. The curvature is calculated with a multiscale approach and values of the original curve are related to values of the smoothed curve. Structural features include area to perimeter ratio, rectangularity, distance relation, temperature and convex hull area measure.

Afterward, SVMs are introduced as a classifier. Features and the classifier were evaluated on synthetic data. For comparison, the SVM was compared to the kNN classifier and showed a better performance. The F-Score was used to calculate the linear separability of the features and therefrom a reduced feature set was derived.

# Chapter 5

## Evaluation and Results

The last and concluding step in evaluating the proposed method is also its core: the classification of drawing tools. All preprocessing steps have been evaluated in Section 3, and the classifier has been tested in the previous section. We evaluate the algorithm on drawn strokes and glagolitic characters.

### 5-1 Drawn Strokes

The input data are test sheets with strokes and stroke formations applied with 9 different drawing tools: brush, black chalk, charcoal, graphite, juniper, reed pen, metal nib pen, goose quill and silver point pen. These sheets were scanned with a flatbed scanner with a resolution of 600dpi. The first test has been performed with eight classes of drawing tools (silver point pen was excluded due to bad segmentation results, see Section 3-1.2).

#### 5-1.1 All Drawing Tools

The tests were performed first with the whole feature set. Then subsets of features were selected according to the F-score presented in Section 4-3.2. If a subset of features gave a result which is less than 5% worse than the one with whole features set it is also shown. The sizes of the subsets are the half of the original set with nonzero features, than the half of the first subset and so on.

The overall classification rate reached 71.79%. Since reducing the feature set according to F-scores did not fall within the 5% limit, all features were used.

Table 5.1 and Table 5-1.1 show the results of the classification of the drawing tools. Table 5.1 shows the confusion matrix for eight classes of strokes. 89.09% of the brush stroke endings are classified as brush, misclassified brush stroke endings include black chalk. Black chalk stroke endings were confused with charcoal, but still almost 55.53% were classified in the right way. Charcoal showed the worst performance of all drawing tools: 28.88% of charcoal stroke endings were classified as black chalk, which can be explained with the similar structure of the material. Both consist of sticks made of black pigment connected through a binder. Its overall classification rate is about 37.44%. Graphite was confused with every other drawing tool, but still reached a classification rate of 56.25%. Juniper was confused with the other dip-pens for about 20.96% of the stroke endings. The classification rate for the metal-nib pen is about 82.45%. Goose quill was misclassified significantly as juniper and reed pen and reached 83.33% of correctly

classified as →	Brush	B. Chalk	Charcoal	Graphite	Juniper	Metal	Quill	Reed	Total
<b>Brush</b>	<b>49</b>	3	1	1	-	-	-	-	54
<b>B. Chalk</b>	3	<b>30</b>	16	4	-	1	-	-	54
<b>Charcoal</b>	5	13	<b>17</b>	8	1	1	-	-	45
<b>Graphite</b>	4	5	4	<b>36</b>	7	3	2	4	65
<b>Juniper</b>	-	2	-	2	<b>45</b>	1	9	3	62
<b>Metal</b>	1	1	1	3	3	<b>48</b>	-	1	58
<b>Quill</b>	-	2	-	1	4	-	<b>55</b>	4	66
<b>Reed</b>	-	-	-	-	5	-	3	<b>56</b>	64
<b>Total</b>	62	56	39	55	65	54	69	68	468

Table 5.1: Absolute results of the classification of 468 stroke endings.

classified strokes. Reed pen reached a classification rate of 87.52% and was confused with the transferential tools juniper and quill.

The performance of the algorithm is over 72% for all transferential drawing tools. In contrast, the recognition of dry drawing tools reached between 37% and 56%. Other drawing tool classification systems used different tools and different numbers of classes. In [LKS04] the classification of strokes into dry and fluid drawing media gained between 65% and 90%. In [KLZS07] the classification was done between three drawing tools (brush, black chalk and graphite). They reached a correct classification rate of 89% with combined boundary and texture features. [LS05] classified six classes of drawing tools with texture features and a classification rate of about 75%.

Drawing tool	Percentage
<b>Brush</b>	<b>89.09</b>
<b>Black Chalk</b>	55.53
<b>Charcoal</b>	37.77
<b>Graphite</b>	56.25
<b>Juniper</b>	<b>72.58</b>
<b>Metal Nib</b>	<b>82.75</b>
<b>Goose Quill</b>	<b>83.33</b>
<b>Reed Pen</b>	<b>87.52</b>
<b>Overall</b>	70.60

Table 5.2: Percentage of correct classified strokes per class.

## 5-1.2 Dry Drawing Tools

The next test includes only dry drawing tools: Black Chalk, charcoal and graphite. Table 5.3 shows the results. The overall classification rate reached 60.97%. Half of the black chalk strokes were classified properly, while 31.48% were classified as charcoal. Charcoal performed again worst with 35.55% of strokes classified correctly, but 40% are classified as black chalk. This emphasized again the similarity of the two drawing tools. In contrast, graphite performed better than in the test with all drawing tool. It reached 87.69% in this test compared to the previous one (56.25%).

classified as →	<b>Black Chalk</b>	<b>Charcoal</b>	<b>Graphite</b>	Total	%
<b>Black Chalk</b>	<b>27</b>	17	10	54	50.00
<b>Charcoal</b>	18	<b>16</b>	11	45	35.55
<b>Graphite</b>	7	1	<b>57</b>	65	87.69
<b>Total</b>	52	34	78	164	60.97

Table 5.3: Absolute results of the classification of 164 dry strokes.

A reduced feature set of six features gained almost the same overall result as the whole feature set. The features ranked by the F-score are:

1. Convex Hull Area Measure
2. Distance from Centroid: Minimum
3. Distance from Centroid: Mean
4. Distance Relation
5. Distance from Centroid: Maximum
6. Chen Moment 4

It can be observed that three features out of six are gained from the distance from the shapes centroid. They results for black chalk strokes are similar, while only 28.88% of black chalk strokes are classified correctly, 53.33% are classified as black chalk. The results for graphite are also comparable to the whole feature set.

classified as →	<b>Black Chalk</b>	<b>Charcoal</b>	<b>Graphite</b>	Total	%
<b>Black Chalk</b>	<b>28</b>	16	10	54	51.85
<b>Charcoal</b>	24	<b>13</b>	8	45	28.88
<b>Graphite</b>	5	4	<b>56</b>	65	86.15
<b>Total</b>	57	33	74	164	59.14

Table 5.4: Results of the classification of 164 dry strokes with reduced feature set.

### 5-1.3 Transferential Drawing Tools

As with the dry drawing tools, a test has performed with only transferential drawing tools. Table 5.5 shows the results. The overall classification rate reached 82.28%. All brush strokes are classified correctly, while juniper reached 69.35% and performed worse than in the test with all drawing tools. It was confused with metal nib pen, quill and reed. 89.65% of the strokes drawn with a metal nib pen were classified correctly, while quill reached 81.81% and performed therefore similar to the test which included all drawing tools. Reed, as juniper, performed also worse than in the test with all strokes and reached 76.56%. Metal nib and brush are highly distinguishable within the transferential drawing tools, while reed and juniper are confused with the other dip-pens.

With the following reduced feature set the same overall classification rate was achieved:

1. Distance from Centroid: Mean
2. Distance from Centroid: Maximum
3. Distance from Centroid: Standard Deviation

classified as →	<b>Brush</b>	<b>Juniper</b>	<b>Metal</b>	<b>Quill</b>	<b>Reed</b>	<b>Total</b>	<b>%</b>
<b>Brush</b>	<b>54</b>	-	-	-	-	54	100
<b>Juniper</b>	-	<b>43</b>	2	10	7	62	69.35
<b>Metal</b>	2	3	<b>52</b>	-	1	58	89.65
<b>Quill</b>	1	5	1	<b>54</b>	5	66	81.81
<b>Reed</b>	-	6	5	4	<b>49</b>	64	76.56
<b>Total</b>	62	65	54	69	68	304	82.28

Table 5.5: Results of the classification of 304 transferential stroke endings.

4. Chen Moment 1
5. Chen Moment 2
6. Distance from Centroid: Minimum

Again, four features out of six are derived from the distance from the centroid. The results are shown in Table 5.6. Brush and juniper performed similar to the test made with the whole feature set. Metal performed worse and was confused with all other transferential tools, including brush. Quill and reed both performed better.

classified as →	<b>Brush</b>	<b>Juniper</b>	<b>Metal</b>	<b>Quill</b>	<b>Reed</b>	<b>Total</b>	<b>%</b>
<b>Brush</b>	<b>53</b>	-	1	-	-	54	98.14
<b>Juniper</b>	-	<b>43</b>	2	11	6	62	69.35
<b>Metal</b>	2	5	<b>48</b>	1	2	58	82.75
<b>Quill</b>	-	2	2	<b>57</b>	5	66	86.36
<b>Reed</b>	-	7	-	6	<b>51</b>	64	79.68
<b>Total</b>	55	57	53	75	64	304	82.28

Table 5.6: Absolute results of the classification of 304 transferential stroke endings with a reduced feature set.

### 5-1.4 Dry and Transferential Drawing Tools

The last test performed on the strokes divides all strokes into two classes, one for the dry drawing tools and the other for the transferential tools. The overall classification rate reached 91.23%. Here again, the classification worked better for the transferential tools: They reached about 96.38% while the dry drawing tools were classified in 81.70% of the cases in the right way, as shown in Table 5.7.

classified as →	<b>Transferential Tools</b>	<b>Dry Tools</b>	<b>Total</b>	<b>%</b>
<b>Transferential Tools</b>	<b>293</b>	11	304	96.38
<b>Dry Drawing Tools</b>	30	<b>134</b>	164	81.70
<b>Total</b>	323	145	468	89.04

Table 5.7: Absolute results of the classification into two classes of all 468 stroke endings.

The best subset of features were the three best according to the F-score:

1. Convex Hull Area Measure
2. Distance from Centroid: Minimum
3. Distance from Centroid: Mean

Here again, the majority of the features are derived from the distance from the centroid. Table 5.8 shows the results. The overall classification rate decreased for about 1.59%, the classification rate for the transferential tools increased for 0.75% and the classification rate for the dry drawing tools dropped of about 6.20%.

classified as →	<b>Transferential Tools</b>	<b>Dry Tools</b>	<b>Total</b>	<b>%</b>
<b>Transferential Tools</b>	<b>295</b>	9	304	97.03
<b>Dry Tools</b>	39	<b>125</b>	164	75.60
<b>Total</b>	334	134	468	86.31

Table 5.8: Absolute results of the classification into two classes of all 468 stroke endings.

## 5-2 Glagolitic Characters

The classification has also been tested on glagolitic characters. The endings of all test characters (Missale and calligrapher sets) examined so far form the training set. The evaluation is again performed with a leave-one-out-cross-validation. Since there are only two different writing tools used, namely reed and a broad metal nib pen, the character endings have been classified into this two classes. Table 5.9 shows the results using the whole feature set. The overall classification rate is 81.73%. 87.65% of the reed pen strokes have been classified correctly, while 67.64% of the broad pen strokes were classified properly. Here must be stated, that the size of the dataset is larger for the reed pen strokes as for the metal nib strokes.

classified as →	<b>Reed Pen</b>	<b>Broad Metal Nib</b>	<b>Total</b>	<b>%</b>
<b>Reed Pen</b>	<b>142</b>	20	162	87.65
<b>Broad Metal Nib</b>	22	<b>46</b>	68	67.64
<b>Total</b>	164	42	230	81.73

Table 5.9: Results of the classification of stroke endings of glagolitic characters written with reed pen and broad metal nib.

Again, a reduced feature set has been found. It led to the results shown in Table 5.10. The reduced set consists of the following features:

1. Distance from Centroid: Skewness
2. Distance from Centroid: Kurtosis
3. Triangularity
4. Rectangularity
5. Bending Energy of Smoothed Curvature
6. Distance from Centroid: Standard Deviation
7. Curvature Standard Deviation Ratio

8. Area to Perimeter Ratio
9. Distance from Centroid: Maximum
10. Distance from Centroid: Minimum
11. Chen Moment 1

The overall classification rate is even higher for the reduced feature set than using the whole feature set: 85.21%. The classification rate of both classes increases.

classified as →	<b>Reed Pen</b>	<b>Broad Metal Nib</b>	<b>Total</b>	<b>%</b>
<b>Reed Pen</b>	<b>149</b>	13	162	91.97
<b>Broad Metal Nib</b>	21	<b>47</b>	68	69.11
<b>Total</b>	164	42	230	85.21

Table 5.10: Results of the classification of stroke endings of glagolitic characters written with reed pen and broad metal nib with a reduced feature set.

Another test has been performed with the glagolitic characters. In addition to the leave-one-out-cross-validation, a  $n$ -fold-cross-validation has been performed. This kind of evaluation divides the training set randomly into  $n$  parts and uses all parts except one as training set and the remaining part as test set. Leave-one-out-cross-validation can be regarded as  $n$ -fold validation where  $n$  is the number of samples minus one. This validation has been performed with the whole feature set and the reduced feature set for different  $n$ . Since the selection of the partitioning is random, the results are the mean of twenty attempts. Table 5.11 gives the results.

<b>n</b>	<b>% All Features</b>	<b>% Reduced Feature Set</b>
<b>2</b>	74.34	80.43
<b>5</b>	74.34	83.91
<b>10</b>	74.34	83.47
<b>15</b>	74.78	83.47
<b>20</b>	74.34	83.04
<b>50</b>	74.78	83.04

Table 5.11: Results of the  $n$ -fold classification of glagolitic characters with the whole and reduced feature set.

The results are quite consistent throughout different values of  $n$ . While the results differ much for the whole feature set ( $\approx 7\%$ ), the reduced feature set proved to be more stable.

## 5-3 Conclusion

The classification was tested with drawn strokes. As the results show, transferential drawing tools are better recognized than dry drawing tools. This originates in the defined cut of the nib, which results in a low variance between stroke endings of one class. The inner-class variance of endings drawn with dry drawing tools is larger, because the ending shape depends more on factors like pressure, or more generally, on the individual style of the artist.

Other drawing tool classification systems used different tools and different numbers of classes. In [LKS04] the classification of strokes into dry and fluid drawing media gained between 65% and 90%. In [KLZS07] the classification was done between three drawing tools (brush, black chalk and graphite). They reached a correct classification rate of 89% with combined boundary and texture features. [LS05] classified six classes of drawing tools with texture features and a classification rate of about 75%.

Glagolitic characters are also classified into reed pen and broad nib pen. Here the classification was also tested with a n-fold-validation, which proved the stability of the chosen reduced feature set.

All tests were performed with the whole and a reduced feature set according to the F-score. Most of the times, the reduced set yield to comparable results. The convex hull measure and the features calculated from the distance from the centroid showed to be the most reliable features as Table 5.12 shows.

<b>Feature</b>	<b># of Appearances</b>	<b>Average Position</b>
Distance from Centroid: Minimum	6	4.50
Convex Hull Area Measure	4	1.25
Distance from Centroid: Mean	4	4.50
Distance from Centroid: Std. Dev.	4	6.26
Distance from Centroid: Maximum	4	6.50
Rectangularity	3	1.66
Chen Moment 2	3	4.00
Distance from Centroid: Skewness	3	4.00
Distance from Centroid: Kurtosis	3	6.00
Area to Perimeter Ratio	3	6.66
Distance Relation	2	7.00
Maximal Curvature	2	7.50
Chen Moment 1	2	7.50
Standard Deviation Curvature	2	9.50
Triangularity	1	3.00
Bending Energy Smoothed Curve	1	5.00
Chen Moment 4	1	6.00
Bending Energy Original Curve	1	11.00
Chen Moment 1	1	12.00

Table 5.12: Appearance of features in a total of six reduced features sets.

# Chapter 6

## Conclusion and Outlook

This thesis presented a drawing and writing tool recognition algorithm based on shape features of stroke endings. After a preprocessing phase, where the stroke endings were extracted from an image, landmarks were set on the resulting curve of a stroke ending. These landmarks were used to calculate features, based on the ending's shape and curvature.

The analysis of stroke endings has never been attempted before. The hypothesis stated at the begin of this thesis was confirmed, although there is still room for improvement.

Nine drawing and writing tools were examined in this thesis: Brush, black chalk, charcoal, graphite, juniper, metal nib, goose quill, reed pen and silver point pen.

The method presented in this thesis started with the segmentation of strokes and stroke formations. The segmentation was achieved by a thresholding method and a snake to refine the contour. A parameter free thresholding algorithm was chosen to apply it on different kinds of input data without changing any parameters. The segmentation was tested with synthetic data, drawn strokes and glagolitic writings. Although standard methods were used, segmentation results were satisfying, with one exception. Silver point pen strokes showed a low contrast to the background and could therefore not be segmented in way that allowed further processing. Therefore they were excluded from the next steps.

After the segmentation, a skeleton of the strokes was calculated. The binarized segmented strokes served as input. This skeleton was beautified with a method based on principal curves. It was also restructured to remove noisy branches and split up junctions. The skeleton beautification was evaluated with the same data as the segmentation. Two additional datasets challenging the restructuring method were used. One consisted of synthetically generated strokes with noisy boundary inconsistencies to test the removal of noisy branches. The False Positive Rate (considering noisy branches which were removed although they were a part of the true skeleton) was about 0.03, while the False Negative Rate (noisy branches which were not removed) reached 0.19. Since the length of the path between the split up junctions is inverse proportional to the crossing angles, the merging of split up junctions was tested on synthetically generated hatches which cross at different angles and have two different distances between strokes. The False Positive Rate was 0.085, while the False Negative Rate was 0.32. The False Negatives occurred only in hatches with acute angles ( $\leq 45^\circ$ ), but in narrow and wide hatches, while false positives appeared only in narrow hatches with acute angles.

With the help of this cleaned skeleton, the strokes and stroke formations were partitioned into static strokes. These strokes were not only the basis for the ending extraction,

but were also useful to gain features which slavists retain useful for a paleographic analysis of Glagolitic characters. These features are: Number of strokes, number of knots, number of straight strokes, number of horizontal strokes, number of vertical strokes, number of bent strokes and number of enclosed areas.

Once gained static strokes, endings were extracted from open and half open strokes. This was done with the help of the fact, that endings are distinguished from the rest of the stroke by their varying width.

Several features are calculated from the shape of the endings. The shape of the ending was resampled with the help of a landmark setting method. The features were statistical features using different shape representations (shape coordinates and distance from centroid), features base on multiscale curvature analysis and structural features.

A Support-Vector-Machine was used as classifier. The features were tested with the classifier either as a whole or with feature subsets. These subsets were derived from the F-score which is a measure for linear separability of features. The statistical features derived from the distance from the centroid and the ratio of the area to the perimeter of an ending proved to be the most reliable features.

The evaluation of the algorithm included different types of data: synthetic data, to ensure the functioning of the method and pointing out pathological cases, strokes drawn with different drawing tools for drawing tool classification and Glagolitic characters from ancient documents and a calligrapher. The SVM was compared to a kNN classifier which was outperformed and SVM was used subsequently. The classification of drawn strokes reached about 70.60%. There was difference between the classification of dry drawing tools and transferential drawing tools. Dry drawing tools were recognized correctly in 49.85% of the cases, while transferential drawing tools reached a classification rate of about 83.5%. This results show that drawing tools with defined nibs gave better results than drawing tools where the tip can be modified and which change aspect with drawing pressure. Therefore transferential drawing tools are recognized better than dry drawing tools.

Future work includes the search for features which are better suited for dry drawing tools. Ending shape analysis can also be combined with stroke texture and boundary analysis. Since segmentation was not the main task of this thesis, here better results could be gained with a better segmentation method.

# Appendix

## Palaeographic Static Features

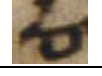
This Section provides the full list of proposed paleographic static features for glagolitic characters introduced in Section 1-2. The following features have been defined by H. Miklas and M. Gau. Their definitions are still under discussion.

1. Multistroke: Number of static strokes / character
2. Multiknot: Number of knots/character
3. Discontinuous: Yes/No
4. Disjunctive: Yes/No
5. Close Ranked: Yes/No
6. Ligature: Yes/No
7. Straight: Number of straight static strokes / character
8. Bent: Number of bent static strokes / character
9. Short: Yes/No
10. Long: Yes/No
11. Descendent: Yes/No
12. High: Yes/No
13. Low: Yes/No
14. Vertical: Number of vertical static strokes/character
15. Horizontal: Number of horizontal static strokes/character
16. Acute-angled: Number of pairs of static strokes joined at a knot with less than 90° or static strokes with a sharp bend
17. Convex: Number of convex static strokes/character, in writing direction
18. Concave: Number of concave static strokes/character, in writing direction
19. Open Water Reservoirs: Number of Water Reservoirs
20. Closed Elements: Number of closed elements (number of holes) per character
21. Horizontal Symmetry: Yes/No
22. Vertical Symmetry: Yes/No
23. Parallel: Number of parallel static strokes/character
24. Up-concentrated: Yes/No
25. Down-concentrated: Yes/No
26. Centered: Yes/No
27. Left-leaning: Yes/No
28. Right-leaning: Yes/No

## Glagolitic Alphabet

The following pages give an overview of the glagolitic alphabet (courtesy M. Gau).

	Latine	Litterae Nomen slavicum	Mis. Sin. Hand A	Mis. Sin. Hand B	Mis. Sin. Hand C
1	a	azъ			
2	b	buki			
3	v	vědě			
4	g	glagoli			
5	d	dobro			
6	e	(j)estъ			
7	ž	živěte			
8	dz	dzělo		-	
9	z	zemlja			
10	i	iže			
11	ï	i		-	
12	ı	(Jagić-) i		-	
13	g'	g'een'na ("Gěrv")		-	-
14	k	kako			
15	l	ljudije			
16	m	myslite			
17	n	našъ			
18	o	опъ			
19	p	pokoi			
21	r	ръci			
22	s	slovo			

23	t	tvъdo			
24	ou	oukъ		-	
25	u	ukъ	-		-
26	f	fgъtъ	 	-	
27	f	fgъtъ		-	-
28	ch	chĕr(ouvim)ъ			
29	ch'	(sonnenförmiges) chĕrъ	-	-	-
30	ω	ω(tъ)	-	-	
31	k'/š(t)	(k'itъ) / š(t)a			
32	c	ci			
33	č	čgvъ			
34	š	ša			
35	ъ	jerъ ("Jor")			
36	y	jery		-	-
37	y	jery	-	-	-
38	ъi	jerъi			
39	ь	jerъ ("Jer")		-	
40	ě	ětъ	 		
41	ü/ju	ju(že)			
44	ę	ęsъ			
45	ǫ	ǫsъ			
46	(j)ę	jęsъ		-	

47	ϥ	јѡѡъ			
50	th	thita	-	-	-
51	ν	уpostasъ (ižica)		-	
Σ			41	31	39

# Bibliography

- [ABE06] B. Allier, N. Bali, and H. Emptoz. Automatic Accurate Broken Character Restoration for Patrimonial Documents. *International Journal of Document Analysis and Recognition*, 8(4):246–261, 2006.
- [AVF05] N. Arica, Y. Vural, and T. Fatos. Shape Similarity Measurement for Boundary Based Features. In M. Kamel and A. Champilho, editors, *Proceedings of the Second International Conference on Image Analysis and Recognition, Lecture Notes in Computer Science*, vol. 3656, pages 431–438, 2005.
- [Bam99] C.C. Bamach. *Drawing and Painting in the Italian Renaissance Workshop. Theory and Practice, 1300-1600*. Cambridge University Press, 1999.
- [BL07] X. Bai and W.-Y. Liu. Skeleton Pruning by Contour Partitioning with Discrete Curve Evolution. *IEEE Transaction Pattern Analysis and Machine Intelligence*, 29(3):449–462, 2007.
- [Bom02] D. Bomford. *Underdrawings in Renaissance Paintings*. Art in the Making. National Gallery Company, London, 2002.
- [Boo96] F.L. Bookstein. Landmark Methods for forms Without Landmarks: Localizing group Differences in Outline Shape. In M.E. Kavanaugh, editor, *Proceedings of the Workshop on Mathematical Methods in Biomedical Image Analysis*, pages 279–289, 1996.
- [BPP05] M. Barni, A. Pelagotti, and A. Piva. Image Processing for the Analysis and Conservation of Painting: Opportunities and Challenges. *IEEE Signal Processing Magazine*, 22(5):141–144, 2005.
- [BPvdH05a] I. Berezhnoy, E. Postma, and J. van den Herik. Authentic: Computerized Brushstroke Analysis. In *Proceedings of the IEEE International Conference on Multimedia and Expo*, pages 1586–1588, 2005.
- [BPvdH05b] I.E. Berezhnoy, E.O. Postma, and J. van den Herik. Computerized Visual Analysis of Paintings. In *Proceedings of the XVI International Conference of the Association for History and Computing*, pages 28–32, 2005.
- [BPvdH07] I. Berezhnoy, E. Postma, and J. van den Herik. Computer analysis of Van Gogh’s complementary colours. *Pattern Recognition Letters*, 28(6):703–709, 2007.

- [BSK<sup>+</sup>06] J. Bacardit, M. Stout, N. Krasnogor, J. D. Hirst, and J. Blazewicz. Coordination Number Prediction Using Learning Classifier Systems: Performance and Interpretability. In M. Keijzer, editor, *Proceedings of the 8th annual conference on Genetic and Evolutionary Computation*, pages 247–254, 2006.
- [Bun03] H. Bunke. Recognition of cursive Roman handwriting: past, present and future. In B. Werner, editor, *Proceedings of the Seventh International Conference on Document Analysis and Recognition*, pages 448–459, 2003.
- [CL01] C.-C. Chang and C.-J. Lin. *LIBSVM: A Library for Support Vector Machines*, 07.03.2008 2001. Software available at <http://www.csie.ntu.edu.tw/~cjlin/libsvm>.
- [CL06] Y.W. Chen and C.J. Lin. Combining SVMs with various feature selection strategies. In I. Guyon, S. Gunn, M. Nikravesh, and L. Zadeh, editors, *Feature extraction, foundations and applications*. 2006.
- [CMCJ00] L. da Fontuora Costa and R. Marcondes Cesar Jr. *Shape Analysis and Classification*. CRC Press, Boca Raton, 2000.
- [CPZ<sup>+</sup>99] E.G. Caiani, A. Porta, P. Zanetti, M. Turiel, S. Muzzupappa, and A. Malliani. Left Ventricular Shape Analysis Applied to Color Kinesis Images. *Computers in Cardiology*, 26:137–140, 1999.
- [CT93] C.-C. Chen and T.-I. Tsai. Improved Moment Invariants for Shape Discrimination. In *Applications of Digital Image Processing XV, Proceedings SPIE*, vol. 1771, pages 270–280, 1993.
- [CT99] H.-P. Chiu and D.-C. Tseng. A novel stroke-based feature extraction for handwritten Chinese character recognition. *Pattern Recognition*, 32(12):1947–1959, 1999.
- [CV95] C. Cortes and V. Vapnik. Support-Vector Networks. *Machine Learning*, 20:273–297, 1995.
- [DC04] F. Drago and N. Chiba. Painting Canvas Synthesis. *The Visual Computer*, 20:314–328, 2004.
- [DCT01] R.H. Davies, T.F. Cootes, and C.J. Taylor. A Minimum Description Length Approach to Statistical Shape Modelling. In M.F. Insana and R.M. Leahy, editors, *Proceedings of the 17th International Conference on Information Processing in Medical Imaging, Lecture Notes in Computer Science*, vol. 2082, pages 50–63, 2001.
- [DK04] C.R.P. Dionisio and H.Y. Kim. New features for affine-invariant shape classification. In *Proceedings of the International Conference on Image Processing*, vol. 4, pages 2135–2138, 2004.
- [DKM86] Y. DuPain, T. Kamae, and M. Mendes. Can one measure the temperature of a curve? *Archive for Rational Mechanics and Analysis*, 94(2):155–163, 1986.

- [DLL03] D. Doermann, J. Liang, and H. Li. Progress in Camera-Based Document Image Analysis. *Proceedings of the Seventh International Conference on Document Analysis and Recognition*, 1:606–616, 2003.
- [DLS07] M. Diem, M Lettner, and R. Sablatnig. Registration of Multi-Spectral Manuscript Images. In *Proceedings of the 8th International Symposium on Virtual Reality, Archaeology and Cultural Heritage VAST (2007)*, pages 113–120, 2007.
- [DM98] I.L. Dryden and K.V. Mardia. *Statistical Shape Analysis*. John Wiley & Sons Ltd, Chichester, 1998.
- [DT97] G. Dudek and J.K. Tsotsos. Shape Representation and Recognition from Multiscale Curvature. *Computer Vision and Image Understanding*, 68(2):170–189, 1997.
- [DTC<sup>+</sup>02] R.H. Davies, C.J. Twining, T.F. Cootes, J.C. Waterton, and C.J. Taylor. A Minimum Description Length Approach to Statistical Shape Modeling. *IEEE Transactions on Medical Imaging*, 21(5):525–537, 2002.
- [dTT95] O. due Trier and T. Taxt. Evaluation of Binarization Methods for Document Images. *IEEE Transactions on Pattern Analysis and Machine Intelligence*, 17(3):312–315, 1995.
- [DvdLB06] A.I. Deac, J. van der Lubbe, and E. Backer. Feature Selection for Paintings Classification by Optimal Tree Pruning. *Multimedia Content Representation, Classification and Security*, 4105:354–361, 2006.
- [EBR07] V. Eglin, S. Bres, and C. Rivero. Hermite and Gabor Transforms for Noise Reduction and Handwriting Classification in Ancient Manuscripts. *International Journal on Document Analysis and Recognition*, 9(2-4):101–122, 2007.
- [EJKCB03] R.L. Easton Jr., K.T. Knox, and W.A. Christens-Barry. Multispectral Imaging of the Archimedes Palimpsest. In B. Werner, editor, *Proceedings of the Applied Imagery Pattern Recognition Workshop*, pages 111–116, 2003.
- [Fal07] C. M. Falco. Novel Expert-Based Approach to Image Analysis. In D.D. Seligmann, editor, *Proceedings of the International Conference on Information Sciences, Signal Processing and its Applications*, pages 8–11, 2007.
- [FK01] K. Franke and M. Köppen. A Computer-Based System to Support Forensic Studies on Handwritten Documents. *International Journal on Document Analysis and Recognition*, 3(4):218–231, 2001.
- [FMR<sup>+</sup>02] J. Freixenet, X. Munoz, D. Raba, J. Marti, and Cufi X. Yet Another Survey on Image Segmentation: Region and Boundary Information Integration. In A. Heyden, G. Sparr, M. Nielsen, and P. Johansen, editors, *Proceedings of the 7th European Conference on Computer Vision-Part III*, pages 408–422, 2002.

- [FRSN03] A.F. Frangi, D. Rueckert, J.A. Schnabel, and W.J. Niessen. Automatic construction of multiple-object three-dimensional statistical shape models: application to cardiac modeling. *IEEE Transactions on Medical Imaging*, 22(8):1114–1126, 2003.
- [Fug05] A. Fuga. *Techniken und Materialien der Kunst, Bildlexikon der Kunst*, vol. 10. Parthas, Berlin, 2005.
- [FY97a] A.M.N. Fu and H. Yan. Effective Classification of Planar Shapes Based on Curve Segment Properties. *Pattern Recognition Letters*, 18:55–61, 1997.
- [FY97b] A.M.N. Fu and H. Yan. Object representation based on Contour Features and Recognition by a Hopfield-Amari network. *Neurocomputing*, 16:127–138, 1997.
- [GGSK01] P. Golland, W.E.L. Grimson, M.E. Shenton, and R. Kikinis. Deformation Analysis for Shape Based Classification. In M.F. Insana and R.M. Leahy, editors, *Proceedings of the 17th International Conference on Information Processing in Medical Imaging*, pages 517–530, 2001.
- [GPH06] U. Garain, T. Paquet, and L. Heutte. On foreground-background separation in low quality document images. *International Journal of Document Analysis and Recognition*, 8(1):47–63, 2006.
- [GPP04] B. Gatos, I. Pratikakis, and S.J. Perantonis. An Adaptive Binarization Technique for Low Quality Historical Documents. In S. Marinai and A. Dengel, editors, *Document Analysis Systems VI, Lecture Notes in Computer Science*, vol. 3163, pages 102–113, 2004.
- [GPW05] X. Guan, G. Pan, and Z. Wu. Automatic Categorization of Traditional Chinese Painting Images with Statistical Gabor Feature and Color Feature. In V.S. Sunderam, G.D. van Albada, P.M.A. Sloot, and J.J. Dongarra, editors, *Proceedings of the 5th Conference on Computational Science, Lecture Notes in Computer Science*, vol. 3514, pages 743–750, 2005.
- [GSH07] B. Gottfried, A. Schuldt, and O. Herzog. Extent, Extremum, and Curvature: Qualitative Numeric Features for Efficient Shape Retrieval. In J. Hertzberg, M. Beetz, and R. Englert, editors, *Proceedings of the 30th German Conference on Advances in Artificial Intelligence, Lecture Notes in Computer Science*, vol. 4667, pages 308–322, 2007.
- [Gum02] J.P. Gumbert. The Pen and its Movement: Some General and Less General Remarks. *Gazette du Livre Medieval*, 40(1):14–24, 2002.
- [Gun98] S. R. Gunn. *Support Vector Machines for Classification and Regression*. Technical Report ISIS-1-98, University of Southampton, 1998.
- [GW01] R.C. Gonzales and R.E. Woods. *Digital Image Processing*. Prentice Hall, 2001.

- [HKZ03] A. Hanbury, P. Kammerer, and E. Zolda. Painting crack elimination using viscous morphological reconstruction. In B. Werner, editor, *Proceedings of the 12th International Conference on Image Analysis and Processing*, pages 226–231, 2003.
- [HL02] C.-W. Hsu and C.-J. Lin. A comparison of methods for multiclass support vector machines. *IEEE Transactions on Neural Networks*, 13(2):415–425, 2002.
- [HPM07] R. Huang, V. Pavlovic, and D.N. Metaxas. Shape analysis using curvature-based descriptors and profile hidden markov models. *Proceedings of the 4th IEEE International Symposium on Biomedical Imaging: From Nano to Macro*, pages 1220–1223, 2007.
- [HTB00] A. Hill, C.J. Taylor, and A.D. Brett. A framework for automatic landmark identification using a new method of nonrigid correspondence. *Transactions on Pattern Analysis and Machine Intelligence*, 22(3):241–251, 2000.
- [IWNL05] E. Ie, J. Weston, W. Stafford Noble, and C. Leslie. Multi-class protein fold recognition using adaptive codes. In *Proceedings of the 22nd International Conference on Machine Learning*, pages 329–336, 2005.
- [JCKL06] K. Jin, M. Cao, S. Kong, and Y. Lu. Homocentric Polar-Radius Moment for Shape Classification. *The 8th International Conference on Signal Processing*, 3:1851–1854, 2006.
- [Kav05] E. Kavallieratou. A binarization algorithm specialized on document images and photos. *Proceedings of the Eighth International Conference on Document Analysis and Recognition*, 1:463–467, 2005.
- [KHE05] S. Kopf, T. Haenselmann, and W. Effelsberg. Enhancing curvature scale space features for robust shape classification. In *Proceedings of the IEEE International Conference on Multimedia and Expo*, pages 4–7, 2005.
- [KK02] B. Kégl and A. Krzyzak. Piecewise Linear Skeletonization Using Principal Curves. *IEEE Transactions on Pattern Analysis and Machine Intelligence*, 24(1):59–74, 2002.
- [KL98] S. Kroener and A.D. Lattner. Authentication of Free Hand Drawings by Pattern Recognition Methods. In H. Emptoz and F. Le Bourgeois, editors, *Proceedings of the 14th International Conference on Pattern Recognition (1)*, pages 462–464, 1998.
- [KLSZ03] P. Kammerer, G. Langs, R. Sablatnig, and E. Zolda. Stroke Boundary Analysis for Identification of Drawing Tools. In *Proceedings of the 8th Iberoamerican Congress on Pattern Recognition*, pages 409–415, 2003.
- [KLZS07] P. Kammerer, M. Lettner, E. Zolda, and R. Sablatnig. Identification of drawing tools by classification of textural and boundary features of strokes. *Pattern Recognition Letters*, 28:710–718, 2007.

- [KO05] A. Kuijper and O. F. Olsen. Geometric skeletonization using the symmetry set. *IEEE International Conference on Image Processing*, 1:497–500, 2005.
- [Kos77] W. Koschatzky. *Die Kunst der Zeichnung*. Residenz Verlag, Salzburg, 1977.
- [KPK06] V. Kokla, A. Psarrou, and V. Konstantinou. Ink recognition based on statistical classification methods. In F. Le Bourgeois and H. Emptoz, editors, *Proceedings of the Second International Conference on Document Image Analysis for Libraries*, 2006.
- [KSG99] A. Kelemen, G. Szekely, and G. Gerig. Elastic model-based segmentation of 3-D neuroradiological data sets. *IEEE Transactions on Medical Imaging*, 18(10):828–839, 1999.
- [KT98] A.C.W. Kotcheff and C.J. Taylor. Automatic construction of eigenshape models by direct optimization. *Medical Image Analysis*, 2(4):303–314, 1998.
- [Kun92] R. Kunze. *DuMont’s Handbuch Kalligraphie. Einführung in Geschichte, Theorie und Praxis der handschriftlichen Gestaltung*. DuMont Buchverlag Köln, 1992.
- [KWT88] M. Kass, A. Witkin, and D. Terzopoulos. Snakes: Active Contour Models’ *International Journal of Computer Vision*, 1(4):321–331, 1988.
- [KZ06] A. Kumar and D. Zhang. Personal recognition using hand shape and texture. *IEEE Transactions on Image Processing*, 15(8):2454–2461, 2006.
- [Lad68] Günther Ladstetter. Zeichnung. In Hans H. Hofstätter, editor, *Geschichte der Kunst und der künstlerischen Techniken*. Ullstein, Frankfurt, 1968.
- [Let05] M. Lettner. Texture based drawing tool classification in infrared reflectograms. Master’s thesis, Vienna University of Technology, 2005.
- [LG06] L.M. Lorigo and V. Govindaraju. Offline Arabic handwriting recognition: A survey. *Transactions on Pattern Analysis and Machine Intelligence*, 28(5):712–724, 2006.
- [LHS99] K. Liu, Y.S. Huang, and C.Y. Suen. Identification of Fork Points on the Skeletons. *IEEE Transactions on Pattern Analysis and Machine Intelligence*, 21(10):1095–1100, 1999.
- [LJN04] C.-L. Liu, S. Jaeger, and M. Nakagawa. Online recognition of Chinese characters: The state-of-the-art. *Transactions on Pattern Analysis and Machine Intelligence*, 26(2):198–213, 2004.
- [LKS04] M. Lettner, P. Kammerer, and R. Sablatnig. Texture analysis of painted strokes. In W. Burger and J. Scharinger, editors, *Proceedings of the 28th Workshop of the Austrian Association for Pattern Recognition*, pages 269–276, 2004.
- [LLS92] L. Lam, S.-W. Lee, and C.Y. Suen. Thinning Methodologies—A Comprehensive Survey. *IEEE Transactions on Pattern Analysis and Machine Intelligence*, 14(9):869–885, 1992.

- [Lon98] S. Loncaric. A survey of shape analysis techniques. *Pattern Recognition*, 31(8):983–1001, 1998.
- [LRF04] S. Lyu, D. Rockmore, and H. Farid. A digital technique for art authentication. *Proceedings of the National Academy of Sciences*, 101(49):17006–17010, 2004.
- [LS95] L. Lam and C.Y. Suen. An evaluation of parallel thinning algorithms for character recognition. *Transactions on Pattern Analysis and Machine Intelligence*, 17(9):914–919, 1995.
- [LS05] M. Lettner and R. Sablatnig. Texture Analysis for Stroke Classification in Infrared Reflectograms. In Parkkinen J., Kälviäinen H., and Hauta-Kasari M., editors, *Proceedings of the 14th Scandinavian Conference on Image Analysis, Lecture Notes in Computer Science*, vol. 3540, pages 459 – 469, 2005.
- [LT02] F. Lin and X. Tang. Off-line handwritten Chinese character stroke extraction. In R. Kasturi, D. Laurendeau, and C. Suen, editors, *Proceedings of the 16th International Conference on Pattern Recognition*, vol. 3, pages 249–252, 2002.
- [LW98] C. Lee and B. Wu. A Chinese-Character-Stroke-Extraction. *Pattern Recognition*, 31(6):651–663, 1998.
- [LW04] J. Li and J.Z. Wang. Studying Digital Imagery of Ancient Paintings by Mixtures of Stochastic Models. *IEEE Transactions on Image Processing*, 13:340–353, 2004.
- [LZLL05] Z. Li, J. Zhang, Y. Liu, and H. Li. The curve-structure invariant moments for shape analysis and recognition. In D.C. Martin, editor, *Proceedings of the 9th International Conference on Computer Aided Design and Computer Graphics*, pages 5–9, 2005.
- [Mai03] F. Mairinger. *Strahlenuntersuchung an Kunstwerken, Bücherei des Restaurators*, vol. 7. E.A. Seemann, Leipzig, 2003.
- [MBEA06] I. Moalla, F. Le Bourgeois, H. Emptoz, and A.M. Alimi. Image Analysis for Palaeography Inspection. In F. Le Bourgeois and H. Emptoz, editors, *Proceedings of the Second International Conference on Document Image Analysis for Libraries*, pages 303 – 311, 2006.
- [MCSP02] K. Martinez, K. Cupitt, J. Saunders, and D. Pillay. Ten years of art imaging research. In R.J. Trew, editor, *Proceedings of the IEEE*, vol. 90, pages 28–41, 2002.
- [MFTM01] D. Martin, C. Fowlkes, D. Tal, and J. Malik. A database of human segmented natural images and its application to evaluating segmentation algorithms and measuring ecological statistics. In B. Werner, editor, *Proceedings of the 8th IEEE International Conference on Computer Vision*, vol. 2, pages 416–423, 2001.

- [Mik03] H. Miklas. Die slavischen Schriften: Glagolica und Kyrillica. In W. Seipel, editor, *Der Turmbau zu Babel. Ursprung und Vielfalt von Sprache und Schrift. Eine Ausstellung des Kunsthistorischen Museums Wien für die Europäische Kulturhauptstadt Graz 2003*, vol. 3a, pages 243–249. Kunsthistorisches Museum Wien, Wien, 2003.
- [Mik04] H. Miklas. Zur Relevanz des neuen Sinaitischen Materials für die Entwicklungsgeschichte der Glagolica. In Dürrigl M.-A., M. Mihaljevic, and F. Velčić, editors, *Glagolijica i Hrvatski Glagolizam. Zbornik radova s međunarodnoga znanstvenog skupa povodom 100. obljetnice Staroslavenske akademije i 50. obljetnice Staroslavenskog instituta (Zagreb - Krk 2.-6. listopada 2002)*, pages 389–399. Zagreb, 2004.
- [Mik08] H. Miklas. St. Catherine’s Monastery on Mount Sinai and the Balkan-Slavic Manuscript-Tradition. <http://slovo-aso.cl.bas.bg/sinai.html>, 08.02.2008 2008.
- [Mok95] F. Mokhtarian. Silhouette-based isolated object recognition through curvature scale space. *IEEE Transactions of Pattern Analysis and Machine Intelligence*, 17(5):539–544, 1995.
- [MR05] R. Manmatha and J.L. Rothfeder. A scale space approach for automatically segmenting words from historical handwritten documents. *Transactions on Pattern Analysis and Machine Intelligence*, 27(8):1212–1225, 2005.
- [MRLM05] N. Mohanty, T.M. Rath, A. Lee, and R. Manmatha. Learning Shapes for Image Classification and Retrieval. In W.-K. Leow, S. L. Michael, T.-S. Chua, W.Y. Ma, L. Chaisorn, and E.M. Bakker, editors, *Image and Video Retrieval, Lecture Notes in Computer Science*, vol. 3568, 2005.
- [MSL01] H. Maitre, F. Schmitt, and C. Lahanier. 15 years of image processing and the fine arts. In *Proceedings of the 2001 International Conference on Image Processing*, vol. 1, pages 557–561, 2001.
- [Nag00] G. Nagy. Twenty Years of Document Image Analysis in PAMI. *IEEE Transactions on Pattern Analysis and Machine Intelligence*, 22(1):38–62, 2000.
- [NEIH98] T. Nakamura, H. Enowaki, H. Itoh, and L. He. Skeleton Revision Algorithm Using Maximal Circles. *14th International Conference on Pattern Recognition*, 2:1607, 1998.
- [NFI+97] W.M. Neuenschwander, P. Fua, L. Iverson, G. Székely, and O. Kuebler. Ziplock snakes. *International Journal of Computer Vision*, 15(8):191–201, December 1997.
- [Nib86] W. Niblack. *An Introduction to Image Processing*. Prentice-Hall, Englewood Cliffs, NJ, 1986.
- [NP01] N. Nikolaidis and I. Pitas. Digital image processing in painting restoration and archiving. In B. Mercer, editor, *Proceedings of the International Conference on Image Processing*, vol. 1, pages 586–589, 2001.

- [Ots79] N. Otsu. A threshold selection method from gray level histograms. *IEEE Transactions on Systems, Man and Cybernetics*, 9:62–66, 1979.
- [Pig05] T. Pignatti. *Die Geschichte der Zeichnung: Von den Ursprüngen bis heute*. Belser Verlag, Stuttgart, 2005.
- [PLM05] V. Pervouchine, G. Leedham, and K. Melikhov. Handwritten character skeletonisation for forensic document analysis. In L.M. Liebrock, editor, *Proceedings of the 2005 ACM symposium on Applied Computing*, pages 754–758, 2005.
- [PS00] R. Plamondon and S. N. Srihari. Online and off-line handwriting recognition: a comprehensive survey. *IEEE Transactions on Pattern Analysis and Machine Intelligence*, 22(1):63–84, 2000.
- [RB05] K. Rapantzikos and C. Balas. Hyperspectral imaging: potential in non-destructive analysis of palimpsests. In *Proceedings of the IEEE International Conference on Image Processing*, vol. 2, pages 618–621, 2005.
- [RC06] P. D. Romero and V. F. Candela. Mathematical models for restoration of baroque paintings. *Advanced Concepts for Intelligent Vision Systems*, 4179:24–34, 2006.
- [SD07] D.G. Stork and M.F. Duarte. Computer Vision, Image Analysis, and Master Art: Part 3. *IEEE Multimedia*, 14(1):14–18, 2007.
- [SJ06] D.G. Stork and M.K. Johnson. Computer Vision, Image Analysis, and Master Art: Part 2. *IEEE Multimedia*, 13(4):12–17, 2006.
- [SKZ98] R. Sablatnig, P. Kammerer, and E. Zolda. Hierarchical classification of paintings using face- and brush stroke models. In A.K. Jain, S. Venkatesh, and B.C. Lovell, editors, *Proceedings of the 14th International Conference on Pattern Recognition*, vol. 1, pages 172–174, 1998.
- [SP00] J. Sauvola and M. Pietikäinen. Adaptive Document Image Binarization. *Pattern Recognition*, 33:225–236, 2000.
- [SS06] H. Sakai and K. Sugihara. Stable and Topology-Preserving Extraction of Medial Axes. In M.L. Gavrilova, editor, *Proceedings of the 3rd International Symposium on Voronoi Diagrams in Science and Engineering*, pages 40 – 47, 2006.
- [Sto06] D.G. Stork. Computer vision, image analysis, and master art: Part 1. *IEEE Multimedia*, 13(3):16–20, 2006.
- [SW93] C.Y. Suen and P.S.-P. Wang. Thinning methodologies for pattern recognition. *International Journal of Pattern Recognition and Artificial Intelligence*, 7(5):965–967, 1993.
- [SZD03] D. Shen, Y. Zhan, and C. Davatzikos. Segmentation of prostate boundaries from ultrasound images using statistical shape model. *IEEE Transactions on Medical Imaging*, 22(4):539–551, 2003.

- [Tho03] H.H. Thodberg. Minimum Description Length Shape and Appearance Models. In G. Goos, J. Hartmanis, and J. van Leeuwen, editors, *Information Processing in Medical Imaging, Lecture Notes in Computer Science*, vol. 2732, pages 51–62, 2003.
- [Tka00] V. Tkadlčik. Über den Ursprung der Glagolica. In H. Miklas, editor, *Glagolitica. Zum Ursprung der slavischen Schriftkultur*, pages 9–32. Verlag der Österreichischen Akademie der Wissenschaften, Wien, 2000.
- [TPR<sup>+</sup>07] S.V. Tracy, C. Papaodysseus, P. Roussopoulos, M. Panagopoulos, D. Fragoulis, D. Dafi, and T. Panagopoulos. Identifying hands on ancient athenian inscriptions: first steps towards a digital approach. *Archaeometry*, 49(4):749–764, 2007.
- [TSB07] A. Tonazzini, E. Salerno, and L. Bedini. Fast correction of bleed-through distortion in grayscale documents by a blind source separation technique. *International Journal on Document Analysis and Recognition*, 10(1):17–25, 2007.
- [TY03] Y.Y. Tang and X. You. Skeletonization of Ribbon-like shapes based on a new wavelet function. *IEEE Transactions on Pattern Analysis and Machine Intelligence*, 25(9):1118–1133, 2003.
- [UH05] R. Unnikrishnan and M. Hebert. Measures of Similarity. In T. Boult, editor, *Proceedings of the Seventh IEEE Workshops on Application of Computer Vision*, vol. 1, pages 394–394, 2005.
- [UPH07] R. Unnikrishnan, C. Pantofaru, and M. Hebert. Toward Objective Evaluation of Image Segmentation Algorithms. *IEEE Transactions on Pattern Analysis and Machine Intelligence*, 29(6):929–944, 2007.
- [VK06] M. Vill and P. Kammerer. Extension of Active Contour Models (Snakes) for Stroke Segmentation in Paintings. In R. Sablatnig, J. Hemsley, P. Kammerer, Zolda E., and Stockinger J., editors, *Proceedings of the 1st EVA Vienna Conference*, pages 11–18, 2006.
- [vO88] P.J. van Otterloo. *A Contour-Oriented Approach to Digital Shape Analysis*. Cip-Data Koninklijke Bibliotheek, Den Haag, 1988.
- [WLLH05] B. Wang, X.-F. Li, F. Liu, and F.-Q. Hu. Color text image binarization based on binary textures analysis. *Pattern Recognition Letters*, 26:1650–1657, 2005.
- [WLW03] I. Widjaja, W.K. Leow, and F.-C. Wu. Identifying painters from color profiles of skin patches in painting images. In L. Torres, editor, *Proceedings of the International Conference on Image Processing*, vol. 1, pages 845–848, 2003.
- [XP97] C. Xu and J.L. Prince. Gradient Vector Flow: A New External Force for Snakes. In D. Plummer and I. Torwik, editors, *Proceedings of IEEE Computer Science Conference on Computer Vision and Pattern Recognition*, pages 66–71, 1997.

- [YF95] D.S. Yeung and H.S. Fong. An off-line approach to extract natural strokes from handwritten Chinese characters. In W.A. Gruver, editor, *Proceedings of the IEEE International Conference on Systems, Man and Cybernetics*, vol. 2, pages 1933–1938, 1995.
- [YFY<sup>+</sup>05] X. You, B. Fang, X. You, Z. He, D. Zhang, and Y.Y. Tang. Skeleton Representation of Character Based on Multiscale Approach. In J.G. Carbonell and J. Siekmann, editors, *Proceedings of the International Conference on Computational Intelligence and Security, Lecture Notes in Computer Science*, vol. 3802, pages 1060–1067, 2005.
- [YJ05] Y. Yan and J.S. Jin. Indexing and Retrieving Oil Paintings Using Style Information. In S. Bres and R. Laurini, editors, *Proceedings of the 8th International Conference on Visual Information and Information Systems, Lecture Notes in Computer Science*, vol. 3736, pages 143–152, 2005.
- [YKD<sup>+</sup>04] I.B. Yosef, K. Kedem, I. Dinstein, M. Beit-Arie, and E. Engel. Classification of Hebrew calligraphic handwriting styles: preliminary results. *Proceedings of the First International Workshop on Document Image Analysis for Libraries*, pages 299–305, 2004.
- [ZL04] D. Zhang and G. Lu. Review of shape representation and description techniques. *Pattern Recognition*, 37(1):1–19, 2004.
- [ZS84] T.Y. Zhang and C.Y. Suen. A fast parallel algorithm for thinning digital patterns. *Communications of the ACM*, 27(3):236–239, 1984.